THERMO-MECHANICAL PERFORMANCE OF DOWELED CONNECTIONS IN TALL TIMBER BUILDINGS

By

Milad Shabanian

A dissertation submitted to the faculty of
The University of North Carolina at Charlotte
in partial fulfillment of the requirements
for the degree of Doctor of Philosophy in
Civil Engineering

Charlotte

2020

Approved by:

_____
Dr. Nicole Braxtan

_____
Dr. Janos Gergely

_____
Dr. Rajaram Janardhanam

_____
Professor David Thaddeus

_____
Dr. Aixi Zhou

_____
David Barber

ABSTRACT

MILAD SHABANIAN. Thermo-mechanical performance of doweled connections in tall timber buildings. (Under the direction of Dr. Nicole L. Braxtan)

Innovations in engineered wood products have led to an increased interest in the design and construction of high-rise timber buildings. However, concerns arise when considering the fire safety of tall timber structures. Similar to other types of structures, the fire resistance (FR) of these types of buildings is greatly affected by the performance of its connections along with the performance of the main structural members. Previously, most of experimental studies focused on the fire-performance (FP) of the metal connections loaded in tension, and parallel to the grain of timber elements, while they were exposed to the standard fire curves. However, contributions in a case study on the fire-performance of tall timber structures confirmed that for the contemporary tall timber buildings, connections would be loaded in different directions and the fire behavior of timber structures directly would be influenced by the percent of exposure of the combustible elements to the fire. Therefore, testing assemblies by prescriptive rules and standard fire curves could not be a precise assumption. In ambient temperature, connections loaded parallel and perpendicular to the grain perform differently. Brittle splitting failure is the dominant failure mode for the connections loaded perpendicular to the grain. Considering the different failure modes at normal temperature and the effect of metal fasteners in increasing the charring in the connection location, raised a question on how the loading direction will affect the fire-performance of doweled connections. In this study heavy timber beam-to-girder and beam-to-wall steel and aluminum doweled connections were tested at three different thermal conditions. Tests were first performed at ambient

temperature where specimens were loaded perpendicular to the grain to determine the capacity of the assembly. Then post-fire-performance (PFP) tests were conducted where the assemblies were exposed to a non-standard fire, allowed to be cooled, and then loaded perpendicular to the grain to investigate the residual capacity of the connection. Finally, the assemblies were loaded perpendicular to the grain while they were exposed to a non-standard fire curve in order to study the fire-performance (FP) of the assemblies. Parameters such as width of the gap between the beam and the girder or wall, beam thickness around the connection, and the thermal material properties influence the fire resistance. A framework to model timber connections at room temperature and elevated temperature, based on a coupled finite-element (FE) heat-displacement model, was developed and applied in a parametric study of the previously tested connection assemblies. Comparison with experimental results showed that the FE models provided good estimates of measured temperatures and the load-carrying capacity at normal temperature and in fire.

DEDICATION

First, I would like to devote this research to my spouse Padideh, my son Diako and my parents for their unconditional love and support.

In addition, the main motivation for doing this research was the several catastrophic fire incidents that propagated to progressive collapse such as 2001, Twin Towers incident in New York, and the 2017, Plasco Building fire in Tehran. Many fire fighters passed away in these tragic events. This research is a dedication to all the brave firefighters who put their lives on the line to save the others.

"MAY WE NEVER FORGET"

ACKNOWLEDGMENTS

It is a great honor for me to acknowledge the roles of several individuals who were instrumental for completion of this research. Foremost, thanks to my committee chair, Dr. Nicole L. Braxtan, for her unlimited support, patience, motivation, consistent guidance, and immense knowledge that made it possible for me to perform this research to a successful conclusion. Besides my advisor, I would like to thank Dr. Janos Gergely, Dr. Rajaram Janardhanam, Dr. Aixi Zhou and Professor David Thaddeus for serving on my committee. Their constructive advice, comments and suggestions were invaluable for this research. My sincere appreciation also goes to a key person in this research, David Barber, my industrial advisor from Arup, who helped me connect with the manufacturers of engineered wood products and doweled connections. His support for this research was unconditional and sincere. I also wish to thank David Impson and Graham Montgomery for their consultation with the case study on the 30 story Cross Laminated Timber (CLT) building for 12th international Society of Fire Protection Engineers (SFPE) conference in Hawaii. Not to mention Mike Beigay from SteelFab, Inc. for generous donation of the required steel material of the test set-up, Sebastian Popp from KLH corporation, provider of CLT material, my friends Rafi Marandi, Matthew Benfield and Austin Parker from UNCC who helped me in preparing the samples and building the test set-up frame, Jacob Nyanja and Hannes Blaas for providing required materials for testing Aluminum connection, and finally Lee Ennis, Chair of the Fire Technology program from Rowan-Cabarrus Community College (RCCC) for letting me to use the RCCC flashover simulator room for the fire tests.

TABLE OF CONTENTS

LIST OF TABLES

LIST OF FIGURES

LIST OF ABBREVATIONS

ASTM	American Society for Testing and Material
CLT	Cross Laminated Timber
FE	Finite Element
FP	Fire Performance
FR	Fire Resistance
FRR	Fire Resistance Rate
Glulam	Glued Laminated Timber
HT	Heavy Timber
JC	Johnson Cook
LT	Light Timber
LVL	Laminated Veneer Lumber
NLT	Nailed Laminated Timber
PBD	Performance Base Design
PFP	Post Fire Performance
RCCC	Rowan-Cabarrus Community College
SFPE	Society of Fire Protection Engineers
TTB	Tall Timber Building
UNCC	University of North Carolina at Charlotte
UTM	Universal Testing Machine
NT	Normal Temperature

1. INTRODUCTION

1.1. Background

In comparison to the other type of construction materials, heavy timber (HT) construction has advantages in architectural appearance, constructability, cost, and sustainability [1]. As such, the use of HT materials has been on the rise in Europe and more recently in the North America where the renaissance of timber construction has also led to a desire to design and build taller timber structures [2].

Metal connections play a critical role in both seismic and fire-performance of contemporary timber structures. They increase the ductility and thereby improve the seismic performance of a structure against lateral forces. On the other hand, steel connections may be seriously affected by fire, losing strength and stiffness, leading to large plastic deformations, and contributing to progressive collapse. Figure 1.1 shows a fire incident in a 17-story steel structure. In this catastrophic incident, failure of the connections propagated a disproportionate collapse, which claimed the lives of 16 firefighters and 10 civilians [3]. Thus, the study of fire behavior of connections is vital.

Beam-to-girder connections and beam-to-wall connections are some of the structural components which were found to be of great importance when considering the structural performance at elevated temperatures in tall timber buildings (TTB). Post-fire investigations of damaged structures confirm the fact that these connections have a notable effect on the survival time of the structure in fire [4].

Figure 1.1. Fire incident occurred in a 17-story Plasco building [3].

Currently, structural fire design methods for timber construction follows prescriptive codes based on standard fire curves [5]. However, for contemporary timber structures with exposed, combustible timber elements it may not be appropriate to follow the structural fire design methods of prescriptive codes and fire standard curves such as ASTM E-119 [6]. Fire safety measures of these types of structures are best to consider using performance-base design (PBD) methods. To date, the fire-performance (FP) of connections in this type of structure has not been investigated through a performance-based approach considering a variety of parameters under realistic fire scenarios.

1.2. Project Goal and Objectives

The goal of this research is to study the fire-performance (FP) and post-fire-performance (PFP) of doweled connections for tall timber structures. Seven intermediate size assemblies were investigated at ambient temperature, during fire, and after fire

exposure. The samples were designed and inspired by a case-study defined by the Society of Fire Protection Engineers (SFPE) 12th International Conference on Fire-performance of a 30-story cross-laminated timber (CLT) building [7]. The assemblies include beam-to-wall and beam-to-girder doweled connections.

This research is comprised of four tasks: (1) experimental testing of connections at ambient temperature (AT); (2) experimental testing of connections after fire (PFP); (3) experimental testing of connections during fire (FP); and (4) finite element model validation and expanded numerical study.

Task 1 benchmarked the performance of the connections at ambient temperatures (AT). The assemblies were loaded at mid-span until failure occurred using a Universal Testing Machine (UTM). The objective of Task 1 was to define the strength and failure mode of the test assemblies under ambient conditions.

Task 2 studied the PFP of metal connections. During these experiments, the assemblies were exposed to fire once for 30 minutes and once for 60 minutes by a propane burner, allowed to cool, and then subject to imposed load until failure occurred. Fire testing was performed off-campus and then the specimens were carefully transported back to campus for testing in the UTM. The objective of Task 2 was to define the residual strength and failure mode of the test assemblies after defined exposure times to fire.

Task 3 studied the fire-performance of the connections. In this set of experiments, test assemblies were exposed to fire while they were loaded at the mid-span of the beam element. Testing was performed off-campus – loading was applied using a mechanical jack while the fire was applied with a propane burner. Deflection of beams was measured using a displacement gage while temperatures were recorded using thermocouples.

Task 4 included a finite element model validated by comparison with experimental results. A fully couple thermal-structural model using the Johnson-Cook (JC) plastic model and temperature dependent thermal and mechanical material properties was developed using Abaqus Finite Element (FE) Software. Once the model was validated, an expanded numerical matrix was considered to investigate the effect of a standard fire exposure on the fire-performance of the connections.

1.3. Overview

This dissertation is organized into chapters as follows. Chapter 2 includes background on heavy timber structures and a brief discussion of a case study on the fire-performance base design of a tall CLT building. Chapter 3 explains the thermo-mechanical behavior of the Glulam beam-to-girder assembly at ambient temperature (AT), during (FP) and after (PFP) non-standard fire (Paper 1). Chapter 4 describes the performance of the Glulam-beam to CLT-wall assembly at ambient temperature, during and after non-standard fire (Paper 2). Chapter 5 represents the thermo-mechanical performance of CLT beam-to-girder assembly at three similar thermal conditions (Paper 3). Chapter 6 describes the numerical simulations and FE modeling of the tested assemblies (Paper 4). Finally, Chapter 7 provides conclusions and recommendations for future work. Appendix A provides more details on the case study and the experiments conducted on steel connection. Appendix B describes the test results related to the aluminum connection.

1.4. REFERENCES

[1] Green, M.C. and J.E. Karsh, *The case for tall wood buildings: how mass timber offers a safe, economical, and environmentally friendly alternative for tall building structures*. 2012: MgbARCHITECTURE+ DESIGN.

[2] Smith, I. and A. Frangi, Use of timber in tall multi-storey buildings. 2014: International Association for Bridge and Structural Engineering (IABSE).

[3] Ahmadi, M., et al., *Collapse of the 16-Story Plasco Building in Tehran due to Fire.* Fire Technology, 2019: p. 1-31.

[4] Newman, G., *Structural fire engineering investigation of Broadgate phase 8 fire.* Steel Construction Institute, Ascot, 1991.

[5] Buchanan, A.H. and A.K. Abu, *Structural design for fire safety*. 2017: John Wiley & Sons.

[6] ASTM-E119-18ce1, *Standard Test Methods for Fire Tests of Building Construction and Materials*. 2018, ASTM International: West Conshohocken, PA.

[7] Bahrani B, Saunders C, Shabanian M, Braxtan NL, Rockwell SR, Zhou A. (2018) High-rise residential building using cross-laminated timber: Charlotte 9th Street Tower- United States Case Study, 12th International Conference on Performance-Based Codes and Fire Safety Design Methods, Honolulu, Hawaii, USA, April 23-27, 2018.

2. A CASE STUDY ON TALL TIMBER BUILDINGS

2.1. Introduction

The Society of Fire Protection Engineers (SFPE) issued a call for a case study on the performance-based design (PBD) of a high-rise timber building utilizing CLT as the main construction material for the 12th International Conference on Performance-Based Codes and Fire Safety Design Methods [1]. A team of UNC Charlotte students and faculty presented their case study at the conference. This chapter presents a relevant background related to heavy timber structures and different types of engineered wood products along with the design of the structural system included in the case study.

2.2. Background on Timber Structures

There are two major types of timber structures: light-timber (LT) and heavy-timber (HT). Figure 2.1 compares light timber construction versus heavy timber construction. Light timber construction typically consists of 2 in by 4 in studs and 2 in by 6 in, 8 in, or 10 in joists in residential buildings up to 6 story (65 ft). The structural elements are typically protected against fire through encapsulation with gypsum board protection [2]. On the other hand, heavy timber construction includes wood columns, walls, posts, and beams with nominal section size usually greater than 6 in by 6 in. Heavy timber members inherently exhibit better fire-performance and structural strength due to their large size. Thus, heavy timber construction may be applicable for use also in high-rise buildings.

The maximum fire resisting rate (FRR) allowed for light timber construction is 2 hours for exterior bearing walls and 1 hour for interior bearing walls and floor construction [3]. Light timber framing is popular in construction due to the speed in construction, lower

construction cost, and simplicity. However, due to the relatively low stiffness and limited fire-performance of this type of constructions, light timber is not allowed to be used in high-rise buildings.

(a) *(b)*

Figure 2.1. Different types of timber structures: (a) LT framing vs. (b) HT framing.

For the benefit of this research and in order to provide a better understanding about heavy timber constructions and their fire performance, more detailed information on heavy timber construction will be presented in the following sections.

2.2.1. History of Tall Timber Buildings

Early man started controlling fire almost 1.7 million years ago. Whereas evidence shows that timber engineering and timber usage as a structural material was born around 300,000 years ago [4]. City wide or district wide conflagrations were the motive force for building regulations dating back to the Roman Empire and Achaemenes Empire [5].

Figure 2.2. Capital part of a pillar from Persepolis remained after fire incident and on display at the Louvre in Paris.

In the Zoroastrianism Achaemenes Empire, fire was a symbol of God and purity on earth and Zoroastrianism fire temples were located along the Achaemenes territory with an active eternal flame [6]. When Alexander the Great invaded the Persian Empire in 334 B.C., he destroyed and burnt Persepolis, the 200 years old capital of the Persian Empire [7]. Persepolis had been built by order of Cyrus the Great, mainly out of solid sawn lumber and stone. Figure 2.2 shows the capital part of a heavy timber column and the bearing connection of two sawn lumber beams.

However, there are still several examples of tall timber structures which have been standing for centuries. For example, tall, wooden pagodas in Japan and China with heights between 9 to 19 stories are reported to be between 1000-1400 years old.

Nevertheless, due in part to the fear caused by some major catastrophic fire incidents such as great fire of London in 1666 [8] and Boston Fire in 1872 [9], and restrictions with fire extinguishing facilities, the use of timber as the main construction material has been limited to four stories. Simultaneously, the Industrial Revolution of 1760, marking the beginning of the modern steel industry in 1850 [10] and reinforced concrete in 1853 [11], greatly influenced the construction of tall superstructures. Specially, after the invention of safety elevators in 1857, the number of high-rise steel and reinforced concrete structures increased significantly.

The contemporary knowledge gained during last century in fire protection and firefighting helped prevent the possibility of the catastrophic fire incidents of before and opened a new door into timber construction. The invention of engineered wood products also contributed to the feasibility of construction of tall timber structures. Table 2.1 lists some of the historical and contemporary tall buildings constructed out of heavy timber products.

Table 2.1. High-rise heavy timber structures.

Year	Name and location	Number of stories	Total height (ft.)
515 BC	Persepolis, Iran (destroyed in fire 330 BC).	1 story	89
1056	Sakyamuni Pagoda, China	9 story	220
1709	Daibutsuden, Japan	N/A	160
1720	Bârsana Monastery, Romania	N/A	203
1890	St. Georges Anglican Catholic Church, Guyana	N/A	142.7
1893	St. Paulus Church, San Francisco, USA (destroyed by fire 1995)	N/A	142.7
1906	Claremont Hotel, Oakland, CA, USA	10 + Cupola	160
1921	Lattice frame industrial building, Cardona, Spain	N/A	106.3
1934	Muhlacker Radio Tower, Germany	N/A	623.36
1935	Gliwice Radio Tower, Poland	N/A	387.13
1942	Tillamook Hanger, OR, USA	N/A	190.94
1942	Hangers 2&3, Moffit Field, CA, USA	N/A	170.60
1992	Sutyagin House, Russia	13	144.35
1992	Tennessee Tree House, USA	10	96.78
2003	Sa ̆pânt ̦a-Peri Church, Romania	N/A	246
2007	E3, Germany	7 story	269
2008	Stadthaus, London, UK	9	98.42
2010	Bridport House, London, UK	8	85.3
2011	Holz8, Bad Aibling, Germany	8	82

2012	Life Cycle Tower One, Dornbirn, Austria	8	88.58
2012	Forté, Melbourne, Australia	10	104.98
2013	Panorama Giustinelli, Trieste, Italy	7	72.17
2013	Maison de l'Inde, Paris, France	7	75.45
2013	Wagramerstrasse, Vienna, Austria	7	72.17
2013	Pentagon II, Oslo, Norway	8	78.74
2013	Cenni di Cambiamento, Milan, Italy	9	88.58
2013	Dalston Lane, London, UK	9	104.98
2014	Contralaminada, Spain	6	65.61
2014	Wood Innovation Centre, Vancouver, Canada	8	95.14
2014	St. Dié-des-Vosges, St. Diè des Vosges, France	8	88.58
2014	Strandparken, Stockholm, Sweden	7	72.17
2015	Puukuokka, Jyväskylä, Finland	8	91.86
2015	Banyan Wharf, London, UK	10	108.26
2016	T3, Minnesota, USA	7	101.7
2016	Arbora, Montréal, Canada	8	88.58
2016	Moholt 50/50, Trondheim, Norway	9	101.7
2017	Brock Commons, Vancouver, Canada	18	173.88
2018	Sanctuary, Glasgow, UK	7	98.42
2018	Carbon 12, Portland, USA	8	82
2018	5 King, Brisbane, Australia	10	170.6

2.2.2. Heavy Timber Structures

Heavy timber framing, or mass timber construction, is a distinctive type of timber framing, comprised of wooden elements such as: columns, beams, bearing walls, shear walls and floor panels. Solid sawn lumber is probably one of the oldest types of wooden elements used in construction of heavy timber structures. Figure 2.3 shows three examples of ancient heavy timber structures built by sawn lumber.

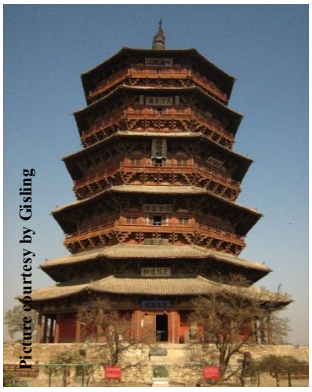

(a) *(b)* *(c)*

Figure 2.3. Ancient heavy timber constructions:(a) Urnes Stave Church, Sweden, (b) Hwangnyungsa Buddhist Temple, South Korea, (c) Yinxian Pagoda, China

The invention and development of engineered wood products during the last century, has led to increased feasibility of construction of tall timber structures. Engineered wood products such as glued-laminated timber (glulam or GL), laminated veneer lumber (LVL), cross-laminated timber (CLT) and nailed-laminated timber (NLT) presented with higher strength and quickly increased in popularity. Figure 2.4 shows examples of contemporary heavy timber construction using engineered wood products as the main structural elements.

(a) *(b)* *(c)*

Figure 2.4. Modern heavy timber constructions: (a) Treat, Norway [16], (b) Brock Commons, Canada, (c) Medienhaus Tamedia, Switzerland.

2.2.3. Engineered Wood Products

The wood industry is rapidly developing and advancing. Most recently, North America has spurred new, powerful companies competing with deep-rooted European companies. Engineered wood products are wood-based composites that are manufactured in order to increase the strength and dimension of structural wooden elements. There is wide variety of engineered wood products such as plywood, oriented strand board (OSB), glued-laminated timber (glulam or GL), cross laminated timber (CLT), nailed laminated lumber (NLT), doweled laminated timber (DLT), structural composite lumber (SCL), laminated veneer lumber (LVL), parallel strand lumber (PSL), laminated strand lumber

(LSL) and oriented strand lumber (OSL). A brief review on some of the main engineered wood products is discussed.

2.2.3.1. Glued-Laminated Timber (Glulam or GL)

Glue laminated timber (glulam or GL) is an innovative engineered wood product that was first used in 1893 to construct an auditorium in Switzerland [12]. Glulam is made up of individual layers of dimensional lumber. These layers are end jointed together in order to have longer lengths and glued together with adhesives to provide larger cross sections. Because of their configuration, large glulam elements can be produced from small trees. Glulam has higher strength compared to solid sawn lumber and due to this high strength glulam can span longer distances. It is very common to use glulam elements as posts and beams in structures. Figure 2.5 shows glulam elements and their application as structural elements.

(a)

(b)

Figure 2.5. (a) Glulam beam and (b) its application as beams and columns in HT construction.

2.2.3.2. Laminated Veneer Lumber (LVL)

LVL is probably one of the most common engineered wood products manufactured by gluing thin layers of wood veneer together under high pressure. Using thin veneer layers

of wood decreases the influence of defects such as knots, cracks, and curves. LVL has applications in walls, floors, beams, and especially headers. Figure 2.6 shows the configuration of LVL and its application as a header.

(a) *(b)*

Figure 2.6. (a) Laminated Veneer Lumber and (b) its application as a header.

2.2.3.3. Cross Laminated Timber (CLT)

Around 1990s, Cross laminated timber, or CLT developed in Switzerland, Germany and Austria [13]. CLT is a wood based composite panel product, comprised of multiple layers of lumbers stacked together with the grains in alternating, perpendicularly orientations in order to achieve higher strength in different directions where the exterior layers are laid out in a direction parallel to the direction of the applied load. CLT can be used as wall, floor, beam, and column elements – however, using CLT as beam and column elements is still uncommon. CLT panels are most applicable for panelized construction. One of the advantages of CLT is that prefabrication is completed off-site, reducing the construction time and cost in addition to increasing the construction accuracy. Figure 2.7 indicates a CLT panel and its application in panelized construction.

(a) *(b)*

Figure 2.7. (a) Cross Laminated Timber (CLT) and (b) its application in panelized construction.

2.2.3.4. Nailed Laminated Timber (NLT)

Nailed laminated timber (NLT) is an engineered wood product consisting of sawn lumbers aligned next to each other side by side and nailed together. NLT panels are applicable for floors and decking systems. Doweled laminated timber, or DLT, is another engineered wood product very similar to NLT, but has timber dowels instead of nails. Figure 2.8 shows the NLT panel and its application as a floor panel.

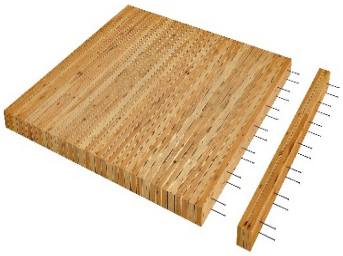

(a) *(b)*

Figure 2.8. (a) NLT Panel and (b) its application as floor panel.

2.2.4. Framing Systems

Balloon and platform framing systems are the two main framing systems traditionally used in light timber construction. The concept behind these two framing

systems has been extended to the other types of construction including heavy timber construction.

2.2.4.1. Platform Framing System

In a platform framing system, each floor is sorted by the wall studs on lower level. The vertical structural elements such as walls and columns span only between two floors and transfer the gravity load from one floor to the underneath level. In this construction system, connections are mostly load bearing type of connections. This means that the vertical structural elements which transfer the gravity load, are fully supported and placed on horizontal structural elements like floor panels or beams. Figure 2.9 illustrates the platform framing system.

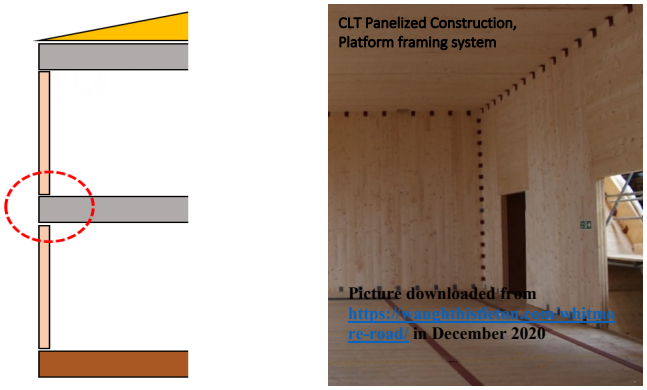

(a) *(b)*

Figure 2.9. (a) Load bearing connection in platform framing system, (b) and its application in panelized construction.

2.2.4.2. Balloon Framing System

Balloon framing consists of continuous vertical structural elements such as columns, load bearing walls, and shear walls transferring the gravity and lateral loads to the foundation. The fire-performance of the platform framing system is better than balloon

framing system as the floor acts as a firestop. Conversely, the chimney effect occurring in the balloon framing system during fire can lead to vertical fire spread within a structure. Therefore, in balloon framing system, it is essential to cover and fill the gaps between the elements by proper fire sealants. Figure 2.10 illustrates the balloon framing system and connection details in this system.

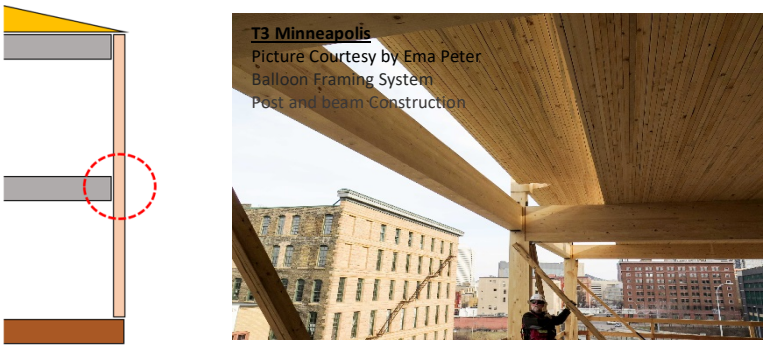

(a) *(b)*

Figure 2.10. (a) Connection configuration in balloon framing system and (b) an example of balloon framing system.

2.2.5. Different Types of Heavy Timber Structures

Heavy timber structures with higher strength in comparison to light timber construction is most common in mid-rise to high-rise timber structures as the invention of engineered wood products made it possible to reach higher strength and elevation. Construction with heavy timber products fall into three main categories: post and beam construction, panelized construction and hybrid construction.

2.2.5.1. Post and Beam

Principal structural components of this type of construction are columns, beams, and braces usually made of solid sawn lumber, glulam or LVL, and shear walls and floor panels mostly consisting of CLT or NLT panels. The post and beam method are suitable

for constructions following the balloon framing system. Figure 2.11 shows examples of heavy timber post and beam construction.

(a) (b) (c)

Figure 2.11. Post and beam constructions. (a) Medienhaus Tamedia, Switzerland, (b) Traditional post and beam construction, (c) Butler Square, USA.

2.2.5.2. Panelized construction

CLT panels are typically used in a platform frame configuration with this type of panelized construction and are suitable for low-rise and mid-rise buildings. CLT panels experience shrinkage due to moisture loss and imposed compressive loads in the thickness direction. Consequently, the cumulative shrinkage of CLT panels make it difficult to use the panelized construction for high-rise buildings [14]. CLT panels are pre-cut off-site and transferred to the site for assembly. Hence, this method of construction is usually faster, safer, and more economical in comparison with post and beam construction. Figure 2.12 shows the panelized construction process using CLT panels.

Figure 2.12. Panelized construction with pre-cut CLT panels.

2.2.5.3. Hybrid Construction

Hybrid construction relates to the cases where a combination of various methods and materials is adopted by the designer in order to achieve different purposes such as decreasing the construction cost, increasing the stiffness, and other architectural considerations. Figure 2.13 shows T3 and Brocks Commons buildings – two recent high-rise hybrid structures, which combine the advantages of engineered wood columns, beams and floor panels with reinforced concrete shear wall cores. Reinforced concrete shear walls resist against lateral loads while the rest of structure is transferring gravity load to the foundation. In addition, there are also other examples of hybrid timber structures including post tensioning technique and mixing structural steel with engineered wood products [2].

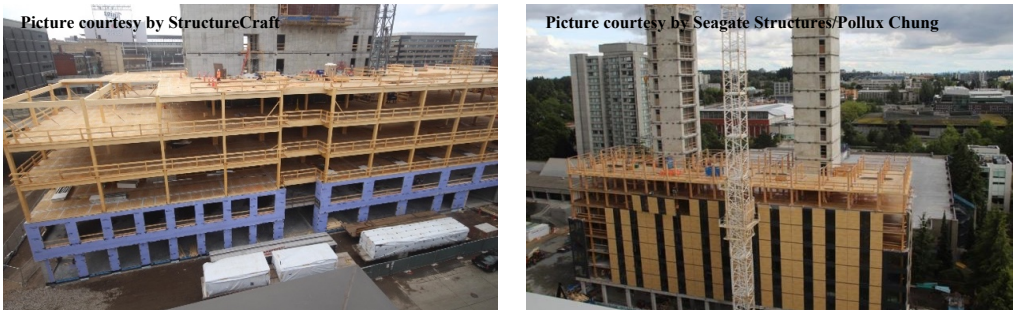

(a) *(b)*

Figure 2.13. Hybrid heavy timber constructions. (a) T3, office building, Minneapolis, MN (b) Brock Commons, residential building, Vancouver, BC.

2.2.6. Fire Protection Systems

Fire performance of unprotected light timber and heavy timber structural elements can be compared to what happens in nature during a wildfire. Figure 2.14 shows the trees in different sizes. When wildfire happens, small branches will burn faster in comparison to the thick trunks, illustrating the inherent fire-resistant behavior of heavy timber. When wood burns, a char layer develops outside and protects the inner cross-section. The post-

fire investigations of wildfire incidents showed that in many cases, large trees did not burn completely and even after the fire incident they continued their lives.

Figure 2.14. Larger sections stand longer during the wildfire incident.

There are two methods of passive fire protection for structural timber construction: encapsulation of the structural members and consideration of a sacrificial char layer on exposed wooden elements.

Encapsulation is the common approach of fire protection in light timber structures. Light timber structures require complete protection against fire as the stud and joists cross sections are not large enough to allow for a sacrificial char layer while maintaining an adequate load carrying core. In this method structural components of the building are completely protected and covered by fire resistant materials such as gypsum boards and intumescent [15]. The timber elements will not be allowed to char and will not contribute to the fire load. This method is easily adopted for different type of structures to provide the

required fire resisting rate (FRR). Figure 2.15 shows the full encapsulation of CLT panelized construction by gypsum boards.

(a) (b)

Figure 2.15. Full encapsulation of panelized structure. (a) Murray Grove building during construction, (b) CLT panels protected by gypsum boards.

The sacrificial layer method uses the inherent fire-resistant behavior of thick wooden elements. A char layer forms on the surface of the elements exposed to fire, protecting the inside layers of timber from burning. Including a sacrificial layer is the desired approach for fire protection when exposed timber elements are present. When considering an exposed timber element, a sacrificial layer will be added to the required cross section of the member. However, the combustible, sacrificial layer contributes to the fuel load of the structure and it is thus necessary to consider the effect of the sacrificial layer in fire calculations [15].

2.3. Tall CLT Building Case Study

An interdisciplinary team consisting of civil engineers, architects, and fire protection engineers completed a case study of a tall timber building as specified by SFPE for the 12th International Conference on Performance-based Codes and Fire Safety Design Methods. The author's specific contributions to the case study include: the architectural design, structural system adoption and providing the final architectural and structural

drawings. Figure 2.16 shows the front elevation view and 3D model of the 30-story structure proposed in the case study.

(a) (b)

Figure 2.16. Designed 30-story CLT building for the 12th SFPE International Conference (a) front view, (b) 3D Model [1].

The structural design, including connection details, are presented here to further illustrate the advancement of heavy timber as a construction material.

2.3.1. Project Background

The 30-story residential concept building was located in a financial district in a city with retail incorporated on the ground floor and two parking levels below the ground. The target market for the building included members of the gig economy with a focus on maximizing transient use. In addition, flexibility had to be provided to facilitate permanent occupants. The owner requested the highest possible environmental standard of sustainability for the project as well as occupant evacuation elevators for emergency situations. The structural behavior of the engineered wood products during a fire event had to be addressed, and there was an architectural desire to expose parts of the engineered wood products as a design feature. The UNC Charlotte student chapter team identified

additional assumptions and completed a performance-based analysis of the building. Figure 2.17 shows the proposed final design, including the recommendations for fire and life safety features to ensure the project goals and objectives were met.

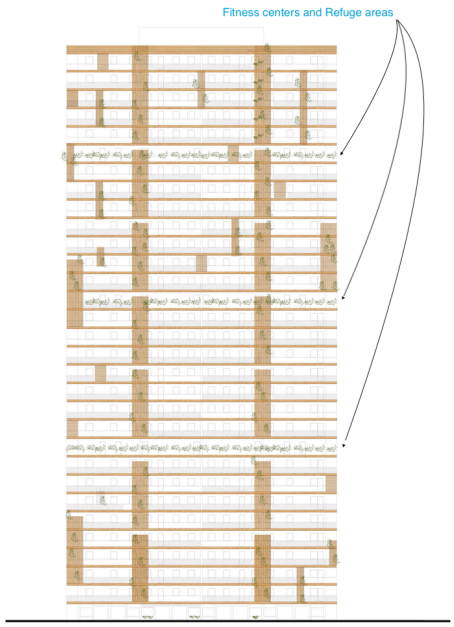

Figure 2.17. Front view of the project [1].

2.3.2. Building Description

The 30-story high-rise residential building with a total height of 433 ft. (102 m.) is located in Charlotte, North Carolina. The building includes a structural podium design with balloon framing system. During the structural design process, the main concern was to use engineered wood products, specifically CLT, as the main construction material. However, there were locations that with considering the required fire resisting rate and required strength, cast in place reinforced concrete was substituted for the engineered wood products.

Figure 2.18 indicates the two car-park levels below ground. All the structural members of these two floors were designed using cast in place reinforced concrete. High

groundwater levels at the site location proved to be one of the most important reasons for preferring reinforced concrete to CLT panels. In addition, dimension of the columns and shear walls would be increased significantly in the lower levels if CLT and GL were employed, which was against the will of the owner. Finally, fire safety of the carparks with a large number of parked cars containing gas was another reason for this adoption.

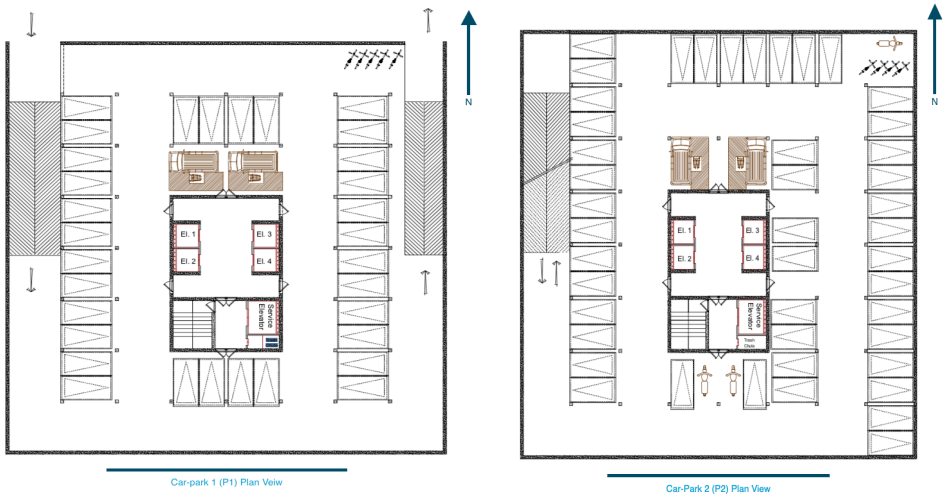

(a) *(b)*

Figure 2.18. Carparks plan view. (a) carpark 1 (b) carpark 2 [1].

Figure 2.19 shows the plan view of the ground floor and residential floors. In the stairways and elevator shafts RC was assigned in order to increase the lateral stiffness of the structure and improve the fire resisting rate of the evacuation system. The remaining above ground level structure is a combination of CLT wall and floor panels, glulam beams and columns, and cast in place reinforced concrete elevator shafts.

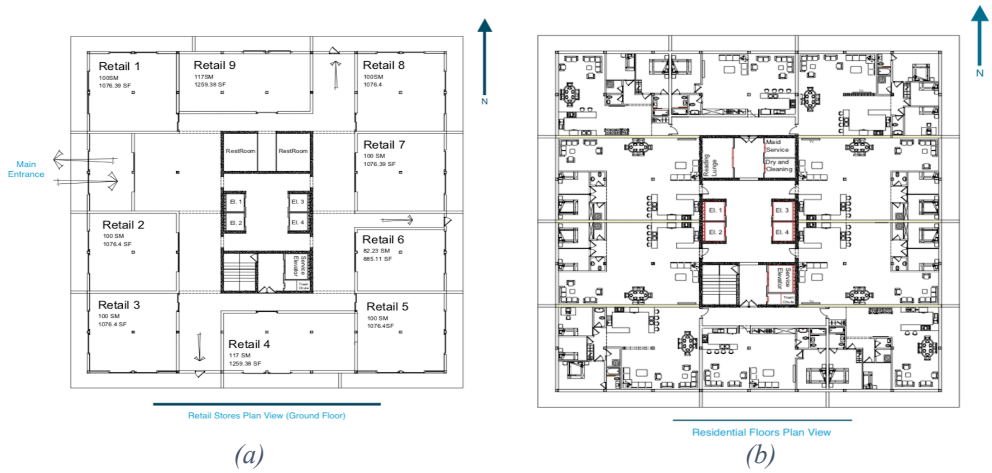

(a) *(b)*

Figure 2.19. Plan view of the (a) Ground floor (b) residential floors [1].

The footprint of the building is rectangular with exterior dimensions of 131ft. (40 m.) by 131ft. (40 m.) and a total area of approximately 17,227 sq. ft. The floor-to-floor height is 9.8 ft. (3 m.) with a mechanical penthouse located on the building roof.

The main entrance to the building is located on the ground floor (west side) and retail areas are located along the perimeter, with each having direct access to the outside (Ground floor plan view). Figure 2.20 reflects the plan view of the refuge areas and fitness centers. The remaining levels are typical and contain 206 condominium style apartment units (plan view of the residential floors), except floors 9, 17, and 25; these floors include building amenities and areas of refuge.

The 3-hr fire-resistance rated central reinforced concrete shear wall core includes: 4 elevators, one service elevator, and an exit stairway, to connect all levels; a 1-hr fire-resistance rated smoke barrier elevator lobby on each level; and trash chutes on each level connected to the basement for disposal. In addition to the active fire protection systems, including an automatic sprinkler/standpipe system, the structural elements were protected from fire through passive methods. The CLT bearing walls are all protected by

encapsulation through gypsum boards and glulam beams and glulam columns are all exposed and protected against fire by adding a sacrificial layer to the element. In addition to the columns and beams, a portion of CLT panels used in the decking system is left exposed as well.

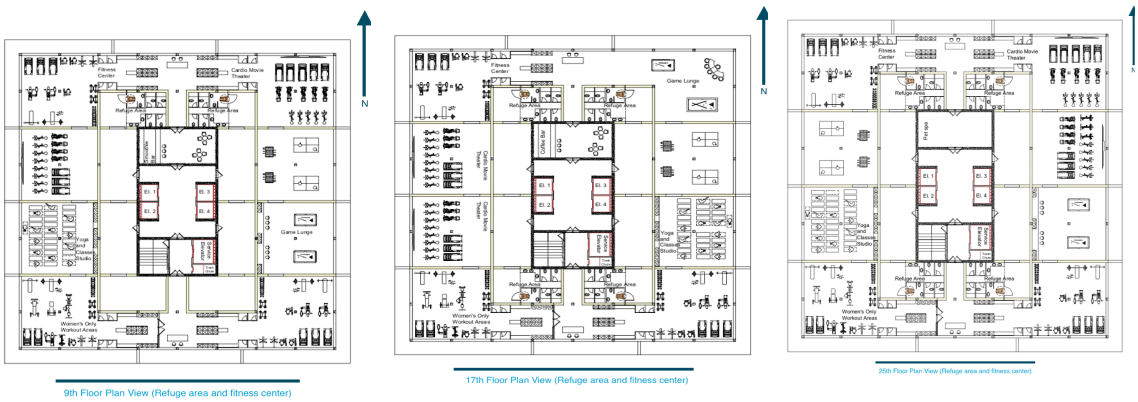

Figure 2.20. Plan view of refuge areas of: (a) 9th floor, (b) 17th floor, (c) 25th floor [1].

2.4. Test Assemblies

The structural system defined for the case study is a hybrid structure with a balloon framing system and consists of cast-in-place reinforced concrete shear walls and columns in the carparks and elevator shaft, glulam columns and beams, and CLT walls. All the structural elements are connected to each other through metal connections. The metal doweled connections such as T-shape steel and aluminum connections are one of the most common type of connections that have been used for this purpose.

For the purpose of this case-study, the doweled steel connections could be used in the following locations:

- Connecting girders to CLT and RC walls.
- Connection between secondary beams and girders.

- Connecting girders to columns.

These locations are very important for improving the structural integrity and performance of the structure at elevated temperatures. Post-fire observations of damaged structures confirmed that the connections have a remarkable effect on the survival time of the structure in fire.

Knowledge gained during this case study resulted in an experimental test matrix of seven intermediate size heavy timber assemblies. Table 2.2 provided a summary of experimental studies performed on these assemblies at ambient temperature (AT), post fire performance (PFP) and fire-performance (FP).

These assemblies were designed to investigate the fire-performance and post-fire performance of doweled connections, connecting glulam beam-to-girder, glulam-beam to CLT-walls, and finally CLT beam-to-girders. Chapter 3,4 and 5 provide detailed information on the experimental studies performed on the A3, A2 and A1. Appendix A provides more drawing details relevant to the case study. Additional information on the experiments addressed in the Appendix B. Also, test result related to the A4-7 provided in Appendix B. Finally, Appendix C offers more pictures taken form assemblies during the experiments.

Table 2.2. Experimental studies summary.

Connection Type	#	Assembly Description	Connection Exposure	Gap	Type of Test	Number of Tests	Test Duration
Steel Doweled Connection	**A1**	CLT beam-to-girders	Exposed	0.5"	AT	4	Failure
			Exposed	0.5"	PFP	1	30 min
			Exposed	0.5"	FP	1	Failure
	A2	GL-beam to CLT-walls	Concealed	No Gap	AT	3	Failure
			Concealed	No Gap	PFP30	1	30 min
					PFP60	1	60 min
			Concealed	No Gap	FP	2	Failure
	A3	GL beam-to-girders	Concealed	No Gap	AT	3	Failure
			Concealed	No Gap	PFP30	1	30 min
					PFP60	1	60 min
			Concealed	No Gap	FP	2	Failure
Aluminum Doweled Connection	**A4**	GL beam-to-girders	Exposed	0.5"	AT	3	Failure
			Exposed	0.5"	PFP30	1	30 min
					PFP60	1	60 min
			Exposed	0.5"	FP	2	Failure
	A5	GL beam-to-girders	Concealed	No Gap	AT	3	Failure
			Concealed	No Gap	PFP30	1	30 min
					PFP60	1	60 min
			Concealed	No Gap	FP	2	Failure
	A6	GL-beam to CLT-walls	Exposed	0.5"	AT	3	Failure
			Exposed	0.5"	PFP30	1	30 min
					PFP60	1	60 min
			Exposed	0.5"	FP	2	Failure
	A7	GL-beam to CLT-walls	Concealed	No Gap	AT	3	Failure
			Concealed	No Gap	PFP30	1	30 min
					PFP60	1	60 min
			Concealed	No Gap	FP	2	Failure

2.5. REFERENCES

[1] Bahrani B, Saunders C, Shabanian M, Braxtan NL, Rockwell SR, Zhou A., *High-rise residential building using cross-laminated timber: Charlotte 9th Street Tower-United States Case Study*, 12th International Conference on Performance-Based Codes and Fire Safety Design Methods, Honolulu, Hawaii, USA, April 23-27, 2018.

[2] Gerard, R., D. Barber, and A. Wolski, *Fire safety challenges of tall wood buildings*. 2013: National Fire Protection Research Foundation.

[3] IBC, I., *International building code.* International Code Council, Inc. (formerly BOCA, ICBO and SBCCI), 2006. **4051**: p. 60478-5795.

[4] Smith, I. and A. Frangi, *Use of timber in tall multi-storey buildings*. 2014: International Association for Bridge and Structural Engineering (IABSE).

[5] Smith, I. and M.A. Snow, *Timber: An ancient construction material with a bright future.* The Forestry Chronicle, 2008. **84**(4): p. 504-510.

[6] Boyce, M., *On the Zoroastrian temple cult of fire.* Journal of the American Oriental Society, 1975: p. 454-465.

[7] Hammond, N.G.L., *Sources for Alexander the Great: An Analysis of Plutarch's' Life'and Arrian's' Anabasis Alexandrou'*. 2007: Cambridge University Press.

[8] Hanson, N., *The Dreadful Judgement*. 2002: Random House.

[9] Christian, P.A., *Boston's Fire Trail: A Walk Through the City's Fire and Firefighting History*. 2007: The History Press.

[10] Brooke, D., *The advent of the steel rail, 1857-1914.* The Journal of Transport History, 1986. **7**(1): p. 18.

[11] Collins, P., *Concrete: the vision of a new architecture*. 2004: McGill-Queen's Press-MQUP.

[12] Moody, R.C. and R. Hernandez, *Glued-laminated timber.* Forest Product Laboratory. USDA Forest Service. Madison, Winconsin, 1997.

[13] Grasser, K.K., *Development of cross laminated timber in the United States of America.* 2015.

[14] Green, M.C. and J.E. Karsh, *The case for tall wood buildings: how mass timber offers a safe, economical, and environmentally friendly alternative for tall building structures*. 2012: MgbARCHITECTURE+ DESIGN.

[15] Buchanan, A.H. and A.K. Abu, *Structural design for fire safety*. 2017: John Wiley & Sons.

[16] Malo KA, Abrahamsen RB, Bjertnæs MA, *Some structural design issues of the 14-storey timber framed building "Treet" in Norway*. European Journal of Wood and Wood Products. 2016 May 1;74(3):407-24.

3. THERMO-MECHANICAL BEHAVIOR OF GLULAM BEAM-TO-GIRDER ASSEMBLIES WITH STEEL DOWELED CONNECTIONS BEFORE, DURING AND AFTER FIRE

Milad Shabanian [a], Nicole Leo Braxtan [a]

[a] University of North Carolina at Charlotte, Department of Civil and Environmental Engineering, 9201 University City Blvd, Charlotte, NC, 28223, United States

Highlights

- Load-carrying capacity and failure modes of a Glulam beam-to-girder assembly connected with T-shaped slotted-in steel doweled connections at ambient temperature illustrated.
- Residual load-carrying capacity and failure modes of the assembly after 30 and 60 minutes of partial exposure to a non-standard fire presented.
- Fire-resistance and failure of the loaded assembly exposed to a non-standard fire on one connection highlighted.

Graphical Abstract

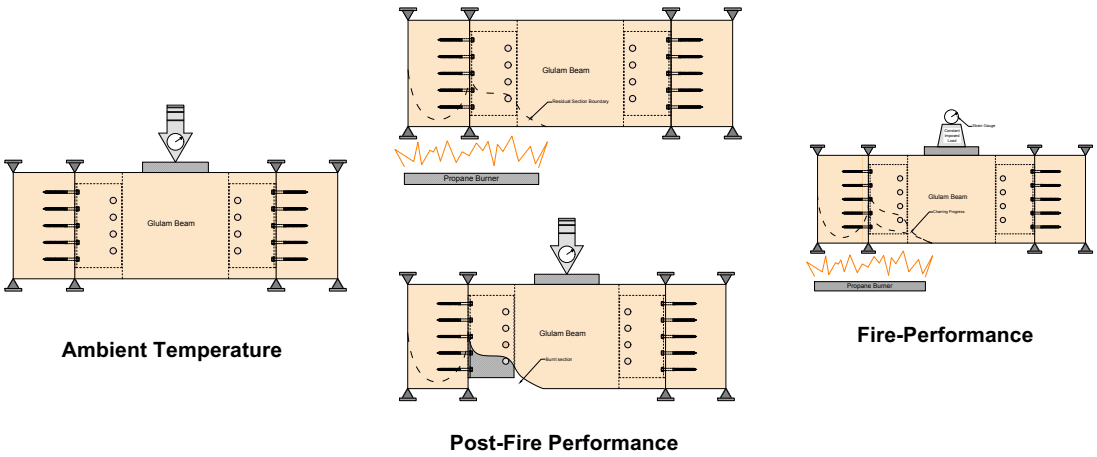

Abstract

In this research, the thermo-mechanical behavior of intermediate-size glued-laminated beam-to-girder assemblies connected with T-shaped slotted-in steel doweled connections is studied at ambient temperature, and then after and during non-standard fire exposure. The ambient temperature tests (AT) evaluated the average load-carrying capacity and failure modes of the assembly at room temperature. Embedment failure and plastic deformation of the dowels followed by the brittle splitting failure of the Glulam beam were found to be the dominant failure modes in the beam members tested at ambient temperature. In the Glulam girders, splitting failure was the major failure mode observed. The post-fire-performance tests (PFP) were conducted to study the impact of 30-min (PFP30) and 60-min (PFP60) partial exposure to a non-standard fire on residual strength of the assembly. The residual strength of the assembly was reduced by 23.7% after 30 minutes and 47.8% after 60 minutes of fire exposure. In both PFP tests, embedment failure and plastic bending of the dowels were the only observed failure modes. During the PFP60, the impact of fire-sealant was also considered for the fire-performance of the steel connections. Results showed that the fire-sealant improved the fire-performance of the connection for the first 30 minutes. The fire-performance test (FP) was conducted to investigate the fire-resistance (FR) of the loaded assemblies during non-standard fire exposure. For this purpose, one assembly was loaded to 67% of its ambient temperature load-carrying capacity while it was partially exposed to a non-standard fire. The fire-performance test continued for 65 minutes while the maximum rate of mid-span displacement occurred at 57 minutes into the fire. Ductile embedment failure of the timber in contact with the dowels was the only failure mode observed at elevated temperature.

Keywords: Beam-to-girder connection; Glued-laminated timber (Glulam); Steel doweled connection; Load-carrying capacity; Fire-resistance; Residual strength; Non-standard fire; Post-fire performance (PFP); Fire-performance (FP).

3.1. Introduction

Development of engineered wood products such as glued-laminated timber (Glulam), cross-laminated timber (CLT), and structural composite lumber (SCL) promote advancements in architectural appeal, constructability, and sustainability leading to what some may call the era of the "renaissance of timber structures". Accordingly, building officials have developed building codes and approved engineered wood products as a suitable material for construction of mid-rise and high-rise structures. However, there are still concerns regarding the fire safety of contemporary timber constructions. In order to properly address these issues, building codes prescribe restrictive design guidelines mostly focused on charring rate and residual cross section of the main structural timber elements such as beams, columns and connections [1-3]. In traditional heavy timber construction, carpentry connections and bearing connections were the most common type of connections with acceptable fire-performance. Over the years, these connections were replaced by a wide range of industrial metal connectors [4]. These connections are usually made from steel or aluminum as metal connections increase the ductility and improve seismic performance of the structure [5-11]. Despite the advantages offered, metal connections may lose strength in elevated temperatures, deform considerably, and potentially propagate a catastrophic incident [12-14]. Beam-to-girder connections are one of the most widely used

type of connections in timber structures. Thus, a need arises for the thorough study and understating of the behavior of these connections in timber structures before, during and after a fire incident.

Previous studies were mostly focused on fire-performance of connections between primary timber members loaded parallel to the grain [15-29]. Additionally, only a limited number of studies concentrated on the fire-performance of beam-to-girder and beam-to-column connections [30-35]. These fire tests were often performed in closed furnaces with limited access, followed standard fire curves that neglected the decay phase of real-fire scenarios and were prescribed for assemblies built based on the prescriptive building codes [36, 37]. Whereas many modern timber structures are constructed with varying percentages of exposed, combustible, wood material and follow performance-based design recommendations. The performance-based design includes determination of a range of design fires. Design fires are particularly important in contemporary heavy timber structures with exposed timber material. In these structures, one of the parameters effecting the charring rate and, as a result, the load carrying capacity is the received heat flux. To this end, a series of experiments was developed to investigate the performance of Glulam beam-to-girder assemblies connected with T-shaped, slotted-in doweled connections before, during and after non-standard fire. Details are provided on the experimental design, procedures followed, results, and conclusions ascertained.

3.2. Research Motivation

American institute of timber constructions (AITC) recommend avoiding the design of connections which create loading perpendicular to the grain of timber elements due to

the propensity of splitting failure in the members [38]. However, this type of connection is growing in popularity with manufacturers producing it both in Europe and the US. Recent testing was performed on Glulam beam-to-column assemblies connected with slotted-in doweled connections (hangers) loaded perpendicular to the grain of the Glulam beam at both ambient and fire conditions [31]. The tests studied the impact of several parameters such as gap size, number of dowels, and location of the dowels. The assemblies included a small gap between the beam and column – a feature often prescribed to avoid splitting failure. The tests also considered the full contact condition (with no gap) during fire exposure but did not include the full contact condition at ambient temperature. The fire performance tests of the assemblies included mechanical load equivalent to 30 percent of the ambient temperature load-carrying capacity of the assembly and thermal loading based on a standard fire curve. Testing confirmed the tendency of brittle failure at ambient temperature and embedment deformation during fire exposure.

There are a limited number of post-fire studies conducted on heavy timber structures. In one recent study, the post-fire performance of glued-laminated lumber and laminated veneer lumber (LVL) beams was addressed after the beam was exposed to a constant radiant heat flux [39]. Results of the testing showed that the degradation beyond the char layer for bending members is at least 11.7 mm for LVL and 12.3 mm for Glulam. In another study, retrofitting the fire damaged Glulam beams through sistering method investigated [40]. Base on the experimental studies conducted in this research, the residual load-carrying capacity of the retrofitted beams decreased to 49%-66% of the failure load of the control members. The current study further considers the critical function of connections in the post-fire performance of structures. Understanding of post-fire

performance of structures may aid in post-fire forensic investigation and retrofitting decisions. Recent code developments provide greater flexibility in the inclusion of exposed heavy timber construction [41]. These heavy timber elements may be costly to replace after a fire incident. However, retrofitting strategies may be employed if appropriate, such as sistering or cleaning and covering/replacing sacrificial layers. Additionally, post-fire performance of structures is critical in the life safety of fire fighters and other emergency responders.

Finally, experimental tests discussed in this chapter will be used to validate a coupled thermal-structural finite element model of a T-shaped dowel connection before, during, and after fire exposure in Chapter 6. The FE model may be expanded in the future to include a parametric study with results informing preliminary decisions about performance-based fire design recommendations.

3.3. Experimental Set-up and Material Properties

Experimental testing was performed on Glulam beam-to-girder assemblies to determine the ambient temperature strength of the connection, the residual strength of the connection after fire, and the strength of the connection during fire. In total, six tests were performed: three at ambient temperature, two post-fire, and one during fire.

3.3.1. Assembly Description

The symmetric, intermediate-size Glulam beam-to-girder assemblies were connected by two T-shaped steel doweled connections, dowels and screws. Figure 3.1 and Table 3.1 provide detailed information on the geometry of the assembly components. All

the Glulam beams used for this research were carefully cut with a table saw and milled with a CNC machine.

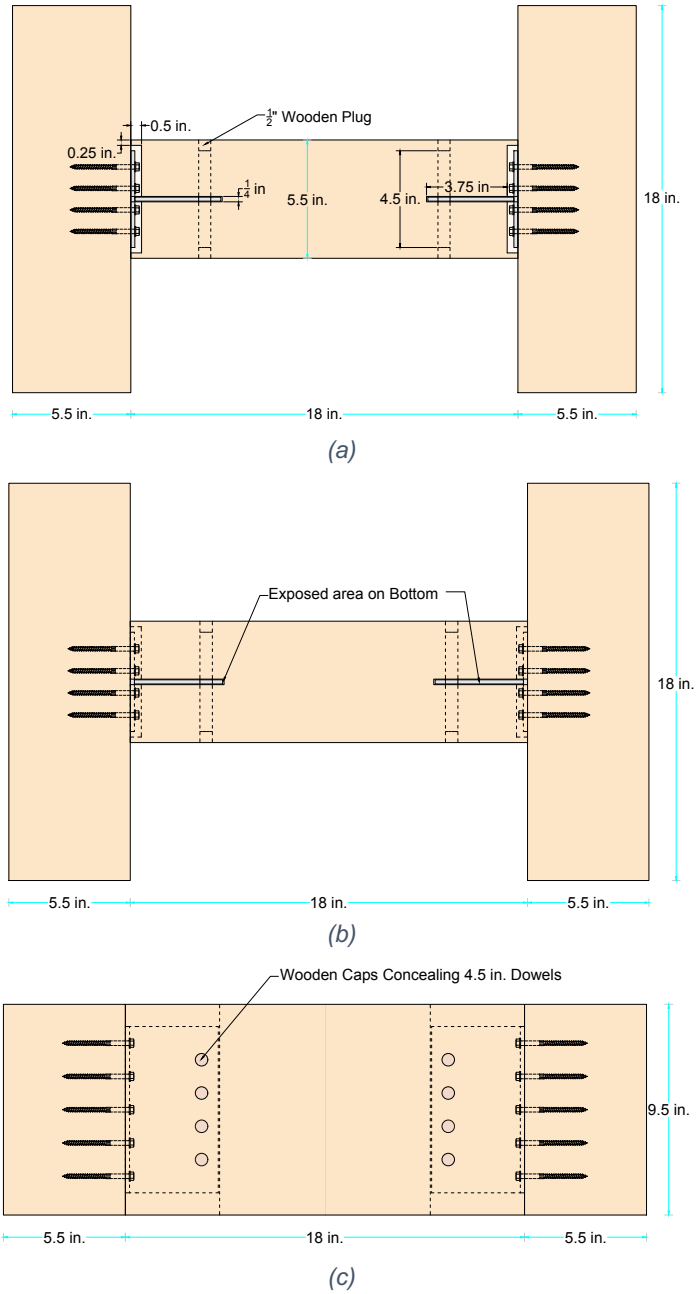

Figure 3.1. Beam-to-girder assembly: (a) top view, (b) bottom view, (c) front view.

Table 3.1. Components of the Glulam beam-to-girder assembly.

Parts	***Quantity***	***Material***	***Dimensions***
Headers (girders)	*2*	*Glued-laminated timber*	*9.5 in. x 5.5 in. x 18 in.*
Joist (beam)	*1*	*Glued-laminated timber*	*9.5 in. x 5.5 in. x 18 in.*
Hangers	*2*	*Steel Connection A572 Gr. 50*	*Plate A: 4.5 in. x 7.5 in. x 3/16 in.* *Plate B: 4 in. x 7.5 in. x 3/16 in.*
Dowels	*2×4*	*Steel A572 Gr. 50*	*1/2 in. diameter, 4.5 in. length*
Screws	*2×20*	*Low-carbon steel wire grade 1022*	*1/4 in. diameter, 3 in. length*

3.3.2. Material Properties

3.3.2.4. Glued-laminated Timber

In each assembly, the glued laminated (Glulam) beams consisted of thin wood laminations of spruce, pine, and fir species (90% black spruce) glued together in parallel using structural adhesives. The Glulam members had an average moisture content of 12% and density of 35 lb./ft^3. Table 3.2 provides the design capacities of the Glulam material.

Table 3.2. Mechanical properties of the glued-laminated timber (in psi).

Stress Grade	*Bending Moment (F_{bx})*	*Compression Perpendicular to Grain (Fcpx)*	*Longitudinal Shear (F_{vx})*	*Compression Parallel to Grain (F_{vx})*	*Tension Parallel to Grain (F_t)*	*Elastic Modulus (E_x)*	*Specific Gravity*
24F-1.9E	*2400*	*600*	*250*	*1150*	*1050*	*1.9E+06*	*0.41*

3.3.2.5. Steel Connections

Figure 3.2 shows the steel connection utilized for this research. The custom designed, T-shaped, slotted-in, welded, steel doweled connections were fabricated out of gauge 7 (3/16 in.) ASTM A572 Gr50 structural steel with 1/8-inch full-length fillet weld on both sides. The steel connection utilized in this research were identical to the steel connections used in Glulam-beam to CLT-wall assemblies (Chapter 4) and CLT beam-to-girder (Chapter 5).

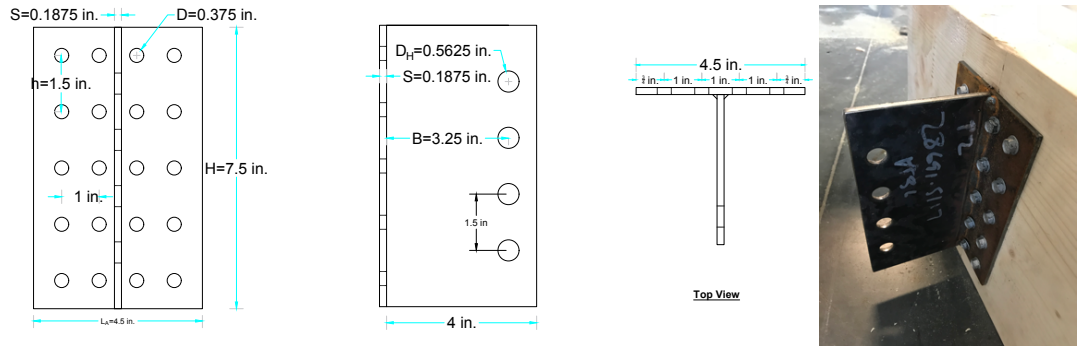

Figure 3.2. T-shaped welded steel connection.

3.3.2.6. Steel Dowels and Fasteners

Figure 3.3 shows the geometry of steel dowels and hexagonal fasteners. The 4.5-in. long dowels were cut from ½-in. structural steel rods (ASTM A572 Gr 50). During the fire tests, the tips of these dowels were covered by ½-in. length wooden plugs. The ¼-in. diameter heavy-duty hexagonal connector screws with 3-in. length and 2-in. thread were manufactured from low-carbon steel wire, grade 1022. This fastener has 164,000 psi bending strength, 1,430 lbf allowable tensile strength and 800 lbf allowable shear strength.

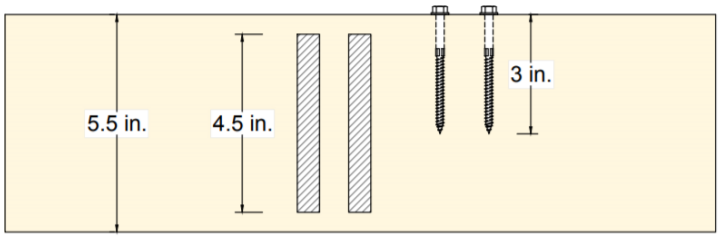

Figure 3.3. Steel dowels and hexagonal connector on Glulam-beam.

3.3.3. Ambient Temperature Test Set-up

The load-carrying capacity of the assembly and relative displacement at the mid-span of the beam were assessed through ambient temperature (AT) tests to establish the baseline condition. Ambient temperature tests were performed in a laboratory where

temperature was maintained at approximately 70 °F. Experimental set-up was developed based on the standard specification for testing and establishing allowable loads of joist hangers [42] which includes blocking for stabilization as shown in Figure 3.4. Each sample was fixed to the Universal Testing Machine (UTM) platform and then a vertical load was imposed at the mid-span of the Glulam-beam at a uniform crosshead rate of 0.05 in. per minute until failure.

Figure 3.4. Modified Glulam beam-to-girder assembly and ambient temperature test set-up.

3.3.4. Post-Fire Performance Test Set-up

The post-fire performance (PFP) tests evaluated the residual strength of the assembly after 30 minutes (PFP30) and 60 minutes (PFP60) of non-standard fire exposure. The PFP experiments included two separate steps: first, fire loading (and subsequent cooling) and second, mechanical loading. To approximate the real boundary conditions during the fire test, the top of the Glulam beam was covered by 1.5" thick mineral wool high temperature insulation boards with foil backing to replicate the 3-sided fire exposure condition. Additionally, the impact of fire-sealant on the fire-performance of the steel

connections was considered in the PFP60 wherein the exposed area of the steel connection on the bottom of the Glulam beam and at the groove location were covered with fire sealant.

Figure 3.5 shows the protected sample and burner installed in the custom-built load frame. A non-standard fire was produced by a 12" x 12" propane burner covered with stainless steel mesh. Temperature of the burner was manually controlled through adjustment of fuel flow through a gas regulator.

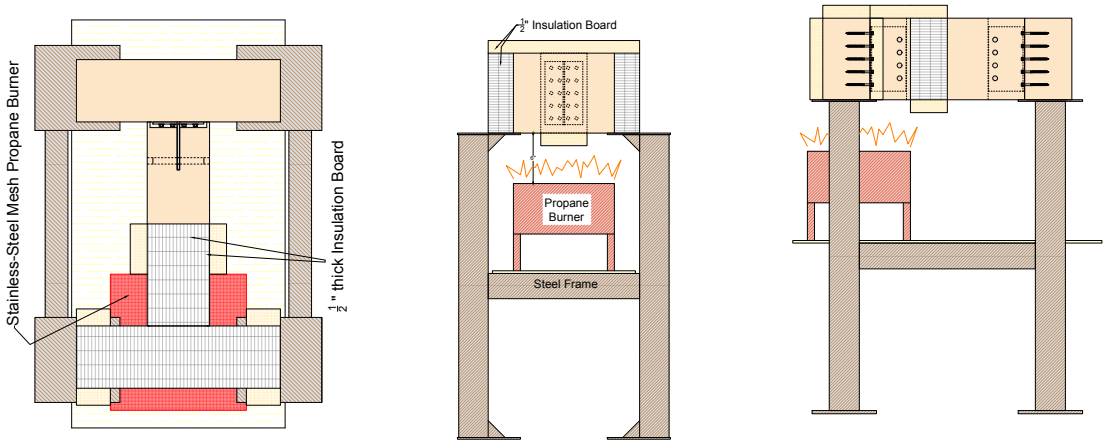

Figure 3.5. PFP fire test set-up, (a) top view, (b) front view, (c) side view.

Figure 3.6 shows the location of the thermocouples used on the test specimens during the fire test. Nine thermocouples captured the temperature distribution along the exposed area of the samples – including the beam, connection, and dowels – while two additional thermocouples measured the temperature at the burner surface. The fire tests were performed in a flashover simulation room at a local fire training facility. Once the fire tests were complete, the fire was extinguished with water and the char layer was carefully removed using a wire wheel brush. The PFP samples were then moved to a curing room in the laboratory to reach to their previous moisture content.

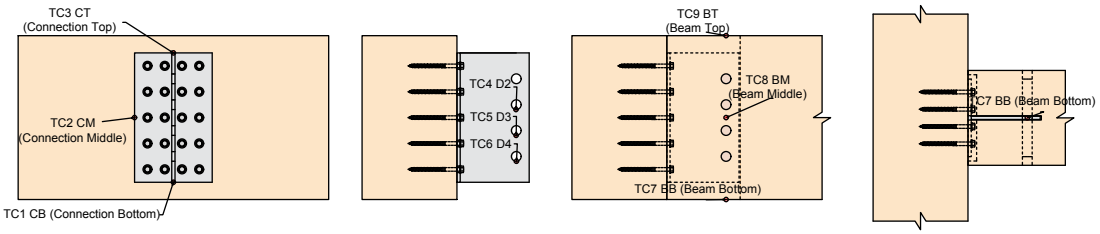

Figure 3.6. Thermocouples arrangement for PFP test.

The second step of the PFP test included mechanical loading of the residual assembly at ambient temperature. This step was, similar to the previous tests performed at ambient temperature, wherein the remaining part of the sample was fixed to the universal testing machine, blocking system installed and loaded downward in the mid-span of the beam until failure occurred. The imposed load and extension at the mid-span were recorded during this step. The boundary condition and blocking system of the samples in this step were similar to the ambient temperature tests.

3.3.5. Fire-Performance Test Set-up

One fire-performance test was conducted on the assembly. In this experiment, the prepared sample was been partially exposed to the non-standard fire while mechanical load was applied at the mid-span of the Glulam beam. This assembly was also protected by insulation boards to simulate typical three-sided fire exposure.

Figure 3.7 shows the FP test set-up, consisting of the partially insulated sample, steel frame, loading system, and propane burner. The assembly was fixed to the steel test frame by custom mechanical clamps. The loading system consisted of two hangers connected to a loading deck by threaded rods positioned at the mid-span of the Glulam beam. A mechanical jack was used to imposed constant load equal to 67% of the ambient

temperature load-carrying capacity of the assembly. The mid-span deflection of the beam was measured by a digital indicator during the fire test.

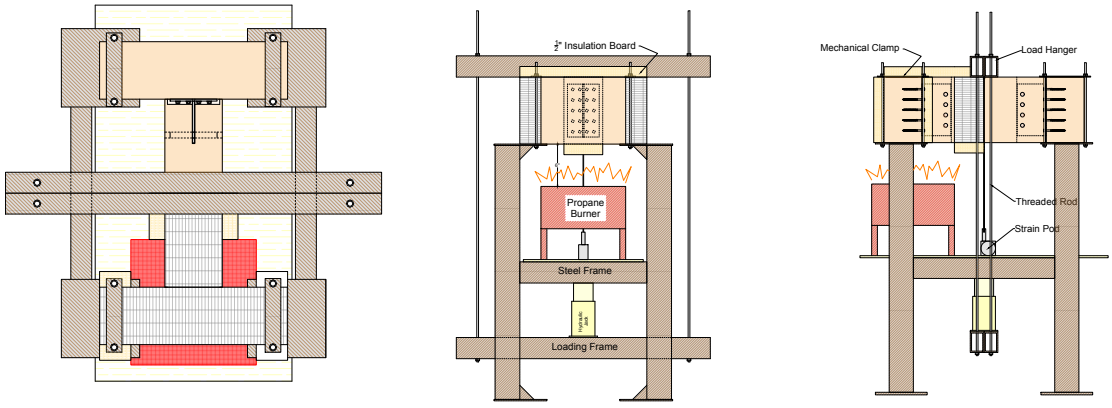

(a) (b) (c)

Figure 3.7. Fire-performance test set-up, (a) top view, (b) front view, (c) side view.

Similar to the PFP tests, 11 k-type thermocouples recorded the heat distribution along the exposed area of the assembly, noted as TC1 through TC11 in the text. Figure 3.8 shows the thermocouple arrangement for the FP test. The FP test was recorded by a video camera aimed at the front view of the test setup to capture the different failure modes and deformation of the assembly during the fire-performance test. The fire-performance test was conducted for 65 minutes and then stopped after considerable deformation was observed.

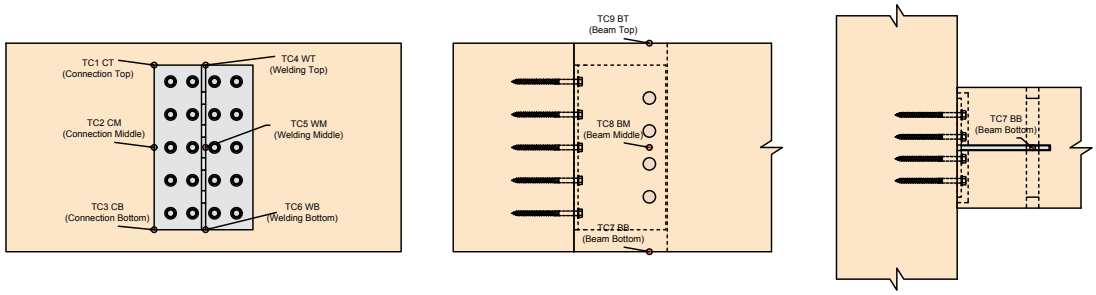

Figure 3.8. Fire-performance test thermocouples arrangement.

3.4. Test Results and Discussion

Results are presented for the ambient temperature tests, the post-fire performance tests, and the fire-performance tests to illustrate the changing behavior of the assembly under different thermal and mechanical loading conditions.

3.4.1. Ambient Temperature Results

Figure 4.10 shows the load-displacement behavior of the Glulam beam-to-girder assemblies tested at ambient temperature. Based on the experiments performed, the average load-carrying capacity of the assembly is 36.7 (kips) and its average elastic stiffness equals to 61.7 (k/in.) at ambient temperature.

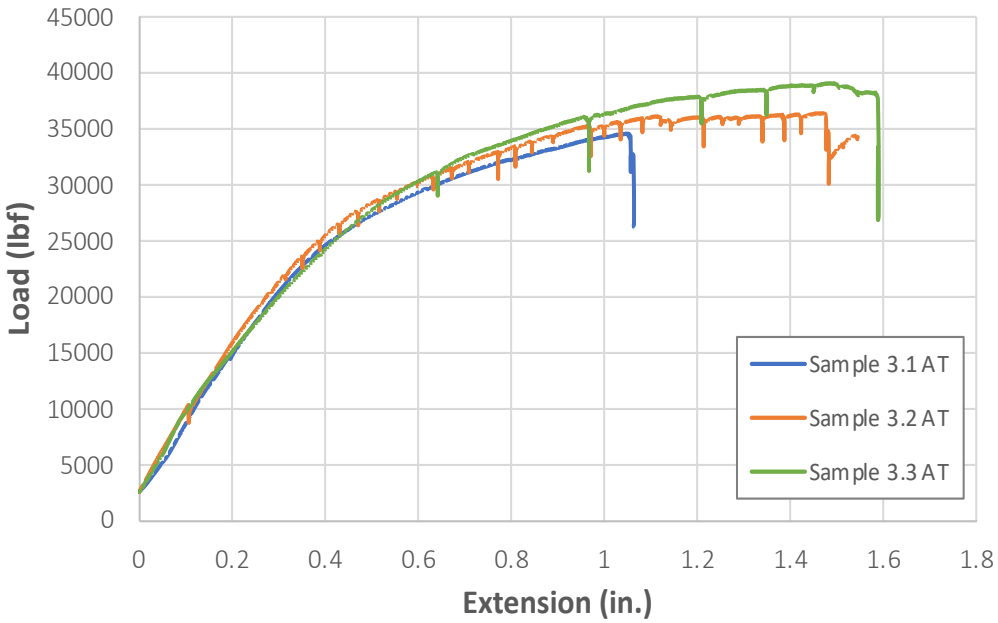

Figure 3.9. Load-displacement of the Glulam beam-to-girder assembly at ambient temperature (AT).

Figure 3.10 shows the sequence of failure modes that occurred during ambient temperature tests. In all samples, failure initiated with plastic embedment failure in the

Glulam beam, continued with plastic bending of steel dowels and then ultimately, brittle splitting failure in beam close to the top dowels and girders. The early, brittle splitting failure of the beam was triggered mostly by contact and friction between the beam and girders. Small drops in the load-displacement curves are related to the splitting failures occurring on the edge of the beam member while the large final drops are related to the girder failure. The ambient temperature tests were stopped once the Glulam girders failed.

(a) (b) (c)

Figure 3.10. Ambient temperature failure modes (a) ductile embedment failure of the Glulam beam around the dowels and bending of the dowels, (b) splitting Failure in the beam and (c) splitting failure of the girder.

3.4.2. Post-Fire Performance Test Results

The PFP tests results include the temperature distribution recorded along the exposed area during fire and the residual load-displacement behavior of the assembly during mechanical loading post-fire. Figure 3.11 and Figure 3.13 display the test results related to the assembly exposed to the non-standard fire for 30 minutes (PFP30) and 60 minutes (PFP60), respectively. After the initial heating phase, the average burner temperature was approximately 920 ˚F in the PFP30 tests, and 1100 ˚F in the PFP60 tests. Figure 3.11 and 3.13 also show the ASTM E119 standard fire curve which, in comparison, reaches 1550°F at 30 minutes and 1700°F at 60 minutes. As expected with fire applied to the bottom of the assembly, in both fire experiments, TC1 recorded the highest temperature

within the steel connection (at the bottom of the connection) and TC7 recorded the highest temperature over the height of the beam (at the beam bottom). Also, the lowest dowel experienced the highest temperature during the PFP30 test. Unfortunately, the TC 3 and TC6 were disconnected during the PFP60 test, but it is assumed that this dowel also had the highest temperature of the dowels. At the completion of the test, there is a temperature range of nearly 400 °F over the height of the connection.

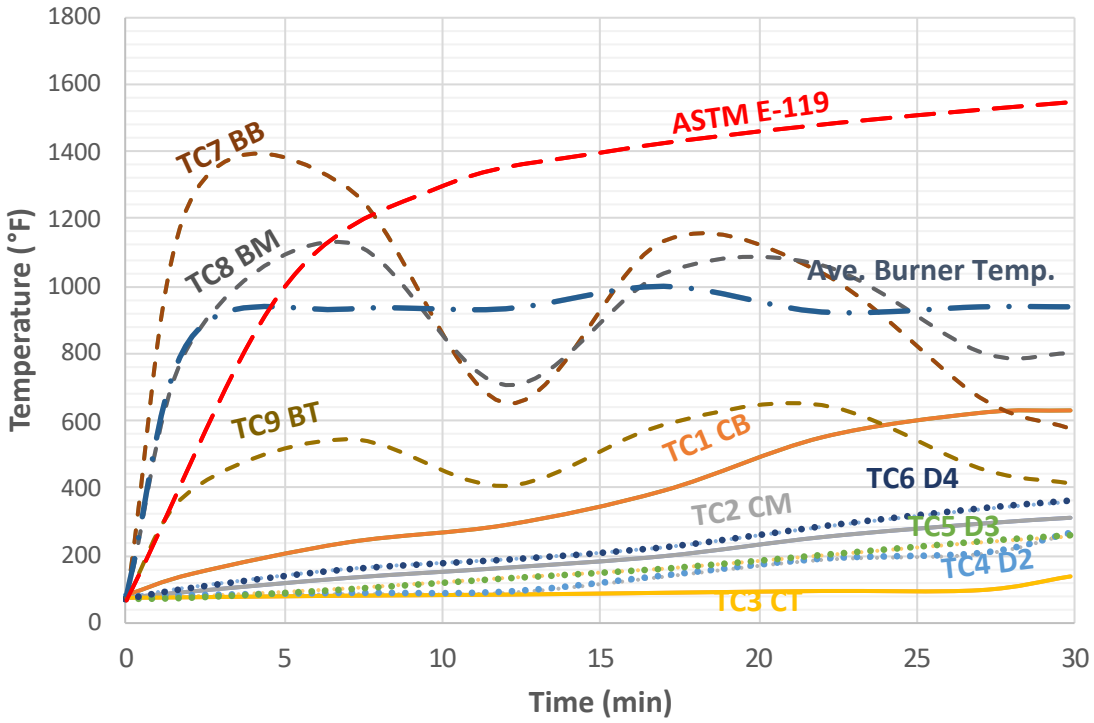

Figure 3.11. PFP30 heat distribution of Glulam beam-to-girder.

During the fire tests, the Glulam beams ignited when their temperature reached the wood ignition temperature of 570 °F. This occurred at approximately 2-3 minutes into the PFP30 test when TC7 and TC8 at the bottom and middle of the beam began to exceed the burner temperature. This is visually confirmed in the captured picture at two minutes shown below (Figure 3.12).

Figure 3.12.PFP30 beam ignition captured from side view of the Glulam beam-to-girder assembly.

At approximately 10 minutes into the PFP30 test, the beam top and beam bottom temperatures converge and then remain very similar for the duration of the test, while the temperature at the beam top lags behind. The beam top did not ignite, and temperatures remained less than the 570 ˚F ignition threshold. Additionally, the top of the beam is not exposed to direct flame from the burner. During the fire exposure, the beam bottom temperature (TC7) decreased almost 800 ˚F while the burner temperature kept constantly around 920 ˚F. At end of the prescribed fire loading, there was a 320 °F gap between prescribed fire curve and average temperature of the beam.

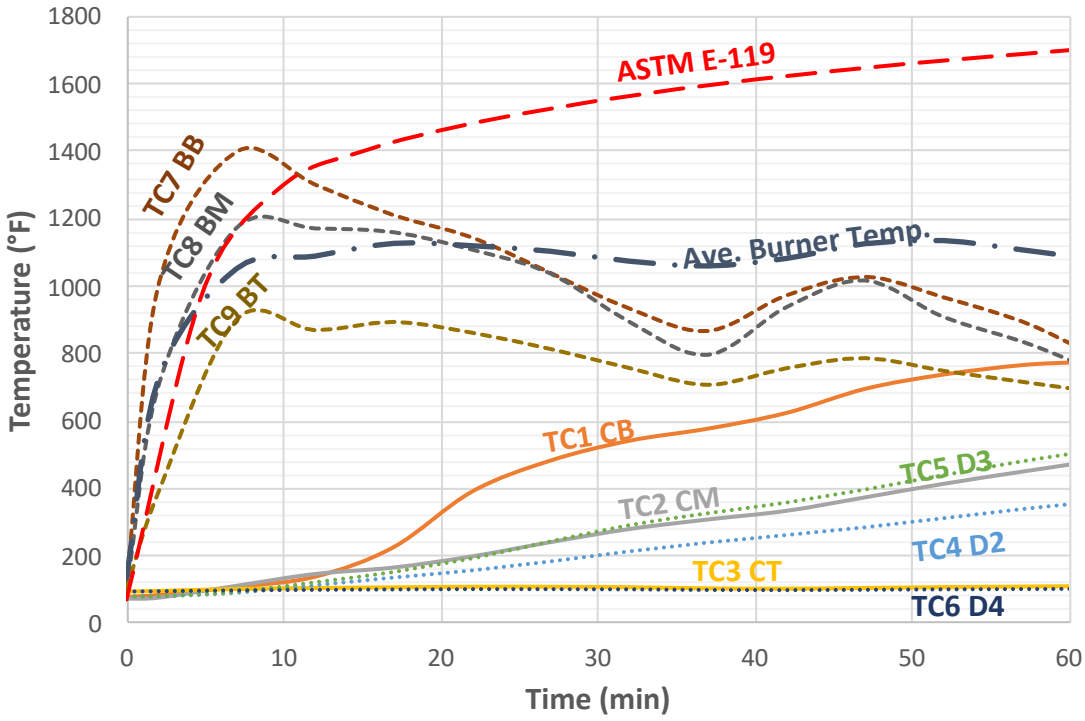

Figure 3.13. PFP60 heat distribution of Glulam beam-to-girder.

The PFP60 test results for the beam temperatures showed similar patterns, with ignition occurring in the beam bottom and middle at approximately 2-3 minutes into the fire test. The temperatures at the beam top were slightly higher in the PFP60 tests than the PFP 30 tests, as expected since the burner temperature in PFP60 was slightly higher than during the PFP30 test. At the completion of the tests, the temperature range over the height of the beam was less than the range in the PFP30 tests, this is a consequence of ignitions over a greater portion of the beam causing more uniform temperatures.

When comparing the connection temperatures between the PFP30 test and the PFP60 tests, the effect of the fire sealant is clear. The maximum temperature in the PFP30 connection was 647 ˚F at 30 minutes into the test with a burner temperature of 900 ˚F. At 30 minutes into the PFP60 test, the connection temperature was 525 ˚F while the burner

temperature was nearly 1100 °F. The sealant, as expected, insulates the connection, and slows the conduction of heat into the connection.

The tips of dowels were covered with wooden plugs during the fire tests and thereby insulated from direct heat input. The temperature in steel connection was not affected by any additional heat transferred through the dowels and the heat distribution along the height of the connection remains linear. In

Previous studies conducted on post-fire performance of structural steel materials indicate reductions in residual strength of steel initiate at 1112 °F [43, 44]. Maximum temperatures in the connection only reach 631 °F in the PFP30 and 776 °F on the PFP60 test. Therefore, the residual (post-fire) mechanical properties of the connections are assumed unaffected after both 30 and 60 minutes of exposure to the prescribed fire studied in this research.

Figure 3.14 compares the load-displacement behavior of post-fire performance tests and the ambient temperature tests. Recall the average ambient temperature capacity was 36.7 kips. Residual capacity of the PFP30 test was reduced to 28.0 kips (76.3% of ambient) and the residual capacity of the PFP60 test was reduced to 19.2 kips (52.3% of ambient). Since the steel connection is assumed to maintain the ambient temperature strength after both PFP exposures, the reduction in load-carrying capacity is attributed to the loss in gross cross-section and strength of the wooden elements. Timber losses strength significantly between 212 °F and 572 °F [2] in the thermal penetration zone, which extends behind the char layer.

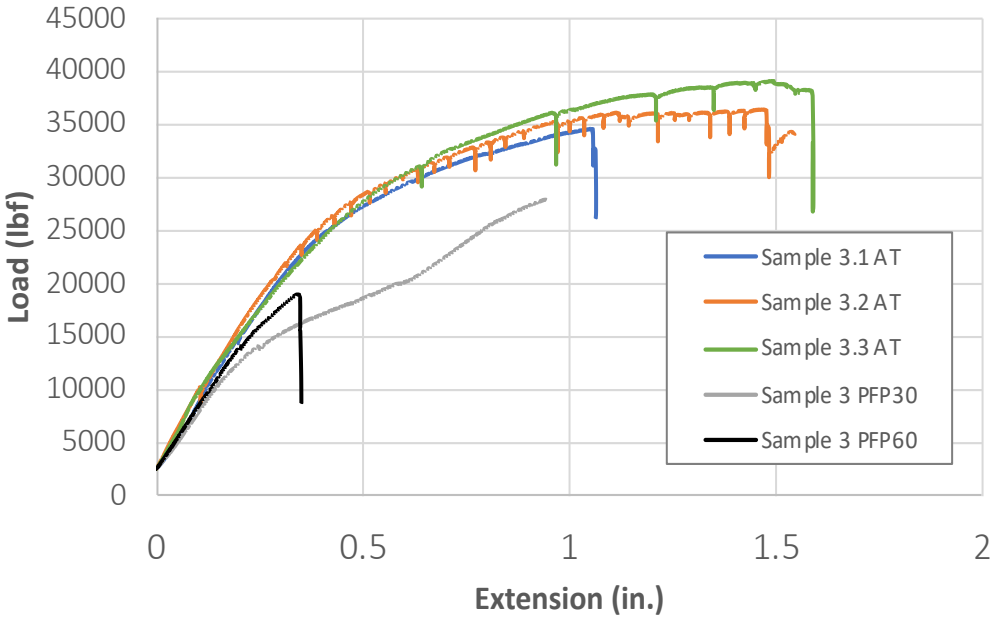

Figure 3.14.Residual strength of assembly after 30 minutes (R30) and 60 minutes non-standard fire exposure.

Figure 3.16 shows the residual assemblies during loading for the PFP30 and PFP60 tests. In both the PFP30 and PFP 60 tests, embedment failure and plastic bending of the dowels were the dominant failure modes, accompanied by premature splitting failure of the beam on the unexposed side of the assembly.

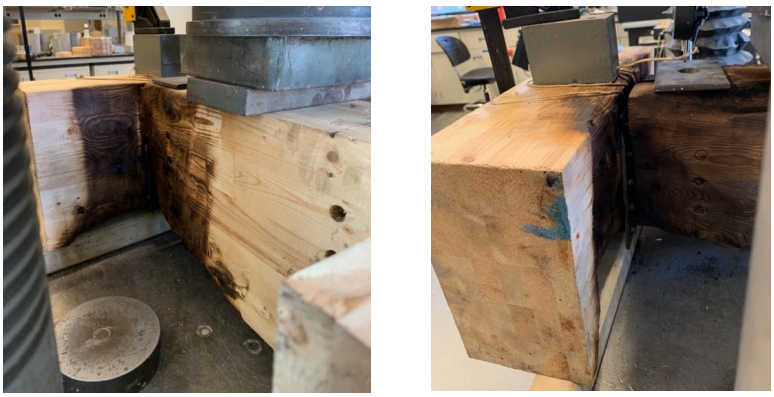

(a) (b)

Figure 3.15. Loaded assemblies exposed to non-standard fire for(a) 30 minutes and (b) 60 minutes.

There was no gap between the beam and girder on the unexposed side of the beam, while a gap formed during fire exposure and due to the charring of the beam section on the exposed side. This newly formed gap then reduced the tendency for splitting failure at the beam on the exposed side. Additionally, the PFP60 sample experienced greater char and thus greater loss in cross section than the PFP30 sample. The PFP60 sample offered less resistance to the loads transferred through the dowels into the beam, causing earlier embedment failure in the beam. Figure 3.16 shows the formed gap and failure on the unexposed side of the assembly after loading step.

(a) (b)

Figure 3.16. Loaded assemblies exposed to non-standard fire for 30 minutes (a) exposed side and (b) nonexposed side.

3.4.3. Fire-Performance Test Results

The fire-resistance (FR) of a Glulam beam-to-girder assembly was studied by applying 66% of the expected failure load (24.6 kips) at the mid-span, holding the load constant, and then applying a nonstandard fire load. The FP test was performed for 65 minutes, until failure occurred. Comparisons are made to the ambient temperature tests, as well as the PFP60 test which had a similar duration of burning and magnitude of prescribed

burner. The first 30 minutes of the FP test is also compared to the PFP30 test, as neither the FP nor PFP30 test assemblies included the fire sealant.

Figure 3.17 displays the temperature distribution along the exposed area of the assembly along with the fire temperature prescribed by the burner – approximately 1100 °F steady state after approximately 8 minutes of initial transient heating.

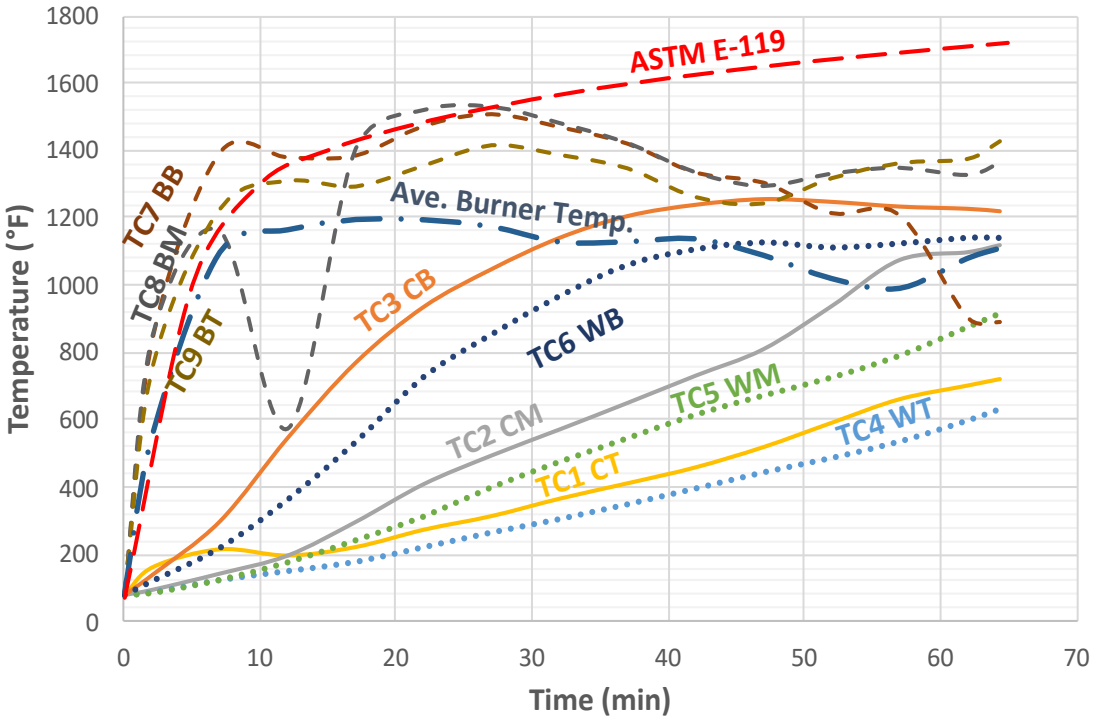

Figure 3.17.Temperature distribution along the exposed area of the assembly during FP test.

Ignition of the beam at the bottom, middle, and top occurred at approximately 2-3 minutes into the fire – similar timing to the PFP60 tests, however the entire beam ignited in the FP test, whereas only the bottom and middle ignited during the PFP60 test. Figure 3.18 shows the to the screen captures from the recorded video of the fire-performance test, confirming that at two minutes into the fire, ignition over the entire height of the beam has occurred. The entire beam remains ignited for the duration of the fire loading.

Beam temperatures reached approximately 1350 ˚F in 10 minutes and remained fairly steady throughout the duration of the fire. The sudden drop of the temperature in the middle of the beam (TC8) was related to malfunctioning of the thermocouple, which was fixed quickly during the test at approximately 12 minutes.

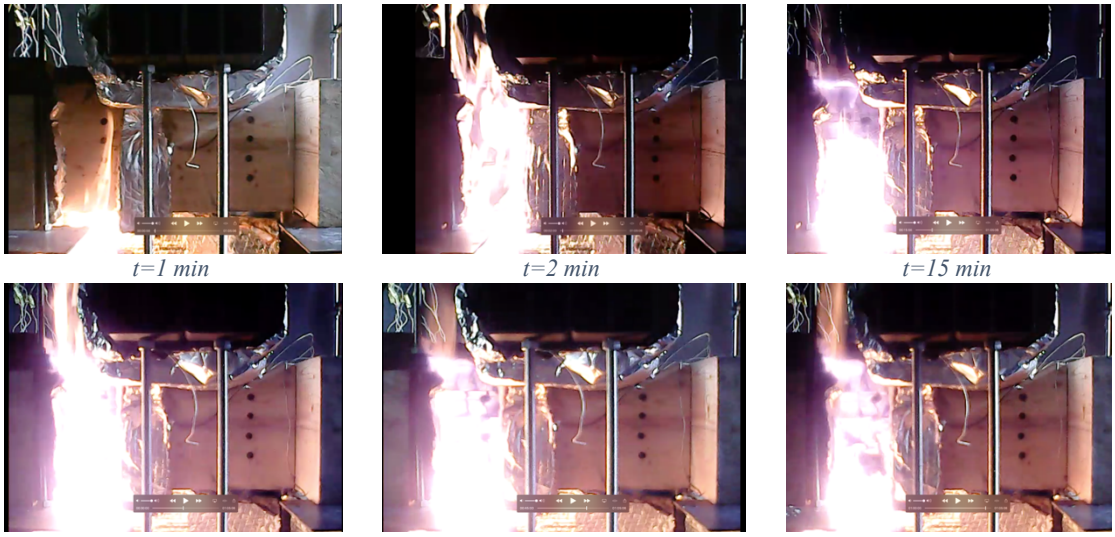

Figure 3.18.Screen shots of FP tests and ignition initiation at t=2 min.

Figure 3.17 also shows the maximum recorded temperature in the steel connection (located in the bottom edge) at 30 minutes was 1110 ˚F, which is nearly the same as the burner temperature of approximately 1130 ˚F. While 30 minutes into the PFP30 tests, the maximum connection temperature was 647 ˚F – approximately 72% of the burner temperature of 900 ˚F. Neither the PFP30 nor the FP tests had fire sealant, yet the FP tests experienced a greater connection temperature in comparison to the applied thermal load of the burner. The increase in temperatures in the connection may be attributed to the initially deformed condition of the assembly due to the applied mechanical load. The PFP tests considered uncoupled fire and mechanical load; the FP test considered these simultaneously wherein the heat flow may have been impacted by potential opening of the

connection due to mechanical load, allowing a path of heat transfer more directly to the connection components. Additionally, the imposed load increased the contact surface between burning beam surfaces and steel connection and this issue promoted more heat transfer.

The maximum connection temperature in the FP test at 60 minutes was close to 1240 °F – while the burner temperature was 1090 °F. Recall that at 60 minutes in to the PFP60 test, the maximum connection temperature was 790 °F, approximately 73% of the burner temperature of 1080 °F. At 60 minutes into both fires with similar burner temperatures, the PFP60 tests experienced connection temperatures nearly 36% lower due to the application of fire sealant to openings/exposed areas of the connection.

Temperatures in the lower portion of the connection reach 750 °F at 15 minutes into the test, while the middle of the connection reaches 750 °F at approximately 40 minutes. At 750 °F, degradation in the yield strength of the steel begins to occur – onset of elastic modulus degradation occurs at only 200 °F. At the maximum temperature of 1240 °F, the yield strength and elastic modulus are expected to be reduced to only 31% and 20%, respectively, of the ambient temperature mechanical properties.

Figure 3.19 shows the midspan displacement of the Glulam beam-to-girder assembly. Note that the displacement gauge was zeroed after the mechanical load was imposed on the assembly and data acquisition commenced after the burner was ignited. Little displacement occurred for most of the test, with displacement then more rapidly increasing at 52 minutes into the fire, with a maximum displacement rate of 0.085 (in/min) occurring at the 57th minute of fire-performance test.

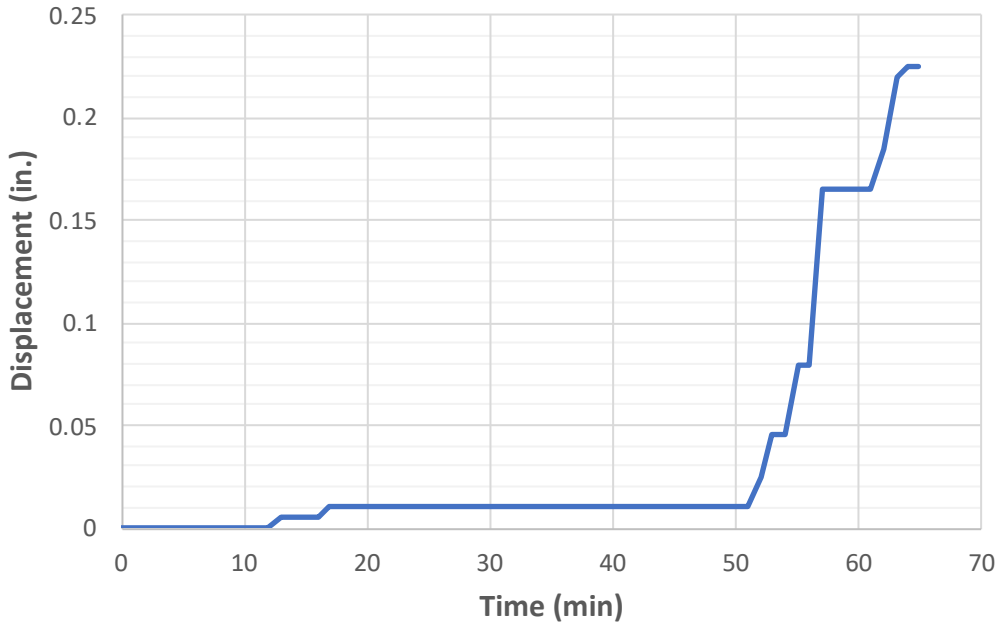

Figure 3.19. Fire-performance time-displacement at the mid-span of the Glulam beam-to-girder assembly.

Figure 3.20 shows the residual section of the assembly after the FP test, and after the char layer was carefully removed. The post-fire investigation of the residual section showed significant charring of the girder, which impacted the anchorage of fasteners. Additional section loss in the connection region showed complete char through the Glulam laminations to the face of the connection, as well as charring to approximately mid-height of the connection, altering the heat distribution on the lower portion of the connection and on the two lower dowels. The maximum charring depth in the beam was 5.5-inch.

Figure 3.20. Residual Section of the Glulam Beam-to-Girder Assembly After the Fire-Performance Test

Finally, Figure 3.21 shows the evidence of embedment failure of the Glulam-beam observed during post-fire investigation. No other failure modes were apparent. This is a critical observation as timber members loaded perpendicular to the grain often experience early, brittle splitting failure. However, in the fire-performance tests, this splitting failure did not occur at all, even with the full-contact (no gap) condition between the connecting members. It is assumed that as significant charring of the girder near the beam connection, the loss of material reduced the contact between the beam and the girder and reduced the tendency for splitting in the Glulam members.

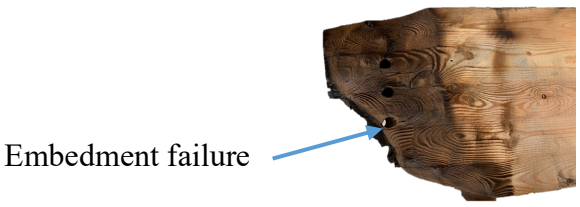

Figure 3.21. Embedment failure of the Glulam-beam occurred during fire-performance test.

3.4.4. Conclusion

Previously, timber assemblies with the timber elements loaded perpendicular to the grain were discouraged due to the propensity for early, brittle failure, particularly in connections with full contact (no gap) between the connecting elements. This research focused on the thermo-mechanical performance of T-shaped, steel doweled connections with no gap, used in Glulam beam-to-girder assemblies at ambient temperatures, after fire exposure, and during combined fire and mechanical loading. Results showed using dowels with adequate ductility was critical in improving the performance of connections with delayed, or in some cases without, splitting failure in the timber elements.

Ductile embedment failure, plastic bending of dowels and splitting failure were the major failure modes of the Glulam beam-to-girder assemblies studied at ambient temperature. The full contact (no gap) condition between the connecting members ultimately contributed to the splitting failure in the Glulam members. However, the ductile steel dowels allowed for large deformations in the assembly prior to the splitting failure, reducing the brittleness of the connection.

Post-fire tests were performed to consider the residual strength of the connection after fire load and subsequent cooling. The maximum temperatures recorded in the steel connection during 30 and 60 minutes of nonstandard fire loading were not high enough to cause permanent degradation of residual material properties of the steel. The elimination of the gap between connecting members in the connection improved the thermal performance by limiting direct exposure to the steel connection. The addition of fire sealant in the 60-minute post fire test, as expected, also improved the thermal performance through

insulation of the connection. This improvement was limited, however, by the evolving exposure surface created through the charring process. The residual load carrying capacity of the connection was substantially reduced compared to the ambient temperature tests due to the loss of gross section caused by charring and loss of strength in the thermal penetration zone behind the charring. Embedment failure and plastic bending of the dowels were the main failure modes in the post-fire performance test. Splitting failure on the fire exposed side of the connection was delayed/prevented as charring near the connection reduced contact between the beam and girder.

During the fire-performance test, mechanical load, equivalent to 67% of the average ambient temperature load-carrying capacity, was applied to the connection and held constant while fire was applied. The test continued for 65 minutes, until failure occurred. Ductile embedment failure of the beam was the only failure mode observed in the fire-performance test. Temperatures were higher in the FP tests than similar PFP tests due to coupled thermal-mechanical effects such as connection opening under mechanical load increasing the direct exposure of heat to the connection. Temperatures in the connection during the FP test were high enough to cause significant degradation in elastic modulus and yield strength of the steel connection plate and the dowels, however as the timber elements failed earlier than steel connection, steel connection never experienced high stress. The key parameters in reducing the strength of the assembly were charring, reduction in gross cross section of assembly and change in boundary condition. However, existence of the steel connection promotes the charring process and facilitates the failure of the wooden beam at the connection area. This is more noticeable where dowels were in

contact with the glulam beam. The embedment failure occurred mostly due to the charring of the glulam beam in contact with the dowels.

3.5. REFERENCES

[1] AWC, *Calculating the fire resistance of exposed wood members.* Technical Report 10 (TR10). American Wood Council, May 2020.

[2] *Eurocode 5. Design of timber structures—part 1-2: general—structural fire design*. 2004, European Committee for Standardization Brussels.

[3] NZS, N.Z.T.S.S., *3603: 1993.* Standards Council. Wellington.

[4] Perkins, N.S., P. Landsem, and G.W. Trayer, *Modern connectors for timber construction*. Vol. 1. 1933: US Government Printing Office.

[5] Gavric, I., M. Fragiacomo, and A. Ceccotti, *Cyclic behaviour of typical metal connectors for cross-laminated (CLT) structures.* Materials and structures, 2015. **48**(6): p. 1841-1857.

[6] Jorissen, A. and M. Fragiacomo, *General notes on ductility in timber structures.* Engineering structures, 2011. **33**(11): p. 2987-2997.

[7] Perkins, N.S., P. Landsem, and G.W. Trayer, *Modern connectors for timber construction*. Vol. 1. 1933: US Government Printing Office.

[8] Dorn, M., K. de Borst, and J. Eberhardsteiner, *Experiments on dowel-type timber connections.* Engineering structures, 2013. **47**: p. 67-80.

[9] Moss, P.J., A.H. Buchanan, and K.L. Wong. *Moment-resisting connections in glulam beams*. in *Proceedings of 6th world conference on timber engineering, Vancouver, Canada*. 2000.

[10] Buchanan, A., P. Moss, and N. Wong. *Ductile moment-resisting connections in glulam beams*. in *Proceedings of NZSEE conference, Wairakei Resort, Taupo, New Zealand*. 2001.

[11] Fragiacomo, M., B. Dujic, and I. Sustersic, *Elastic and ductile design of multi-storey crosslam massive wooden buildings under seismic actions.* Engineering structures, 2011. **33**(11): p. 3043-3053.

[12] Peng, L., et al., *Fire resistance performance of unprotected wood–wood–wood and wood–steel–wood connections: A literature review and new data correlations.* Fire Safety Journal, 2010. **45**(6-8): p. 392-399.

[13] Maraveas, C., K. Miamis, and C.E. Matthaiou, *Performance of timber connections exposed to fire: a review.* Fire Technology, 2015. **51**(6): p. 1401-1432.

[14] Carling, O., *Fire Resistance of Joint Details in Loadbearing Timber Construction: A Literature Survey*. 1990: Building Research Association of New Zealand.

[15] Norén, J., *Load-bearing Capacity of Nailed Joints Exposed to Fire.* Fire and materials, 1996. **20**(3): p. 133-143.

[16] Kruppa, J., T. Lamadon, and P. Rachet, *Fire resistance test of timber connections.* CTICM Ref. INC-00/187-JK/NB, 2000.

[17] Lau, P., *Fire resistance of connections in laminated veneer lumber.* Fire Engineering Research Report, 2006. **6**(3): p. 2006.

[18] Harris, S., *Fire resistance of epoxy-grouted steel rod connections in laminated veneer lumber (LVL)*. 2004, University of Canterbury.

[19] Austruy, C., et al., *Fire resistance of timber connections.* Ecole Normale Superieure de Cachan, Cachan, France, 2007.

[20] Chuo, T.C.B., *Fire performance of connections in laminated veneer lumber.* 2007.

[21] Moss, P., et al., *On the design of timber bolted connections subjected to fire.* 2008.

[22] Moss, P.J., et al., *Fire performance of bolted connections in laminated veneer lumber.* 2009.

[23] Erchinger, C., A. Frangi, and M. Fontana, *Fire design of steel-to-timber dowelled connections.* Engineering Structures, 2010. **32**(2): p. 580-589.

[24] Frangi, A., C. Erchinger, and M. Fontana, *Experimental fire analysis of steel-to-timber connections using dowels and nails.* Fire and Materials, 2010. **34**(1): p. 1-19.

[25] Racher, P., et al., *Thermo-mechanical analysis of the fire performance of dowelled timber connection.* Engineering Structures, 2010. **32**(4): p. 1148-1157.

[26] Peng, L., et al., On the Fire Performance of Double-shear Timber Connections. Fire Safety Science, 2011. 10: p. 1207-1218.

[27] Audebert, M., et al., Behavior of dowelled and bolted steel-to-timber connections exposed to fire. Engineering Structures, 2012. 39: p. 116-125.

[28] Khelifa, M., et al., Analysis of the behavior of multiple dowel timber connections in fire. Fire Safety Journal, 2014. 68: p. 119-128.

[29] Peng, L., et al., *Predicting the fire resistance of wood–steel–wood timber connections.* Fire technology, 2011. **47**(4): p. 1101-1119.

[30] Oksanen, T., et al., *Ruostumattomasta teräksestä valmistettujen puurakenteiden liitosten palonkestävyys.* 2005.

[31] Palma, P., *Fire behaviour of timber connections*. 2016, ETH Zurich.

[32] Palma, P., et al. *Fire resistance tests on steel-to-timber dowelled connections reinforced with self drilling screws*. in *2nd CILASCI–Ibero-Latin-American*

Congresso n Fire Safety Engineering. 2013. Eidgenösische Technische Hochschule Zürich.

[33] Palma, P., et al., *Fire resistance tests on beam-to-column shear connections.* 2014.

[34] Palma, P. and A. Frangi, *Modelling the fire resistance of steel-to-timber dowelled connections loaded perpendicularly to the grain.* Fire Safety Journal, 2017.

[35] Hofmann, V., et al., *Fire resistance of primary beam–secondary beam connections in timber structures.* Journal of Structural Fire Engineering, 2016. **7**(2): p. 126-141.

[36] ASTM-E119-18ce1, *Standard Test Methods for Fire Tests of Building Construction and Materials*. 2018, ASTM International: West Conshohocken, PA.

[37] EN, B., *1-1: 2004 Eurocode 5: Design of timber structures—General—Common rules and rules for buildings*. 1995, NA to BS EN.

[38] Linville, J.D., *Timber construction manual*. 2012: John Wiley & Sons.

[39] Chorlton, B. and J. Gales, *Mechanical performance of laminated veneer lumber and Glulam beams after short-term incident heat exposure.* Construction and Building Materials, 2020. **263**: p. 120129.

[40] Chorlton, B. and J. Gales, *Structural Repair of Fire-Damaged Glulam Timber.* Journal of Architectural Engineering. **27**(1): p. 04020043.

[41] Breneman, S. and D. Richardson, *Tall wood buildings and the 2021 IBC: Up to 18 stories of mass timber.* American Wood Council, 2019(2019): p. 13.

[42] ASTM-D7147-11, *Standard Specification for Testing and Establishing Allowable Loads of Joist Hangers*. 2018, ASTM International: West Conshohocken, PA.

[43] Sajid, H.U. and R. Kiran, *Post-fire mechanical behavior of ASTM A572 steels subjected to high stress triaxialities.* Engineering Structures, 2019. **191**: p. 323-342.

[44] Lee, J., M.D. Engelhardt, and E.M. Taleff, *Mechanical properties of ASTM A992 steel after fire.* 2012.

4. THERMO-MECHANICAL BEHAVIOR OF GLULAM-BEAM CONNECTED TO CLT-WALL ASSEMBLIES WITH STEEL DOWELED CONNECTIONS BEFORE, DURING AND AFTER FIRE.

Milad Shabanian [a], Nicole Leo Braxtan [a]

[a] University of North Carolina at Charlotte, Department of Civil and Environmental Engineering, 9201 University City Blvd, Charlotte, NC, 28223, United States

Highlights

- Load-carrying capacity of a Glulam-beam connected to CLT-wall headers with T-Shape steel doweled connections at ambient temperature presented.
- Residual strength of the assembly after 30 and 60 minutes partially exposure to a non-standard fire highlighted.
- Fire resistance of the loaded assembly partially exposed to a non-standard fire emphasized.
- The failure modes of the assembly before, during, and after non-standard fire tests provided.

Graphical Abstract

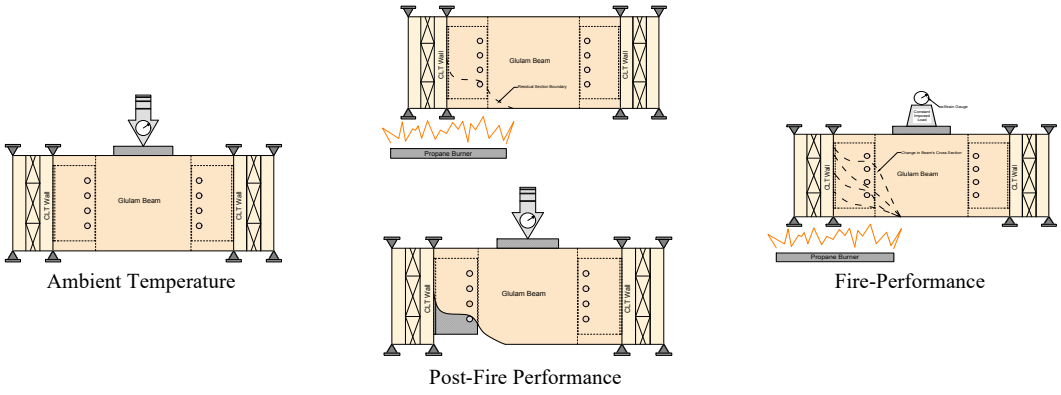

Abstract

In this research, the thermo-mechanical behavior of intermediate-size beam-to-wall assemblies including Glulam-beams connected to CLT walls with T-shape steel doweled connections was investigated. To mimic the performance of 3-ply CLT walls, the outside layers of the CLT members aligned vertically while the mid-layer was laid out horizontally. This paper presents, the results of experimental studies conducted on such an assembly at ambient temperature (AT), as well as the post-fire performance (PFP) and fire-performance (FP) of the assembly. The ambient temperature tests were performed three times to evaluate the load-carrying capacity of the assembly and investigate the failure modes that occurred at room temperature. Embedment failure and plastic deformation of the dowels followed by brittle splitting failure were the dominant observed failure modes in the beam members at ambient temperature. Additionally, tensile failure of the epoxy was observed between the layers of the CLT walls. The PFP tests were performed twice to study the residual strength of the assembly, considering partial exposure to 30-min and 60-min non-standard fires. The residual strength of the assembly was reduced 14% after 30 minutes and 37% after 60 minutes of fire exposure. During the loading phase of the PFP test, the plastic bending of the dowels was the only observed failure mode. The FP test was conducted to investigate the fire-resistance (FR) of the loaded assemblies during the non-standard fire exposure. For this purpose, a similar assembly was loaded up to 65% of its load-carrying capacity at ambient temperature while it was partially exposed to the non-standard fire at one connection. The FP test was conducted for 70 minutes while the maximum mid-span displacement occurred at 51 minutes into the fire exposure. Ductile embedment failure of

the timber in contact with the dowels was the only major failure mode at elevated temperature.

Keywords: Beam-to-wall connection; Cross-Laminated Timber (CLT); Glued-Laminated Timber (Glulam); Steel doweled connection; Load-carrying capacity; Fire-resistance; Residual strength; Non-Standard fire; Post-Fire performance (PFP); Fire-Performance (FP).

4.1. Introduction

The application of engineered wood products such as CLT and Glulam has been increased significantly in Europe and more recently in North America [1-6]. In comparison to the other types of construction materials, engineered wood products provide advantages in architectural appeal, constructability, sustainability, and cost, encouraging engineers to design tall timber structures again [7-13]. It is very common to use CLT as large dimensional wall and floor panels in low to mid-rise panelized construction. Similar to platform framing systems, bearing type of connections with acceptable fire-performance are common in CLT panelized construction. However, due to the complications with accumulative shrinkage [10], it is challenging to employ CLT panelized construction for high-rise structures. On the other hand, current studies confirm the feasibility of using the concept of balloon framing and post and beam construction to reach higher elevations with engineered wood products [8-12]. In this type of construction, columns and beams are usually fabricated from Glulam, walls and floors are CLT, and connections are a combination of bearing, shear, and moment-resisting. As has been well-documented in

other types of structures, connections play a crucial role in providing integrity, stability, and ductility of contemporary high-rise timber structures.

Previously, a wide range of connections has been used for timber structures [14]. These connections are usually constructed from metal or wood. Metal connections are one of the most common types of connections employed in heavy timber construction. They increase the ductility and improve the seismic performance of the structure [15-21], while in a fire incident, they may lose strength and stiffness, and deform considerably [22-24]. Accordingly, it is essential to study the behavior of metal connections in timber structures during and after a fire incident. The fire-performance (FP) of metal connections in timber structures is a function of several variables such as fire exposure time and severity, thermo-mechanical material properties, and geometry of the connected components, magnitude and direction of the imposed mechanical load, and boundary conditions.

A wide range of studies have been conducted to investigate the fire-performance of metal connectors in timber structures [25-45]. Most of these studies focused on fire-performance of the connections between members loaded parallel to the grain [25-39]. Only a limited number of studies covered fire-performance of beam-to-beam and beam-to-column connections with beam members loaded perpendicular to the grain [40-45]. These fire experiments were mostly performed in closed furnaces with accessibility restrictions, following standard fire curves [46, 47] which neglect the decay phase of a real fire incident [48] and are prescribed for constructions designed using prescriptive building codes. However, contemporary high-rise timber structures with varying exposed combustible timber material should follow a performance-based design procedure. For this purpose, a range of design fires including the ASTM standard fire should be considered. The fire load

is important as it will impact the charring rate and load carrying capacity of the timber elements.

This paper describes a series of experiments developed and conducted to investigate the performance of Glulam girder to CLT-wall assemblies connected with T-shape slotted-in doweled connections before, during and after non-standard fire exposure. Experiments were designed considering the restrictions imposed by standard fire tests, previous studies on fire-performance of different connections, and the increasing demand for the use of CLT as a vertical, principal structural member.

4.2. Research Motivation

Timber assemblies loaded perpendicular to grain are vulnerable to brittle splitting failure mode. An experimental study performed on Glulam-beam-to-column assemblies connected with slotted-in doweled connections [49] confirmed this issue. In this study increasing the gap from 10 mm to 20 mm did not impact the failure mechanism at ambient temperature. According to the experiments conducted in this research, reducing the gap will improve the fire-performance of the assembly exposed to the standard fire curve.

Experimental testing on Glulam-beam-to-girder assemblies connected with slotted-in doweled connections (Chapter 3), showed that ductility of the dowels plays a vital role in avoiding the splitting failure. This study also illustrated that removing the gap between connecting members will cause a premature splitting failure and reduce in the load carrying capacity of the assembly at ambient temperature. Results showed that embedment failure was the dominant failure mode on the beam side and splitting failure was the main failure mode on the girder side. The non-standard fire experiments conducted in this research,

highlighted the impact of timber elements mass loss and change in geometry on fire-performance of the assembly. This research also studied the post-fire performance of Glulam-beam-to-girder assemblies after non-standard fire exposure. In these experiments, embedment failure of the Glulam-beams and plastic bending of the dowels occurred before the splitting failure of the Glulam girders.

The current study now considers Glulam-beam to CLT-wall assemblies. Modern mid- to high rise timber panelized construction often relies upon balloon framing wherein the CLT walls are continuous over two to three stories and floor beams are hung from the wall panels. This is fundamentally different from the bearing type connections previously designed for use in platform construction of low-rise timber structures. Additionally, due to its architectural appeal, CLT-wall panels are often left exposed – which contributes to the potential fire load in a structure. The change in grain orientation of CLT-wall panels will also change the failure mechanism. In the beam-to-girder assembly the girders were loaded perpendicular to the grain and experienced brittle failure. It is assumed that using CLT-wall for the headers where the laminations are vertically oriented, as in Figure 4.1, will change the failure mechanism.

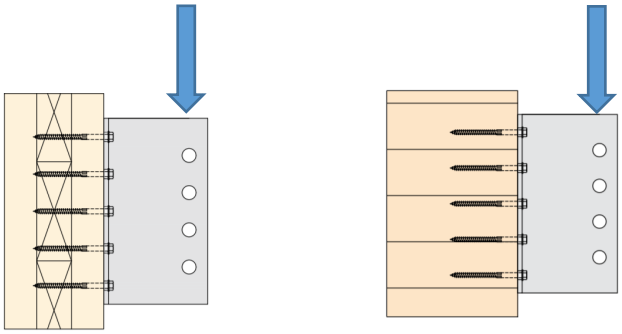

(a) *(b)*

Figure 4.1. (a) CLT-wall header vs (b) Glulam girder header layout in comparison to the load direction

An experimental study performed on behavior of steel to CLT-wall connection showed that screwed connections performed with high ductility [51].

4.3. Experimental Set-up and Material Properties

Experimental testing was performed on Glulam-beam to CLT-wall assemblies to determine the ambient temperature strength of the connection, the residual strength of the connection after fire, and the strength of the connection during fire. In total, six tests were performed: three at ambient temperature, two post-fire, and one during fire.

4.3.1. Assembly Description

Experiments were performed on symmetric, intermediate-size assemblies, consisting of two 3-ply CLT-walls connected to a Glulam-beam with two T-shape steel doweled connectors. Figure 4.2 and Table 4.1 provide additional details of the assembly.

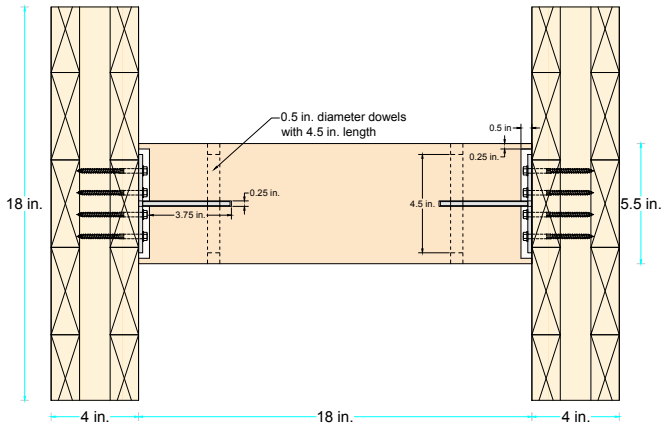

(a)

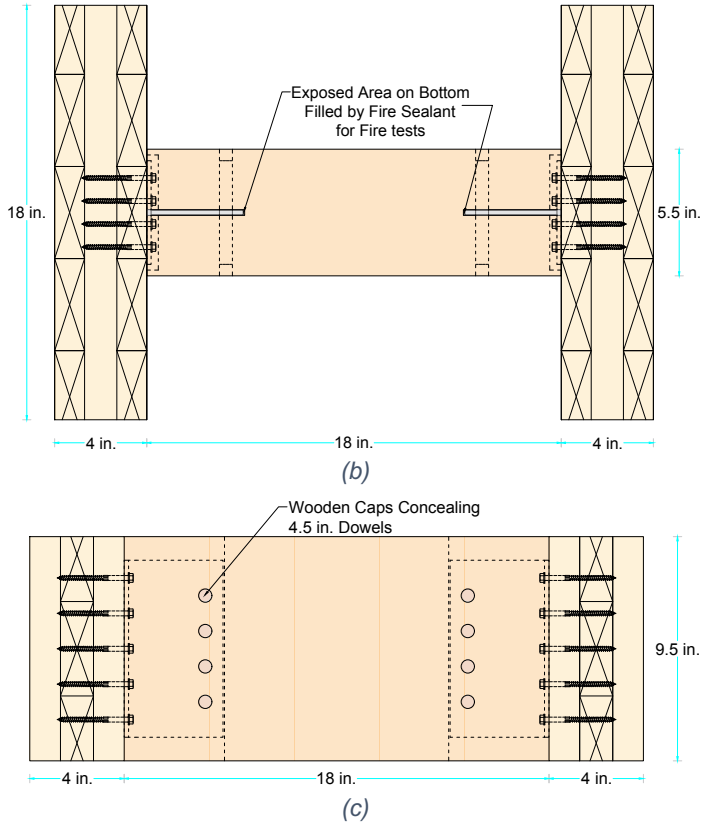

Figure 4.2. Assembly geometry: (a) top view, (b) bottom view, (c) front view.

Table 4.1. Consisting parts of the Glulam-beam to CLT-wall assembly.

Parts	***Quantity***	***Material***	***Dimensions***
Headers	*2*	*3-Ply CLT-wall (105-3s)*	*9.5 in. x 4. in. x 18 in.*
Joist	*1*	*Glulam-beam*	*9.5 in. x 5.5 in. x 18 in.*
Hangers	*2*	*Steel Connection A572 Gr. 50*	*Plate A: 4.5 in. x 7.5 in. x 3/16 in.* *Plate B: 4 in. x 7.5 in. x 3/16 in.*
Dowels	*2×4*	*Steel A572 Gr. 50*	*1/2 in. diameter, 4.5 in. length*
Screws	*2×20*	*Low-carbon steel wire, grade 1022*	*1/4 in. diameter, 3 in. length*

4.3.2. Material Properties

4.3.2.1. CLT-wall Headers

The headers of the assemblies were constructed from 3-ply CLT panels, consisting of three orthogonal layers of graded sawn lumber (Spruce-Pine-Fir) laminated with

structural adhesives. The panel moisture content (MC) was approximately 12% (+/-2%) and density was 32 lb./ft^3. The outside layers of the CLT panels were oriented vertically to simulate the CLT layout for a typical wall condition. Table 2 provides the allowable design capacities of the CLT-wall panel loaded parallel to the outermost layer.

Table 4.2. Mechanical properties of the CLT panel loaded parallel to the outermost layer.

Stress Grade	*Compression Capacity (P_0)*	*Bending Moment Capacity (M_0)*	*Shear Capacity (V_0)*	*Bending Stiffness ($EI_{eff,0}$)*	*Shear Rigidity ($GA_{eff,0}$)*	*Elastic Modulus (E)*
E1	*59 (10^3 lbf/ft)*	*4525 (10^6 lbf-ft/ft)*	*1490 (lbf/ft)*	*115 (10^6 lbf-in.^{2}/ft)*	*0.46 (10^6 lbf/ft)*	*1.7x10^6 (psi)*

4.3.2.2. Beam Member

In each assembly, the Glulam-beam consisted of small wood laminations of spruce, pine, and fir species (90% black spruce) bonded together in parallel using structural adhesives. The Glulam-beams had an average moisture content of 12% and density of 35 lb./ft^3. Table 3.2 shows the design capacities of the Glulam-beams.

Table 4.3. Mechanical properties of the Glulam-beam (in psi).

Stress Grade	*Bending Moment (F_{bx})*	*Compression Perpendicular to Grain (Fcpx)*	*Longitudinal Shear (F_{vx})*	*Compression Parallel to Grain (F_{vx})*	*Tension Parallel to Grain (F_t)*	*Elastic Modulus (E_x)*	*Specific Gravity*
24F-1.9E	*2400*	*600*	*250*	*1150*	*1050*	*1.9E+06*	*0.41*

4.3.2.3. T-shape Steel Connection

The custom designed T-shape slotted-in welded steel doweled connection were fabricated from 7 gauge (3/16 in.) ASTM A572 Grade 50 structural steel with 1/8 in. full-length fillet weld on both sides [50]. Figure 4.3 details the geometry of the connection.

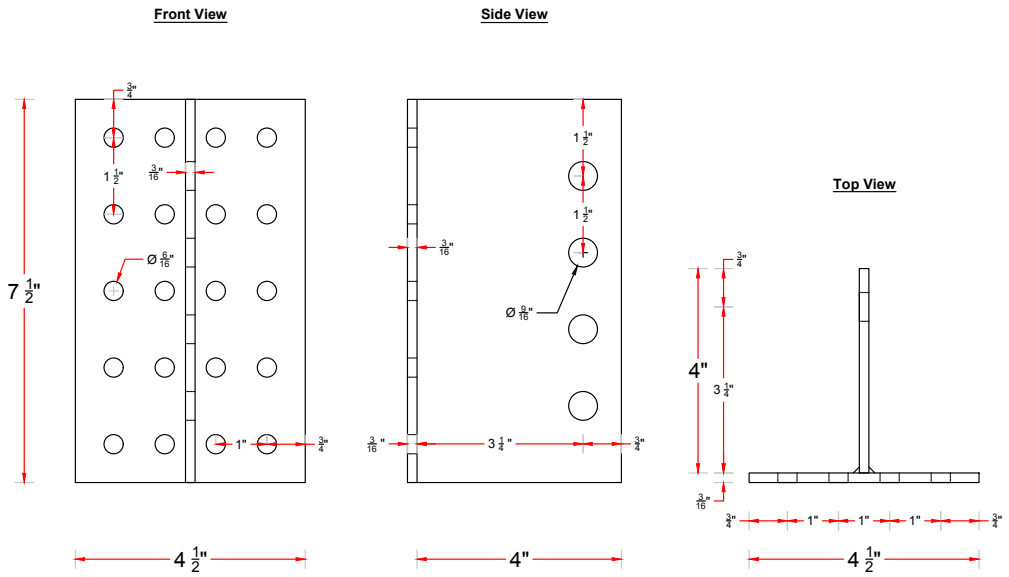

Figure 4.3. Geometry of T-shape welded steel connection

4.3.2.4. Steel Dowels and Fasteners

Figure 4.4 shows the steel dowels and screws in relation to the dimension of the CLT-Wall headers and the Glulam-beam. The 4.5 in. length dowels are cut from ½" structural steel rods (ASTM A572 Gr 50). The ¼" diameter heavy-duty hexagonal connector screws with 3" length and 2" thread were manufactured from low-carbon steel wire, grade 1022. This fastener has 164,000 psi bending strength, 1,430 lbf allowable tensile strength, and 800 lbf allowable shear strength.

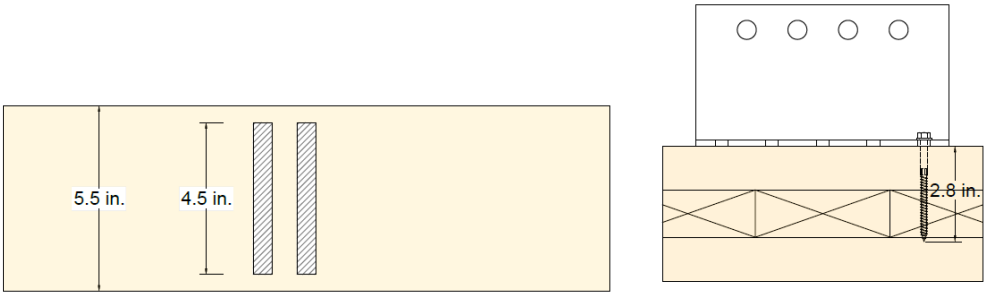

Figure 4.4. 3-Ply CLT-wall and Glulam-beam vs. hexagonal connector and steel dowels.

4.3.3. Experimental Set-up

Figure 4.5, Figure 4.6, and Figure 4.7 show the experimental setup for the ambient, post fire, and fire performance tests performed on the Glulam-beam to CLT-wall connections. Additional details on the test setup can be found in Chapter 3. Ambient temperature experiments considered only mechanical load on the assembly, post-fire tests considered sequential (uncoupled) thermal and mechanical loading, and fire performance tests considered coupled thermal and mechanical loading. Post-fire performance tests were performed after 30 and 60 minutes of nonstandard fire loading. The only difference between the post-fire performance test performed on this assembly compare to the glulam beam to girder assembly was that the CLT-wall was only exposed on the connection side (1-side exposure) in this assembly. Fire performance tests were performed with a constant load applied, equivalent to 65% of the ambient temperature capacity of the assembly, along with a nonstandard fire exposure.

Figure 4.5. Test set-up and instrumentation utilized for testing at ambient temperature.

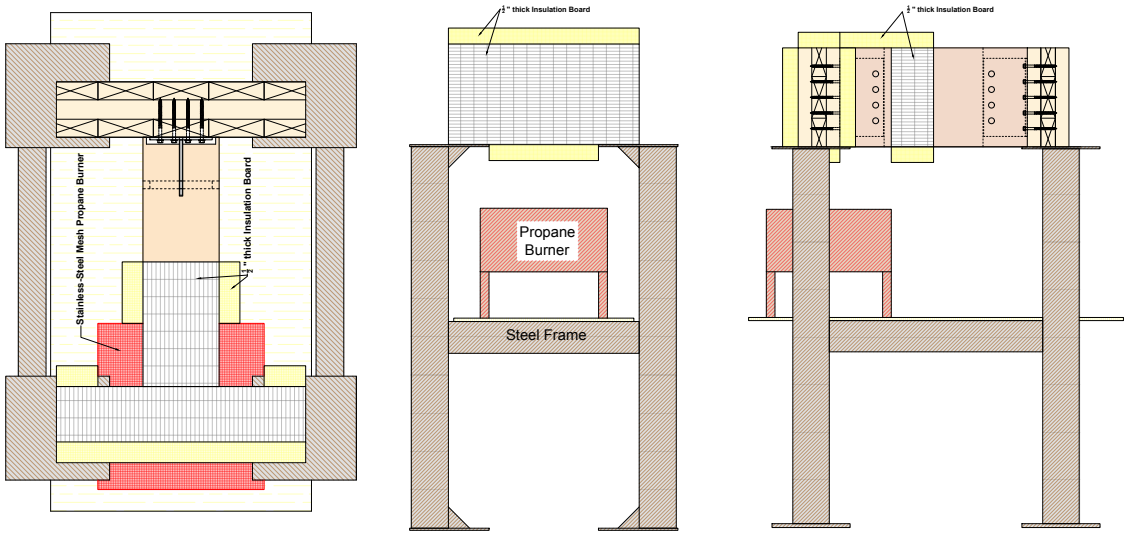

Figure 4.6. PFP fire test set-up, (a) top view, (b) side view, (c) front view.

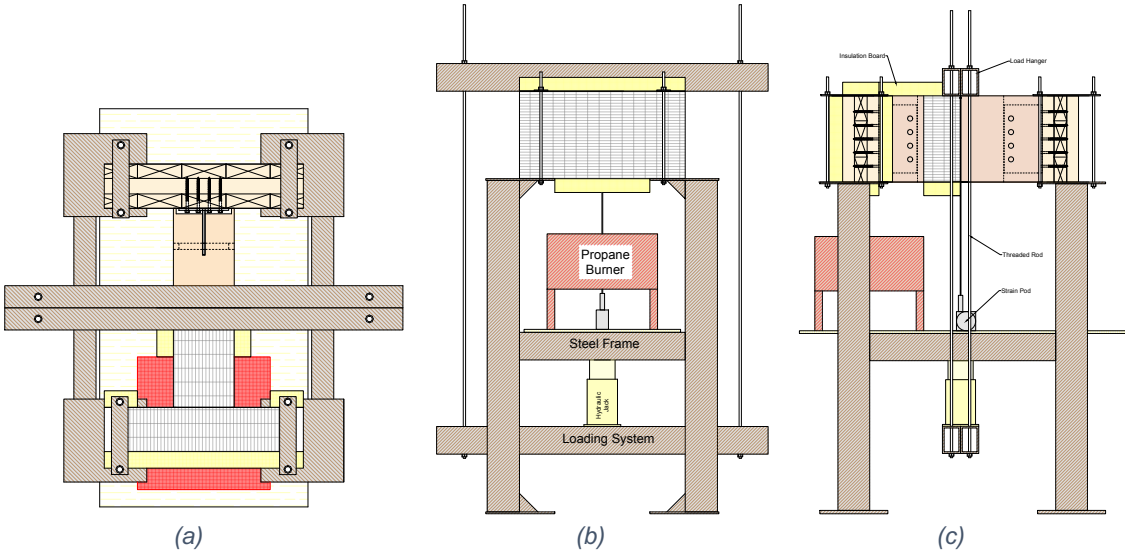

Figure 4.7. Fire-Performance test set-up, (a) top view, (b) side view, (c) front view.

Figure 4.8 and Figure 4.9 show the location of the thermocouples in the fire exposed area of the connection for the Post-fire and fire performance tests, respectively.

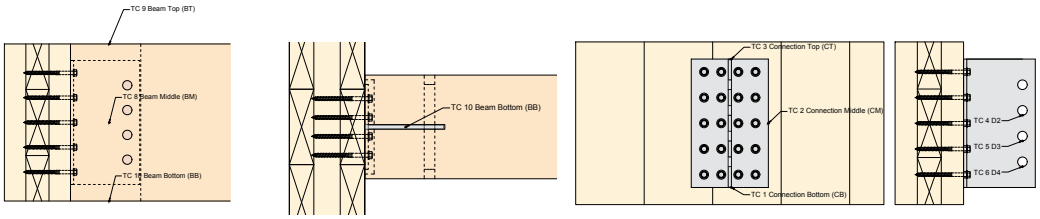

Figure 4.8. Thermocouples arrangement for PFP test.

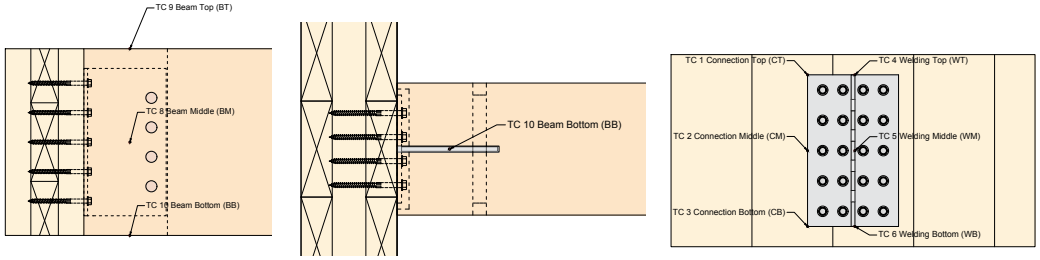

Figure 4.9. Thermocouples arrangement for FP test.

4.4. Test Results and Discussion

4.4.1. Ambient Temperature Results

Figure 4.10 shows the load-displacement curves of the Glulam-beam to CLT-wall assemblies tested at ambient temperature (AT). The average load-carrying capacity of the assembly was 37.5 kips. According to these curves, the average elastic stiffness of the assembly was around 88.9 (k/in.).

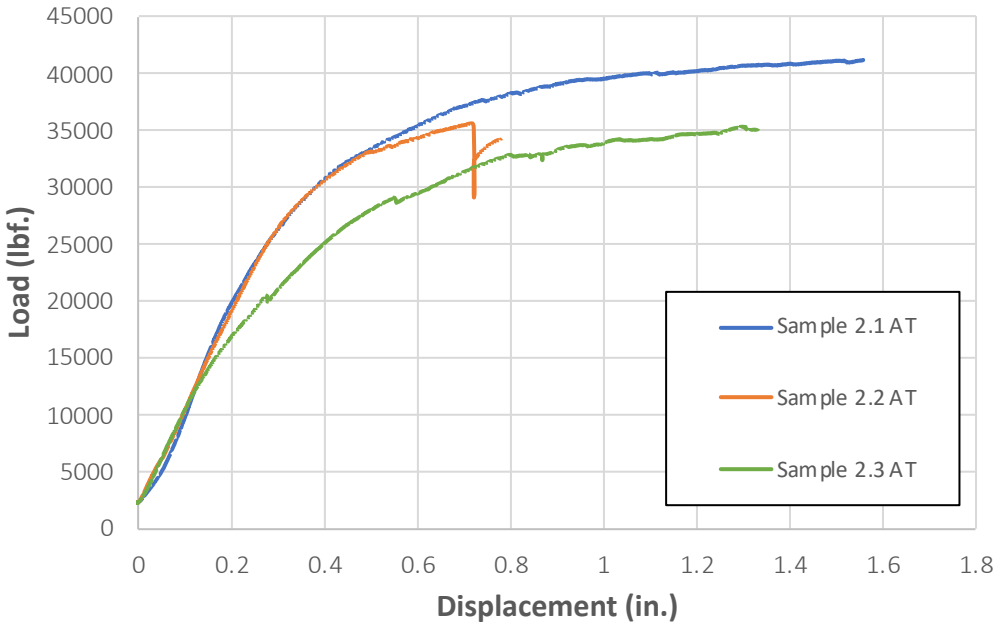

Figure 4.10. Load-displacement of the Glulam-beam to CLT-wall assembly at ambient temperature (AT).

Figure 4.11 shows the failure modes that occurred during ambient temperature tests. In all ambient temperature tests, failure of the Glulam-beam was initiated by the plastic embedment failure of the Glulam-beam at the dowels' contact locations and continued by plastic bending of the steel dowels (Figure 4.11.a). Tests were stopped after brittle splitting failure occurred close to the top dowels (Figure 4.11.b). On the CLT-walls, the tensile withdrawal force of the screws near the top half of the assembly resulted in a tensile plug-out between the CLT-wall layers (Figure 4.11.c). However, this failure may not occur in taller CLT-wall panels with more resistance against tension.

Figure 4.11. Ambient temperature failure modes (a)ductile embedment failure and bending of the dowels, (b)brittle splitting failure, (c) plug-out tensile failure of the CLT-wall.

4.4.2. Post-Fire Performance Test Results

Two post-fire performance tests were conducted to study the degradation in residual load-carrying capacity of the Glulam-beam to CLT-wall assembly exposed to 30- and 60-minute non-standard fires. In both experiments, the temperature of the burner increased during the first five minutes, and then was held constant near 1000 °F. The temperature of the burner can be compared to the ASTM E119 standard fire curve in Figure 4.12. The ASTM fire also reaches 1000 °F in the first five minutes, but then continues to slowly increase for the duration of the fire loading. At 30 minutes fire duration, the ASTM E1119 fire reaches 1550 °F, approximately 50% higher than the burner temperature reached in this research. Also, of note is the addition of fire sealant to the 60-minute test assembly. Results of these tests included measurements of the heat distribution during the fire tests and the midspan load-displacement behavior of the burnt samples during the loading phase.

Figure 4.12 shows the post-fire-performance heat distribution for the 30-minute fire (PFP30) without the fire sealant. Thermocouples 1, 2, and 3 (TC1, TC2, and TC3) recorded the temperature at the bottom, middle, and top of the steel connection, respectively. As it was expected, TC1 recorded the highest temperature in the steel connection. After 30

minutes of fire exposure, the maximum connection temperature occurred in the bottom of the connection (708 °F) while the minimum recorded temperature was at the top of the connection (163°F). According to the former studies [52, 53] the post-fire mechanical properties of ASTM A572 Gr 50 remain unaffected after exposure to temperatures up to 1112 °F. Hence, no reduction in residual strength of the steel connection is expected. Temperatures of the steel connection at the point of contact with the three lower dowels were also recorded by TC4, TC5, and TC6. These temperatures followed the same increasing pattern as the other parts of steel connection. TC4, located closer to the beam bottom had the highest temperature (293°F) of the temperatures recorded at the lower dowels.

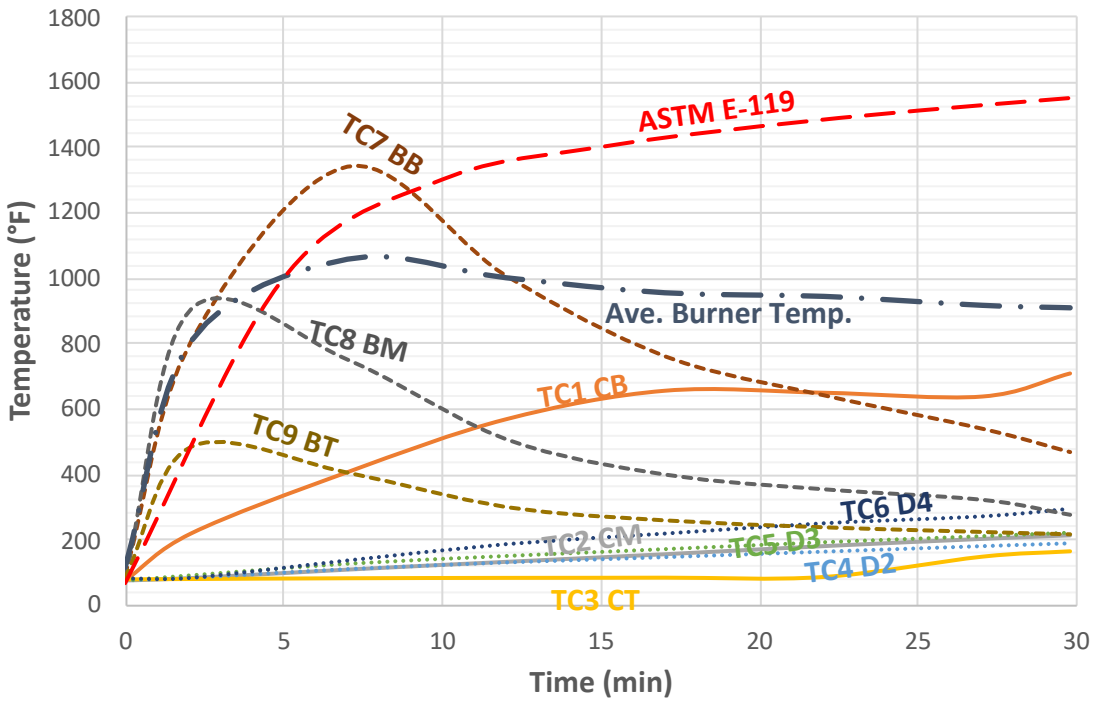

Figure 4.12. PFP30 heat distribution along the exposed area.

Thermocouples TC7, TC8, and TC9 measured the Glulam-beam temperatures at the bottom, middle, and top of the beam. The Glulam-beam temperature increased at first then decreased during the combustion of the beam's surface began to decay. Based on the visual observations, the Glulam-beam ignited after 1 minute on the exterior sides and after 2 minutes on the bottom. The beam temperatures recorded by TC7 and TC8 confirm ignition as the data as temperatures begin to exceed the temperature of the burner and reach the ignition temperature of wood at approximately 2 minutes in to the and 570 °F. Figure 4.13 shows the assembly during and after 30 minutes fire exposure. At the end of this experiment, the average temperature of the exposed beam was 310 °F when exposed to the nearly constant 1000 °F. It is assumed that exposure to the higher intensity ASTM E119 fire would lead to greater beam temperatures and more extensive charring.

(a) (b)

Figure 4.13. Glulam-beam to CLT-wall assembly (a) during, and (b)after PFP30 fire test.

Figure 4.14 shows the heat distribution of the assembly exposed for 60-minutes to the prescribed fire (PFP60). Figure also shows the continually increasing ASTM E119 fire, which reaches 1700 °F at 1-hour fire duration in contrast to the nearly constant burner temperature of 1000 °F. Similar to the PFP30 test, the Glulam-beam bottom ignited when

the beam temperature reached the wood ignition temperature of 570°F. In this case the maximum temperature experienced by the beam was 1430°F. The decay phase on the beam's surface fire began after 12 minutes and the resulting beam temperatures decreased. TC1 recorded the highest temperatures along the steel connection and after 60 minutes of fire exposure the maximum temperature in the bottom of the connection was 803°F.

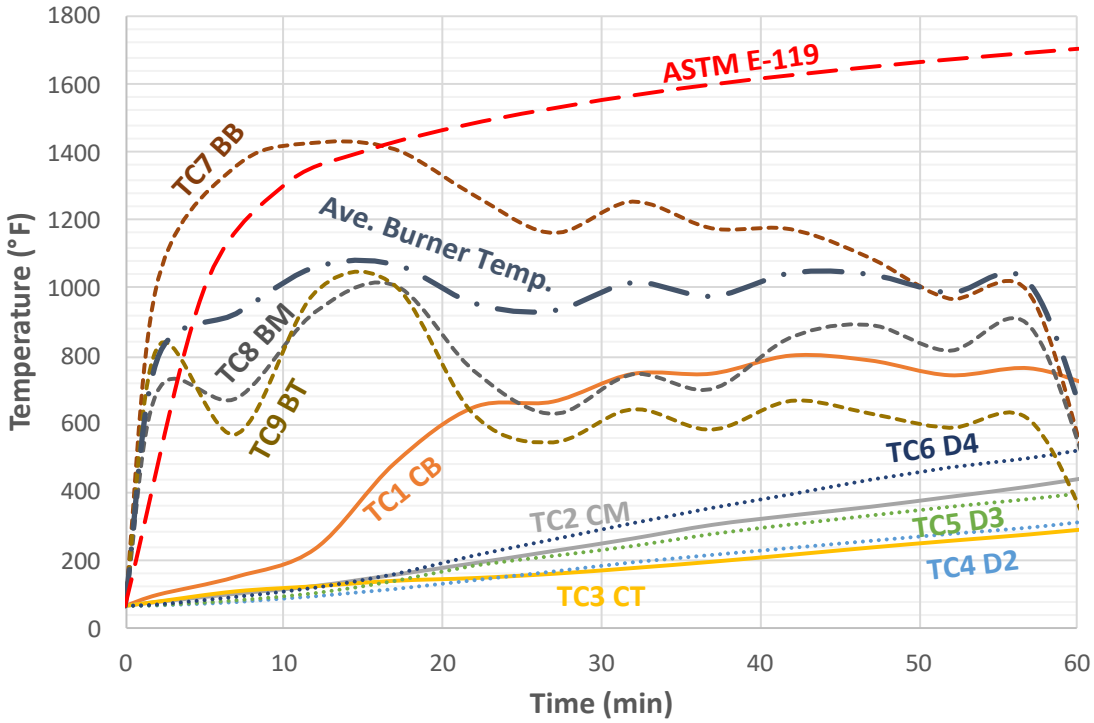

Figure 4.14. PFP60 heat distribution along the exposed area.

Consequently, the fire exposure did not impact the residual strength of the steel connection after cooling. The fire-sealant had a considerable impact on the temperature of the connection for the first 12 minutes of the fire, and then the temperature in the connection began to increase more rapidly. Finally, at the end of this experiment, the average temperature of the beam at the exposed area to the non-standard fire was 520 °F, was 1180 °F less than ASTM E-119. At the end of this experiment, the average

temperature of the exposed beam was 529 °F when the temperature of the burner was 720 °F.

Figure 4.15 shows the Glulam-beam to CLT-wall assembly during and after the PFP60 fire test. While the temperature in the connection began to more rapidly increase after 12 minutes of fire, Figure 4.15 (c) shows that the fire sealant stays in place until the end of fire experiment insulating the connection from the heat. During both fire tests, the temperature of the beam increased due to the consumption of the combustible timber fuel while temperature of the connection increased it exposed more due to the progress in charring.

(a) (b) (c)

Figure 4.15. (a) Fire sealed Glulam-beam to CLT-wall assembly (b) during, and (c) after 60 minutes PFP test.

According to Figure 4.16, the residual load-carrying capacity of the assembly after 30 minutes of fire exposure was reduced to 32.5 kips (86% of the ambient capacity). The embedment failure of the beam and plastic bending of the dowels were the dominant captured failure modes.

Figure 4.16 also shows that the load-carrying capacity of the assembly after 60 minutes was reduced to 23.7 kips (63% of the ambient capacity). The embedment failure of the beam and plastic bending of the dowels were the main failure modes in this

experiment. Since in both tests, the steel connection itself is expected to maintain the ambient temperature strength, the reduction in load-carrying capacity is likely caused by the loss in gross cross-section of the wood due to the charring and strength reduction in the thermal penetrated zone behind the char layer.

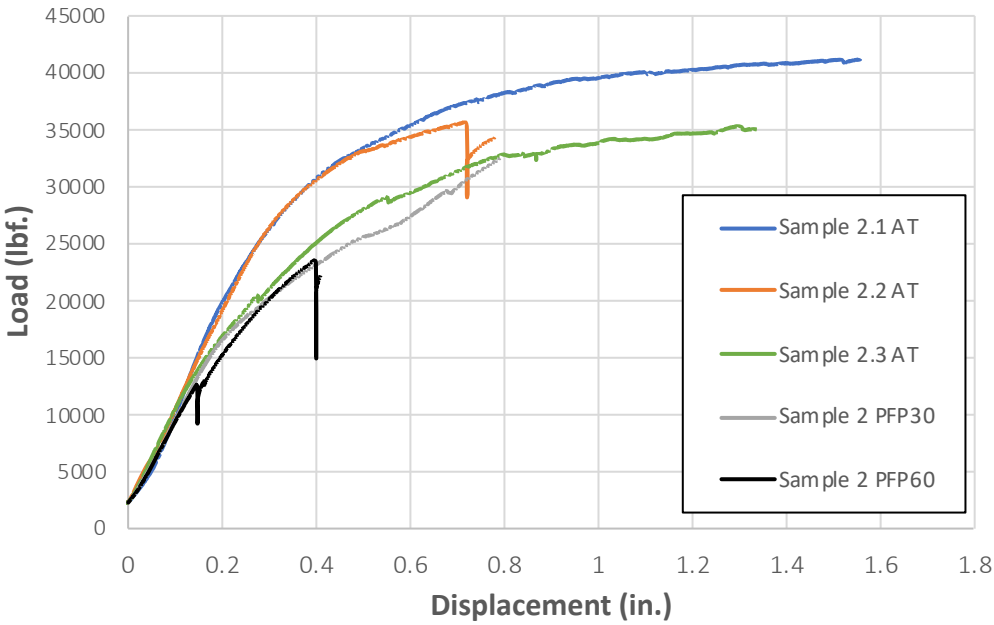

Figure 4.16. Load-displacement of Glulam-beam to CLT-wall assembly exposed 30 and 60 minutes.

Figure 4.17 shows the assemblies exposed for 30 and 60 minutes to the non-standard fire after failure. Extensive charring appears on the heated side of the assembly for both the 30 and 60-minute PFP tests. The right side of the connection remained unaffected during the PFP tests. In both PFP30 and PFP 60, the premature splitting occurred only on the unexposed side while both sides experienced the embedment failure. Ultimately, the assemblies failed due to embedment on the fire exposed side of the beam.

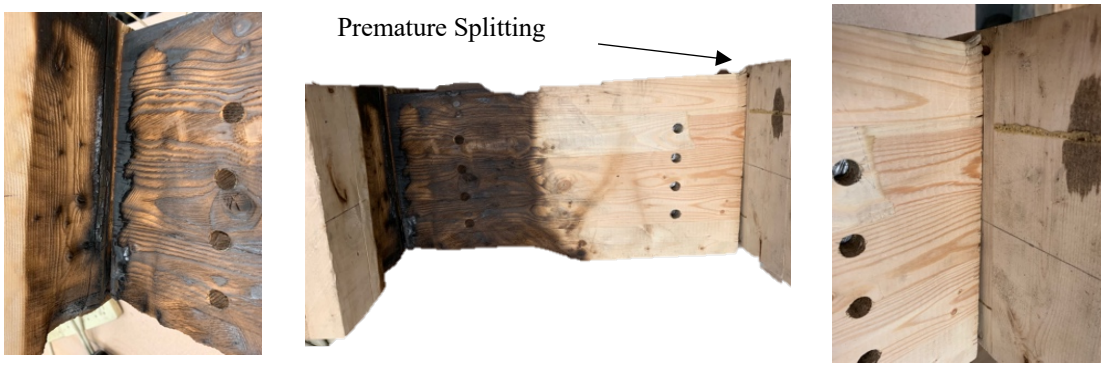

Exposed side *PFP30 after loading step* *Unexposed side*

Figure 4.17. Glulam-beam to CLT-wall assemblies after loading step.

4.4.3. Fire-Performance Test Results

The FP test were conducted to study the fire-resistance (FR) of a loaded assembly partially exposed to a non-standard fire. The sample was loaded with a constant downward load of 24.6 kips at the mid-span of the Glulam-beam during the fire test. Figure 4.18 shows the heat distribution along the exposed area of the Glulam-beam during the fire test. According to this figure, the Glulam-beam ignited after 2 minutes. During fire-performance test, the temperature of the burner was held constant at approximately 1200 °F. Although, the beam bottom temperature increased up to 1400 °F and decreased afterwards when the beam's surface charred and degraded. The FP test was terminated after 70 minutes. During this time, the maximum experienced temperature of the steel connection was 1090 °F in the bottom of the connection.

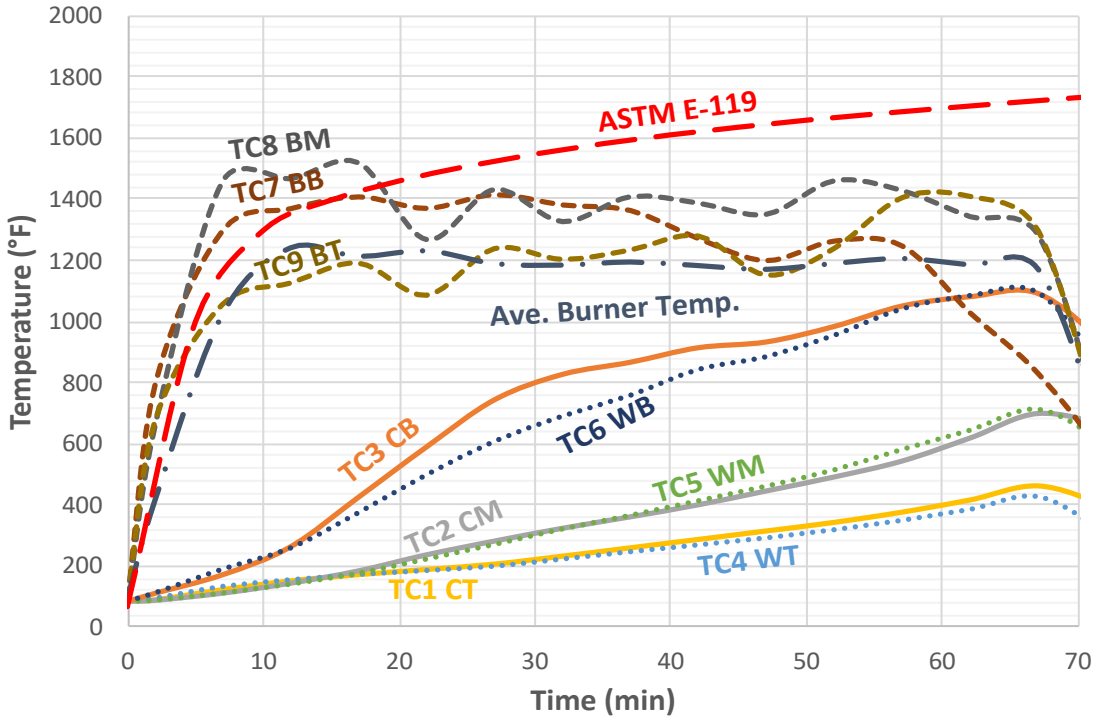

Figure 4.18. Heat distribution along the exposed area of the assembly during FP test.

According to Figure 4.19 and based on the visual observation, the maximum displacement of the sample occurred 51 minutes into the non-standard fire exposure. The maximum rate of displacement occurred at this time and it was 0.131 (in/min). At 51 minutes into the fire, the steel is expected to maintain 80% of its ambient temperature yield strength and 58% of its ambient temperature elastic modulus. While the mechanical properties of the steel connection were degraded, the reserve capacity of the connection prevented failure within the connection itself.

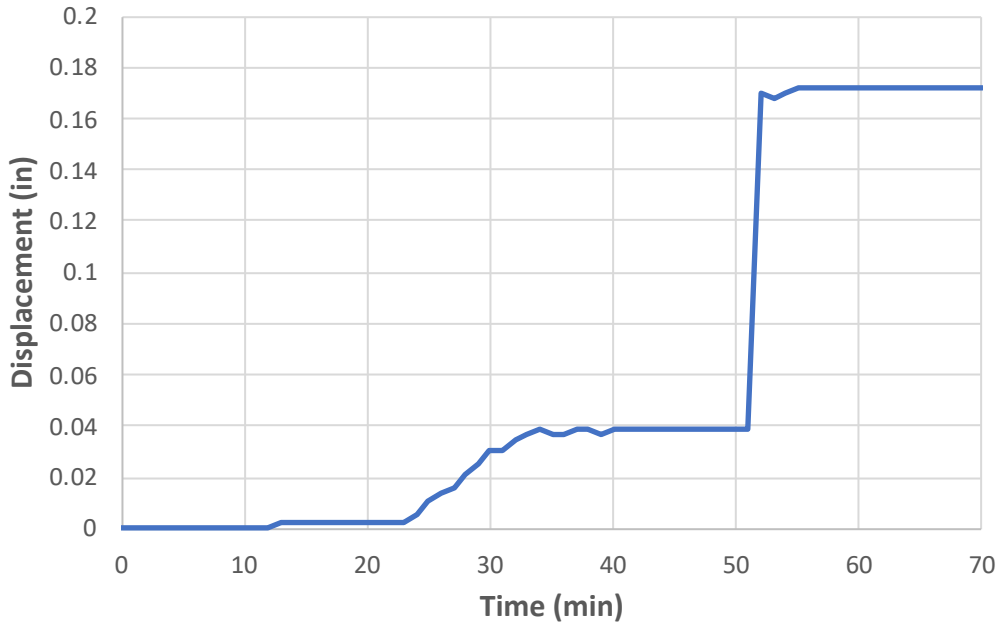

Figure 4.19. Time-displacement at the mid-span of the Glulam-beam loaded in FP test.

The entire fire-performance test was recorded by a fixed video camera. The recorded videos and captured pictures were used for further investigation on the fire-performance of the assembly. Figure 4.20 shows video captures of the fire-performance test at different times.

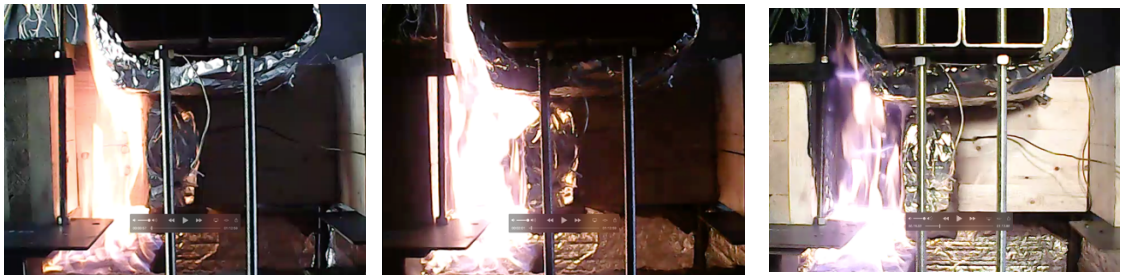

t=1 min *t=2 min* *t=15 min*

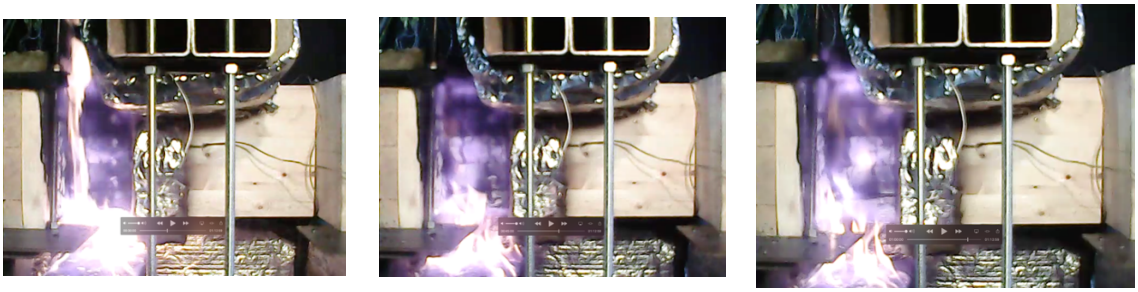

t=30 min t=45 min t=60 min

Figure 4.20.Fire-performance test video shots.

Figure 4.21 shows the residual section of the Glulam-beam to CLT-wall assembly after the FP test. The embedment failure of the Glulam-beam was the only failure occurred in this assembly. During the FP test, the CLT-wall exposed to fire only from one side (the side in contact with connection). The char depth on the exposed side was almost equal to the thickness of the surface layer of the CLT (4/3 in.). This depth was decreased by moving toward the top of CLT wall member, specifically in contact with the steel connection. Higher temperature of the steel connection in the bottom resulted deeper char layer. Consequently, due to the change in geometry and boundary condition, the steel connection rotated around top screws, and caused a displacement in the beam member. The displacement of the beam and connection put the top and bottom dowels in more stress. The connection rotation followed by beam displacement stopped when the beam member seated on the top screws. Figure 4.21 also shows the contact area of the Glulam-beam and change in boundary condition.

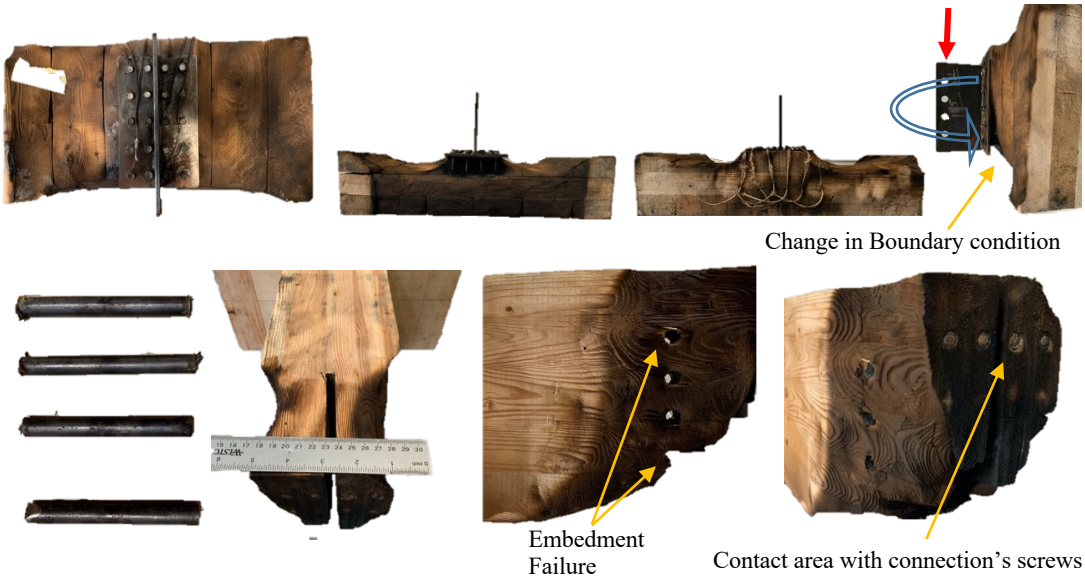

Figure 4.21. Residual section of the Glulam-beam to CLT-wall assembly after the fire-performance test.

4.5. Discussion and Conclusion

This research focused on the performance of Glulam-beam to CLT-wall assemblies connected with T-shaped slotted-in steel connections exposed to mechanical load before, during and after non-standard fire.

According to the tests performed at ambient temperature, the average load-carrying capacity of the assembly was 37.5 kips. The failure of the assembly initiated by the ductile embedment failure of the Glulam-beam, followed by plastic bending of dowels, and ultimately splitting failure of the Glulam-beam. Tensile plug-out also occurred in the CLT wall, but this failure mode may be less likely in an actual wall structure with a greater height than the wall segment tested.

For the assembly loaded after 30 minutes of non-standard fire exposure (PFP30), the embedment failure of the Glulam-beam and plastic bending of the dowels were main failure modes. The load-carrying capacity of the assembly was reduced by 14% after 30

minutes fire exposure. The maximum recorded temperature of the steel connection during the PFP30 test was 708 °F. Therefore, the reduction in load-carrying capacity of the assembly is attributed to the loss of wooden members cross-section and strength in the thermal penetration zone behind the char layer.

The post-fire-performance of the assembly exposed to the non-standard fire for 60 minutes (PFP60) followed the same pattern as the PFP30 specimen. However, the load carrying capacity of the assembly was reduced by 37% after 60 minutes fire exposure. The maximum recorded temperature of the steel connection during the PFP60 test was 803 °F.

For the loaded assembly tested during the non-standard fire (FP), the imposed load was 65% of the expected load-carrying capacity of the assembly. The ductile embedment failure of the beam was the only observed failure mode. The loaded assembly experienced the maximum displacement after 51 minutes non-standard fire exposure. The temperature within the connection was 900 °F at 51 minutes, and although the steel material properties were degraded due to the elevated temperature, the reserve capacity of the connection prevented failure in the connection itself and the main final failure mode for the assembly was embedment failure in the beam.

The fire-sealant utilized for the PFP60 and FP tests protected the steel connection. However, the change in boundary condition and advancing fire surface dictated by charring, limited the impact of fire-sealant.

During all the fire tests, the increase in temperature of the connection did not significantly affect the performance of the connection, and the key parameters in reducing the strength of the assembly were charring, reduction in gross cross section and strength of the exposed part of the assembly and change in boundary condition. Additionally, it was

found that the, presence of the steel connection promoted the charring process and facilitated the failure of the wooden beam at the connection area.

Finally, the CLT-wall to Glulam-beam assembly considered in this chapter was subject to similar ambient temperature, post-fire, and fire performance testing as the Glulam-beam-to-girder connection tested in Chapter 3. The Glulam-beam and steel connection were the same in both tests, but the headers varied – CLT-wall compared to Glulam girder. In both cases, however the controlling failure mode occurred in the Glulam-beam despite the altered geometry and orientation of the CLT wall. Similar trends were observed in the post-fire and fire performance thermal results as well.

4.6. REFERENCES

[1] Manninen, H., *Long-term outlook for engineered wood products in Europe.* European Forest Institute, Joensuu, Finland, 2014.

[2] Pei, S., et al., *An overview of CLT research and implementation in North America.* In: WCTE 2016, August 22-25, 2016 Vienna, Austria, 2016.

[3] Espinoza, O., et al., *Cross-laminated timber: Status and research needs in Europe.* BioResources, 2016. **11**(1): p. 281-295.

[4] Brandner, R., et al., *Cross laminated timber (CLT): overview and development.* European Journal of Wood and Wood Products, 2016. **74**(3): p. 331-351.

[5] Laguarda-Mallo, M.F. and O. Espinoza, *Awareness, Perceptions and Willingness to Adopt CLT by US Engineering Firms.* BioProducts Business, 2018: p. 1-14.

[6] Pierobon, F., et al., *Environmental benefits of using hybrid CLT structure in midrise non-residential construction: An LCA based comparative case study in the US Pacific Northwest.* Journal of Building Engineering, 2019. **26**: p. 100862.

[7] Kuzman, M.K., et al., *Architect perceptions of engineered wood products: An exploratory study of selected countries in Central and Southeast Europe.* Construction and Building Materials, 2018. **179**: p. 360-370.

[8] Smith, I. and A. Frangi, *Overview of design issues for tall timber buildings.* Structural Engineering International, 2008. **18**(2): p. 141-147.

[9] Waugh, A., M. Wells, and M. Lindegar. *Tall timber buildings: application of solid timber constructions in multi-storey buildings*. in *International convention of*

society of wood science and technology and United Nations economic commission for Europe. 2010.

[10] Green, M.C. and J.E. Karsh, *The case for tall wood buildings: how mass timber offers a safe, economical, and environmentally friendly alternative for tall building structures*. 2012: MgbARCHITECTURE+ DESIGN.

[11] Salvadori, V., *The develoment of a tall timber building. The architectural challenges, the examples, the opportunities.* 2017.

[12] Ramage, M., et al., *Super Tall Timber: design research for the next generation of natural structure.* The journal of architecture, 2017. **22**(1): p. 104-122.

[13] Kuzmanovska, I., et al. *Tall timber buildings: Emerging trends and typologies*. in *2018 World Conference on Timber Engineering*. 2018.

[14] Perkins, N.S., P. Landsem, and G.W. Trayer, *Modern connectors for timber construction*. Vol. 1. 1933: US Government Printing Office.

[15] Gavric, I., M. Fragiacomo, and A. Ceccotti, *Cyclic behaviour of typical metal connectors for cross-laminated (CLT) structures.* Materials and structures, 2015. **48**(6): p. 1841-1857.

[16] Jorissen, A. and M. Fragiacomo, *General notes on ductility in timber structures.* Engineering structures, 2011. **33**(11): p. 2987-2997.

[17] Dorn, M., K. de Borst, and J. Eberhardsteiner, *Experiments on dowel-type timber connections.* Engineering structures, 2013. **47**: p. 67-80.

[18] Blaß, H.J. and P. Schädle, *Ductility aspects of reinforced and non-reinforced timber joints.* Engineering Structures, 2011. **33**(11): p. 3018-3026.

[19] Moss, P.J., A.H. Buchanan, and K.L. Wong. *Moment-resisting connections in Glulam-beams*. in *Proceedings of 6th world conference on timber engineering, Vancouver, Canada*. 2000.

[20] Buchanan, A., P. Moss, and N. Wong. *Ductile moment-resisting connections in Glulam-beams*. in *Proceedings of NZSEE conference, Wairakei Resort, Taupo, New Zealand*. 2001.

[21] Fragiacomo, M., B. Dujic, and I. Sustersic, *Elastic and ductile design of multi-storey crosslam massive wooden buildings under seismic actions.* Engineering structures, 2011. **33**(11): p. 3043-3053.

[22] Peng, L., et al., *Fire resistance performance of unprotected wood–wood–wood and wood–steel–wood connections: A literature review and new data correlations.* Fire Safety Journal, 2010. **45**(6-8): p. 392-399.

[23] Maraveas, C., K. Miamis, and C.E. Matthaiou, *Performance of timber connections exposed to fire: a review.* Fire Technology, 2015. **51**(6): p. 1401-1432.

[24] Carling, O., *Fire Resistance of Joint Details in Loadbearing Timber Construction: A Literature Survey*. 1990: Building Research Association of New Zealand.

[25] Norén, J., *Load-bearing Capacity of Nailed Joints Exposed to Fire.* Fire and materials, 1996. **20**(3): p. 133-143.

[26] Kruppa, J., T. Lamadon, and P. Rachet, *Fire resistance test of timber connections.* CTICM Ref. INC-00/187-JK/NB, 2000.

[27] Lau, P., *Fire resistance of connections in laminated veneer lumber.* Fire Engineering Research Report, 2006. **6**(3): p. 2006.

[28] Harris, S., *Fire resistance of epoxy-grouted steel rod connections in laminated veneer lumber (LVL)*. 2004, University of Canterbury.

[29] Austruy, C., et al., *Fire resistance of timber connections.* Ecole Normale Superieure de Cachan, Cachan, France, 2007.

[30] Chuo, T.C.B., *Fire performance of connections in laminated veneer lumber.* 2007.

[31] Moss, P., et al., *On the design of timber bolted connections subjected to fire.* 2008.

[32] Moss, P.J., et al., *Fire performance of bolted connections in laminated veneer lumber.* 2009.

[33] Erchinger, C., A. Frangi, and M. Fontana, *Fire design of steel-to-timber dowelled connections.* Engineering Structures, 2010. **32**(2): p. 580-589.

[34] Frangi, A., C. Erchinger, and M. Fontana, *Experimental fire analysis of steel-to-timber connections using dowels and nails.* Fire and Materials, 2010. **34**(1): p. 1-19.

[35] Racher, P., et al., *Thermo-mechanical analysis of the fire performance of dowelled timber connection.* Engineering Structures, 2010. **32**(4): p. 1148-1157.

[36] Peng, L., et al., *On the Fire Performance of Double-shear Timber Connections.* Fire Safety Science, 2011. **10**: p. 1207-1218.

[37] Peng, L., et al., *Predicting the fire resistance of wood–steel–wood timber connections.* Fire technology, 2011. **47**(4): p. 1101-1119.

[38] Audebert, M., et al., *Behavior of dowelled and bolted steel-to-timber connections exposed to fire.* Engineering Structures, 2012. **39**: p. 116-125.

[39] Khelifa, M., et al., *Analysis of the behavior of multiple dowel timber connections in fire.* Fire Safety Journal, 2014. **68**: p. 119-128.

[40] Oksanen, T., et al., *Ruostumattomasta teräksestä valmistettujen puurakenteiden liitosten palonkestävyys.* 2005.

[41] Palma, P., et al. *Fire resistance tests on steel-to-timber dowelled connections reinforced with self drilling screws*. in *2nd CILASCI–Ibero-Latin-American Congresso n Fire Safety Engineering*. 2013. Eidgenösische Technische Hochschule Zürich.

[42] Palma, P., et al., *Fire resistance tests on beam-to-column shear connections.* 2014.

[43] Hofmann, V., et al., *Fire resistance of primary beam–secondary beam connections in timber structures.* Journal of Structural Fire Engineering, 2016. **7**(2): p. 126-141.

[44] Palma, P., *Fire behaviour of timber connections*. 2016, ETH Zurich.

[45] Palma, P. and A. Frangi, *Modelling the fire resistance of steel-to-timber dowelled connections loaded perpendicularly to the grain.* Fire Safety Journal, 2017.

[46] ASTM-E119-18ce1, *Standard Test Methods for Fire Tests of Building Construction and Materials*. 2018, ASTM International: West Conshohocken, PA.

[47] EN, B., *1-1: 2004 Eurocode 5: Design of timber structures—General—Common rules and rules for buildings*. 1995, NA to BS EN.

[48] Gales, J., B. Chorlton, and C. Jeanneret, *The Historical Narrative of the Standard Temperature–Time Heating Curve for Structures.* Fire Technology, 2020: p. 1-30.

[49] Palma, Pedro. *Fire behaviour of timber connections*. Diss. ETH Zurich, 2016.

[50] ASTM A572 / A572M-18, *Standard Specification for High-Strength Low-Alloy Columbium-Vanadium Structural Steel*, ASTM International, West Conshohocken, PA, 2018, www.astm.org.

[51] Hassanieh, A., H. R. Valipour, and M. A. Bradford. *Load-slip behaviour of steel-cross laminated timber (CLT) composite connections*. Journal of Constructional Steel Research 122 (2016): 110-121.

[52] Sajid, H.U. and R. Kiran, *Post-fire mechanical behavior of ASTM A572 steels subjected to high stress triaxialities.* Engineering Structures, 2019. **191**: p. 323-342.

[53] Lee, J., M.D. Engelhardt, and E.M. Taleff, *Mechanical properties of ASTM A992 steel after fire.* 2012.

5. THERMO-MECHANICAL BEHAVIOR OF CLT BEAM-TO-GIRDER ASSEMBLIES CONNECTED WITH T-SHAPED DOWELED CONNECTIONS BEFORE, DURING AND AFTER FIRE EXPOSURE.

Milad Shabanian [a], Nicole Leo Braxtan [a]

[a] University of North Carolina at Charlotte, Department of Civil and Environmental Engineering, 9201 University City Blvd, Charlotte, NC, 28223, United States

Highlights

- Load carrying capacity and failure modes of CLT beam-to-girder assembly with T-shaped steel doweled connections at ambient temperature presented.
- Residual strength and failure modes of the assembly after 30-min partially exposure to the non-standard fire provided throughout the post-fire performance test.
- Fire resistance of the assembly partially exposed to the non-standard fire highlighted.

Graphical Abstract

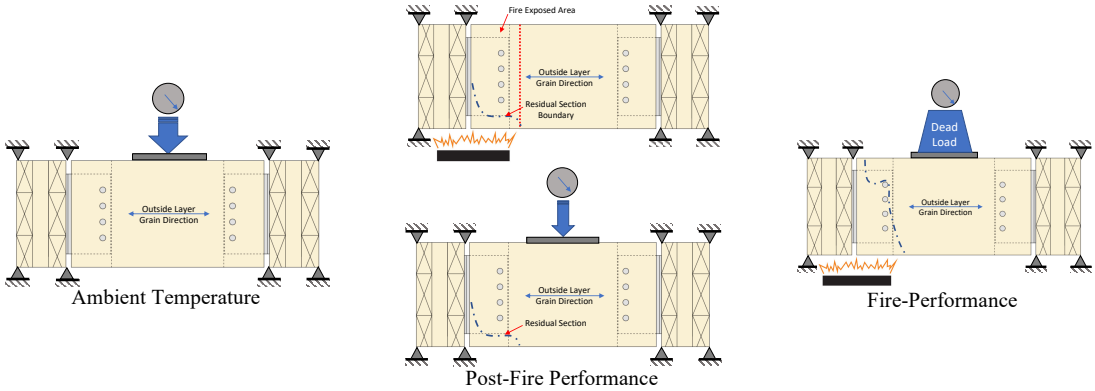

Abstract

3-ply Cross-Laminated Timber (CLT) is utilized to investigate the thermo-mechanical performance of intermediate-size assemblies comprised of T-shaped welded slotted-in steel doweled connections and CLT beams. The outside layers of the CLT beams were aligned horizontally while the mid-layer was laid out vertically in the test assemblies. This paper presents the results of experimental studies conducted at three different thermal conditions: ambient temperature (AT), post-fire performance (PFP) and fire-performance (FP). The first set of experiments was performed as a benchmark to find the load-carrying capacity of the assembly and investigate the failure modes at room temperature. Embedment failure and plastic deformation of the dowels in the beam were the dominant failure modes at the ambient temperature. Additional failure modes of row shear parallel to the grain of the mid-layer and partial splitting failure of the outside layers in the CLT beam were observed. The post-fire performance test was performed to investigate the residual strength of the assembly after 30-min exposure to a non-standard fire. The load-carrying capacity of assembly was reduced to 45% of the ambient capacity after 30 min of fire exposure. Plastic bending of the dowels was the principal failure mode, with row shear in mid-layer of the CLT beam and tear out failure of the header sides also observed. The fire-performance tests were conducted to investigate the thermo-mechanical behavior of the loaded assembly during non-standard fire exposure. In this case, the assembly loaded to 67% of ambient temperature load carrying capacity and partially exposed to a non-standard fire for 75 minutes. Ductile embedment failure of the timber in contact with the dowels was the major failure mode at elevated temperature.

Keywords: Timber connection; Cross-Laminated Timber (CLT) beam; Steel doweled connection; Non-Standard fire; Fire-resistance; Residual strength; Post-Fire performance; Fire-Performance.

5.1. Introduction

In comparison to other types of construction materials, Cross-Laminated Timber (CLT) has advantages in architectural appearance, constructability, cost, and sustainability [1]. As such, the use of CLT has been on the rise in Europe and more recently in North America [2-4]. Although CLT has been employed mainly as large dimensional wall and floor panels in contemporary heavy timber structures, it is also possible to bring CLT into service as a 2D beam element [5]. It has been assumed that using the CLT beam will improve the performance of the beam member against brittle splitting failure. There are different retrofitting methods such as FRP strengthening [6-9], utilizing steel strips [10] and self-drilling screws [11,12] to overcome this undesirable failure, however, these solutions may cause a negative influence on the performance of the member at the dowel locations during the fire [11-13]. Additionally, steel connections play a crucial role in both seismic and fire-performance of contemporary timber structures, increasing the ductility and thereby improving the seismic performance of the structure against lateral forces.

In contrast, steel connections may be seriously affected by fire, losing strength and stiffness, leading to large plastic deformations, and contributing to progressive collapse. In general, fire-performance (FP) of steel connections in timber structures is influenced by parameters like material thermal properties, temperature dependent mechanical properties and geometry of the assembly. This is a complex thermo-mechanical problem and the

research conducted on the fire-performance of the doweled steel connections is limited to the fire tests performed in accordance with the standard fire curves [14-23]. These standard fire curves are mostly adopted by prescriptive codes, while most of the contemporary timber structures with different amount of exposed combustible timber material have been designed through performance-based design (PBD) guidelines. The design fires determined for the PBD method, include but are not limited to the standard fire curves. The heat flux of these design fires plays a significant role in charring depth and, as a result, load carrying capacity of the structural timber elements.

Additionally, most of the standard fire curves do not capture the decay phase of the real-fire and they are more suitable for comparing the performance of different type of assemblies with each other [24]. Furthermore, performing the standard fire test in the furnace restricts the loading condition, measurements, and visual access. To overcome some of these restrictions, a set of experiments was designed to investigate the thermo-mechanical behavior of CLT beam-to-girder assemblies connected by T-shaped slotted-in doweled type connections before, during and after non-standard fire.

P. Palma studied the performance of glulam beam-to-column connections at ambient and fire conditions [25]. Results showed reducing the gap between connecting members improved the fire performance of the connection. Past research, however, showed that removing the gap between connecting members led to undesirable brittle splitting failure in the glulam members (Chapter 3 and 4).

Chapter 3 presented ambient, post-fire, and fire performance tests of glulam beam-to-girder connections with full contact (no gap) between connecting elements. Results showed that ductile dowels were critical in connection performance where brittle splitting

failure in the glulam beam members was delayed or eliminated. Splitting failure in the glulam beam occurred at ambient temperatures, but only after large deformations in the connection; splitting failure was not observed in the post-fire and fire performance tests on the fire exposed connection as charring during the fire degraded the wood properties and decreased the contact between connected elements. Embedment failure in the glulam beam was the controlling failure mechanism during the fire and post-fire tests.

Chapter 4 presented ambient, post-fire, and fire performance tests of CLT wall to glulam beam connections with full contact (no gap) between connecting elements to consider the effect of changing the geometry and timber lamination orientation of the header. Results showed that the controlling failure mechanism remained to be splitting failure at ambient temperature and embedment failure in the beam during post-fire and fire performance tests despite this change in geometry.

The current study now presents a CLT beam-to-girder connection in an effort to reduce the splitting failure in the beam members. Again, ambient temperature, post-fire, and fire performance tests are considered in this research. The CLT beam-to-girder connection is a more unique configuration and research is limited on the subject.

5.2. Experimental Program

5.2.1. Assembly Description

Experimental tests were conducted on symmetric, intermediate-size CLT beam-to-girder assemblies. Figure 5.1 illustrates the CLT beam-to-girder assembly and its geometry. Each assembly was comprised of two 3-ply CLT girders connected to a CLT beam with steel connections. Each steel connection included 4 full-length steel dowels to

the joist member and 20 Type 316 stainless steel screws to each girder. Table 5.1 provides more detailed information on the dimensions and material type of each component.

Table 5.1. Components of the CLT beam-to-girder assembly.

Parts	***Quantity***	***Material***	***Dimensions***
Headers	*2*	*3-Ply CLT Girders*	*10 in. x 4.625 in. x 18 in.*
Joist	*1*	*3-Ply CLT Beam*	*10 in. x 4.625 in. x 18 in.*
Hangers	*2*	*Steel Connection A572 Gr. 50*	*Plate A: 4.5 in. x 7.5 in. x 3/16 in.* *Plate B: 4 in. x 7.5 in. x 3/16 in.*
Dowels	*2×4*	*Steel A572 Gr. 50*	*1/2 in. diameter, 4.625 in. length*
Screws	*2×20*	*Low-carbon Steel Wire Grade 1022*	*1/4 in. diameter, 3 in. length*

(a)

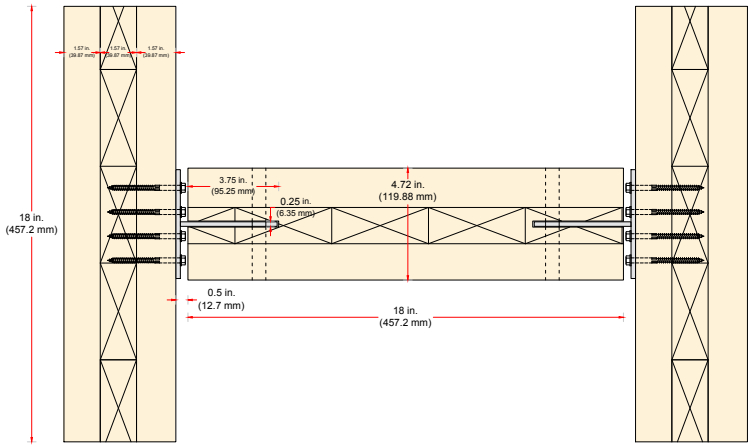

(b)

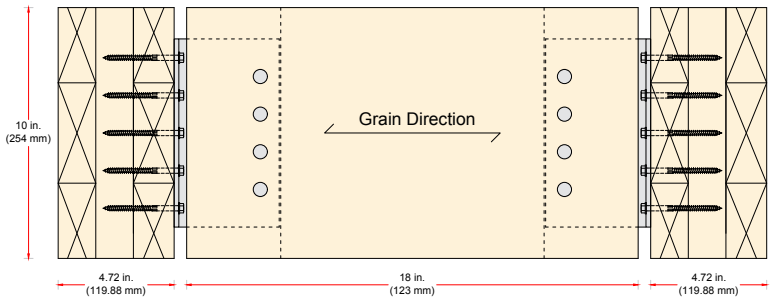

(c)

Figure 5.1. Assembly geometry: (a) test specimen, (b) top/ bottom view, (c) front view.

5.2.2. Material Description

5.2.2.1. Cross-Laminated Timber (CLT)

Both the beam and girders in the assembly studied were 18 in. long by 10 in. deep, 3-ply spruce CLT with total thickness of 4.72-inch. All the samples were loaded downward at the mid-span of the beam, in the direction perpendicular to the grain of the outside layers and parallel to the grain of the mid-layer. The CLT panels had an average moisture content (MC) of 12% (+/-2%) and density of 35 lb./ft^3 (560.7 kg/m^3). Table 5.2 shows the allowable design capacities of the CLT material used for this research.

Table 5.2. Mechanical properties of the CLT (in psi).

CLT Grade	*Bending (F_b)*	*Tension Parallel to the Grain (F_t)*	*Compression Parallel to the Grain (F_c)*	*Shear Parallel to the Grain (F_v)*	*Shear in the Plane (F_s)*	*Elastic Modulus (E)*
CV3M1	*975*	*550*	*1450*	*175*	*55*	*$1.6x10^6$*

**Note: For SI: 1psi = 0.006895 MPa*

5.2.2.2. Steel Connection

The custom T-shaped welded steel doweled connection fabricated from gauge 7 ASTM A572 Gr 50 [26] structural steel welded with 1/8" full-length fillet weld on both sides. Figure 5.2 displays the welded steel doweled connection and its geometry.

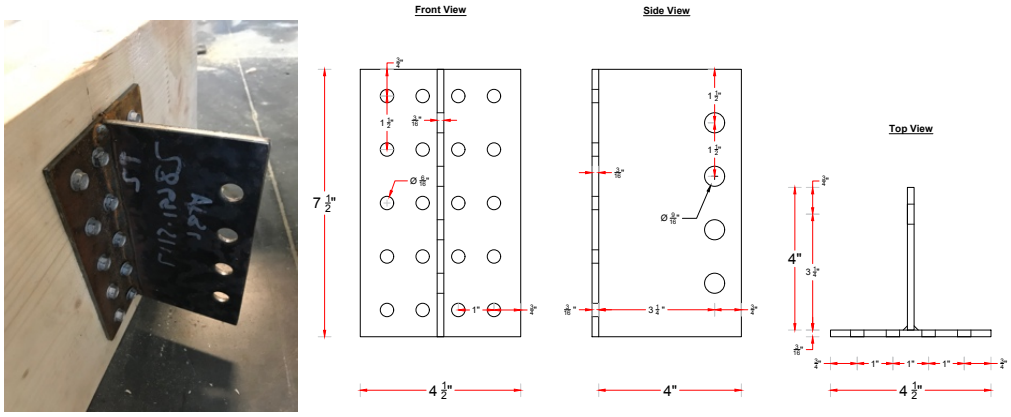

Figure 5.2. Image and geometry of T-shaped welded steel connection.

5.2.2.3. Steel Dowels and Fasteners

The full-length dowels (4.72 in.) are cut from ½" steel rods with similar material property as the steel connection (ASTM A572 Gr 50). The ¼" diameter heavy-duty hexagonal connector screws with 3" length and 2" thread are manufactured from low-carbon steel wire grade 1022. This fastener has 164,000 psi bending yield strength, 1,430 lbf allowable tensile strength and 800 lbf allowable shear strength. Figure 5.3 shows the steel dowels and screws placed on top of the CLT beam.

Figure 5.3. 3-Ply CLT beam, full-length steel dowels and heavy-duty screws.

5.2.3. Experimental Setup

Six CLT beam-to-girder assemblies were tested in total – four at ambient temperature, one post-fire and one during fire. Figure 5.4, Figure 5.5, and Figure 5.6 show the ambient temperature, post-fire, and fire performance test setup, respectively. Additional details on each of the test setup is found in Chapter 3.

Figure 5.7 shows a photo of the two-step post-fire test, including 30 minutes of nonstandard fire exposure of approximately 900 °F and subsequent cooling, followed by mechanical loading to failure. Figure 5.8 shows a photo of the fire performance test, including the application of constant mechanical load equivalent to 66% of the ambient temperature assembly capacity along with nonstandard fire exposure of approximately 900 °F until failure. Figure 5.9 and Figure 5.10 show the locations of the thermocouples used in the post fire and fire performance tests, respectively.

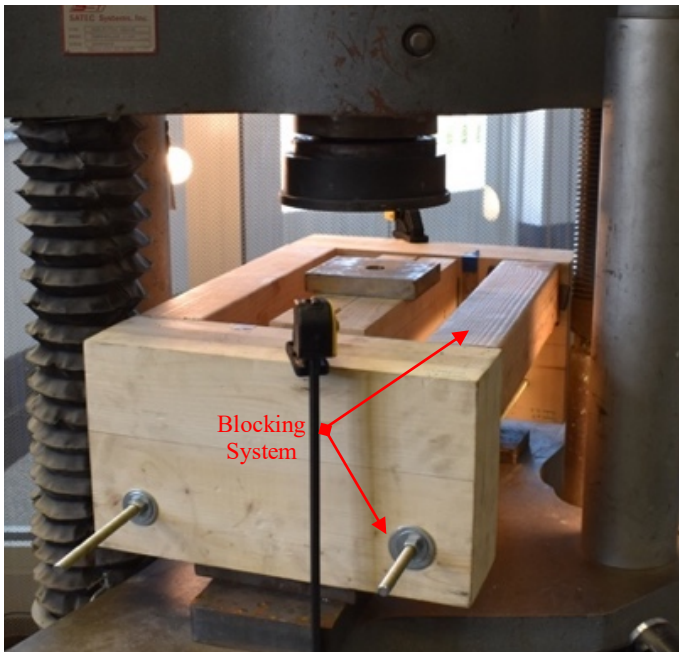

Figure 5.4. Test set-up and instrumentation utilized for testing at ambient temperature.

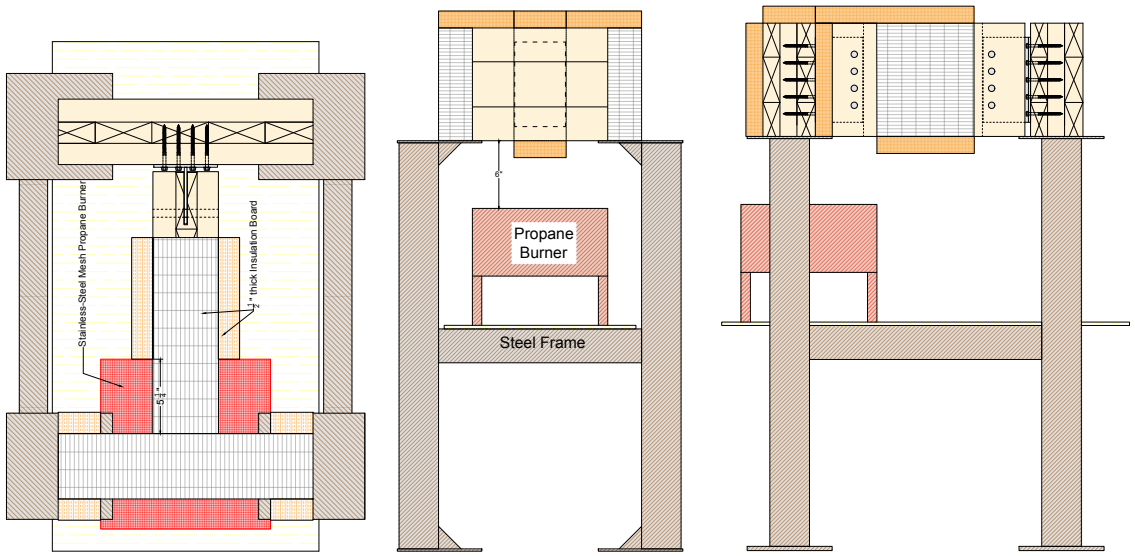

(a) *(b)* *(c)*

Figure 5.5. PFP30 fire test set-up, (a) top View, (b) side view, (c) front view.

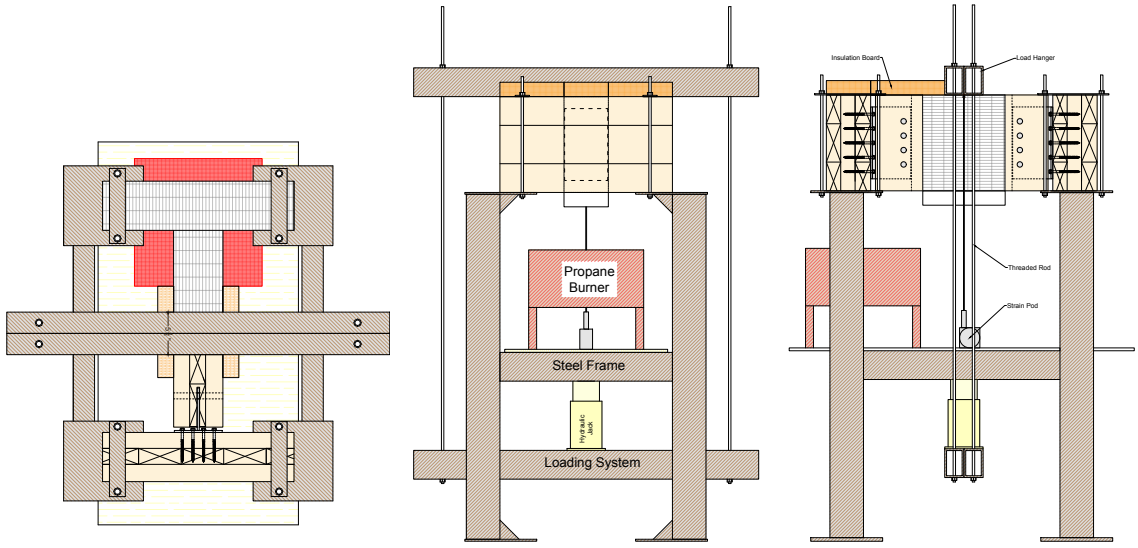

(a) *(b)* *(c)*

Figure 5.6. FP test set-up, (a) top view, (b) side view, (c) front view.

(a) (b)

Figure 5.7. PFP30 test procedure: (a) non-standard fire test, (b) loading at ambient temperature.

Figure 5.8. Fire-performance test of the CLT beam-to-girder assembly.

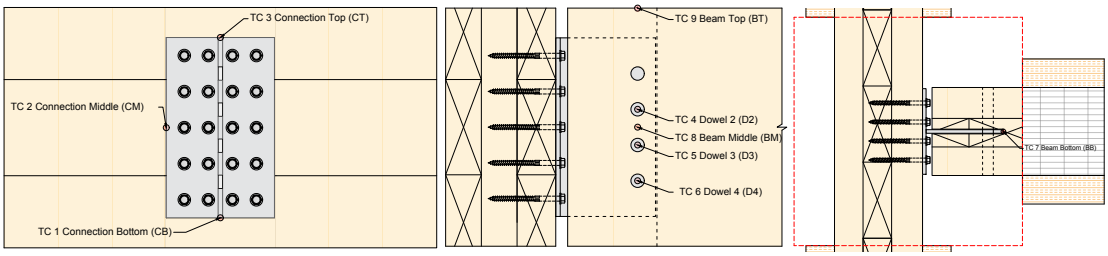

Figure 5.9. Thermocouples arrangement for PFP30 test.

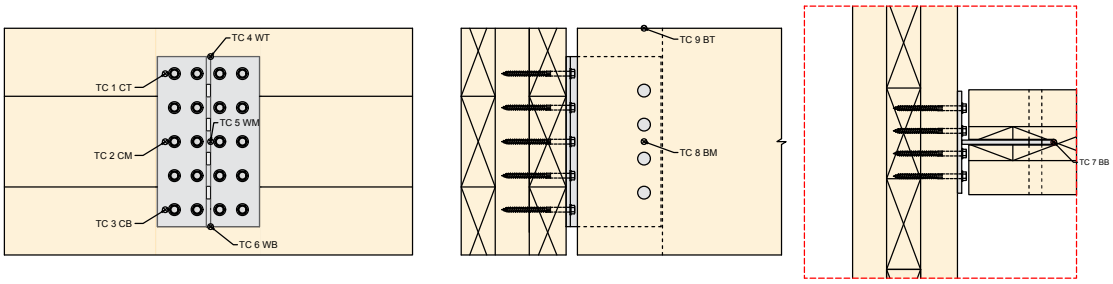

Figure 5.10. Thermocouples arrangement for FP test.

5.3. Test Results and Discussion

5.3.1. Ambient Temperature Results

Four replicas of the CLT beam-to-girder assembly were tested at ambient temperature. The first two tests were stopped after initial failure occurred and investigated to establish the primary failure modes. Assemblies 3 and 4 were loaded until failure and the load-carrying capacity and deflection at the mid-span of the assemblies were recorded. Figure 5.11 shows the load-displacement of the CLT beam-to-girder assemblies tested at ambient temperature (AT) for replicas 3 and 4. The average load-carrying capacity of this assembly was 33 kips. The elastic region of the curve has an average slope of 60 (k/in).

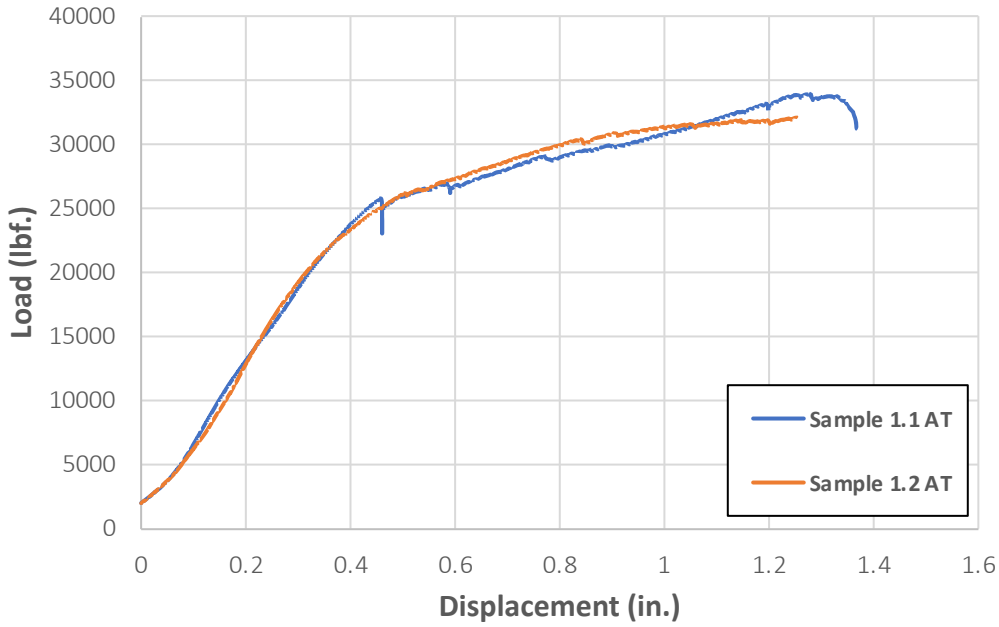

Figure 5.11. Load-displacement of the CLT beam-to-girder assembly at ambient temperature (AT).

Figure 5.12 shows the failure modes that occurred during the ambient temperature test in the order observed. The failure in this assembly was triggered by the plastic embedment failure and bending of the dowels. Then row shear failure occurred in the mid-vertical layer of the CLT beam loaded in shear parallel to the grain at the dowel location (drop in the curve around 0.6 in. displacement) and finally the test stopped after the partial splitting failure occurred at the outside layer of CLT beam and girders. In the outside layers where the dimensional lumbers laid out horizontally, the transferred shear load produced a tension perpendicular to the grain direction and a brittle splitting failure occurred.

Figure 5.12. Ambient temperature failure modes sequence (a) embedment and bending of the dowels, (b) Row shear in the mid-layer, (c) splitting failure of the header side, (d) splitting failure of the beam side.

5.3.2. Post-Fire Performance Test Results

One sample was tested to study the post-fire performance, stiffness degradation and residual load-carrying capacity of the CLT beam-to-girder assembly after heating and subsequent cooling. The results of the 30-minute post-fire performance (PFP30) test include the heat distribution during the 30 minutes of fire exposure and the load-displacement behavior of the burnt sample at the mid-span.

Figure 5.13 shows heat distribution along the sample during the post-fire test. The burner temperature rapidly increased for the first 3-4 minutes to approximately 900 °F and then ranged from approximately 640 °F to 1040 °F for the duration of the fire, with the

slight fluctuations in temperature due to the manually controlled through a gas flow. The figure also shows the ASTM E119 standard fire curve for comparison.

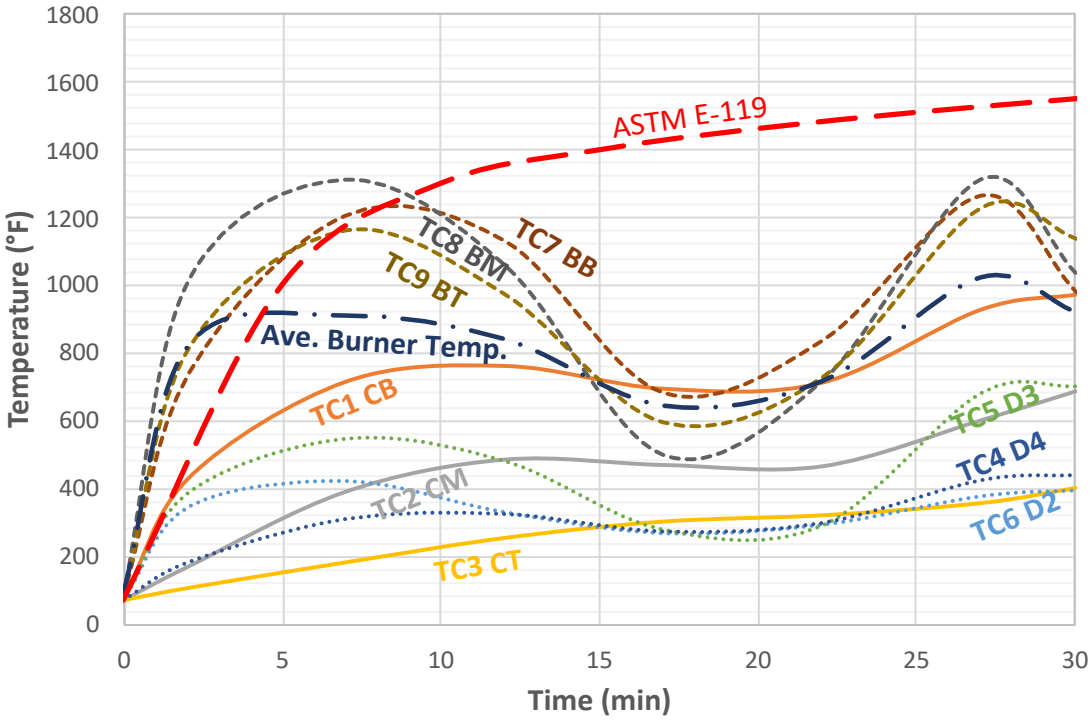

Figure 5.13. PFP30 test result; heat distribution along the exposed area.

The beam temperatures at the location of TCs 7, 8 and 9 (bottom, middle, and top of the beam) reached the wood ignition temperature (570°F) and then began to increase in comparison to the burner temperature after one minute. Figure 5.14 Shows visual confirmation of ignition over the height of the beam 1 minute into the fire test.

Temperature of the three lower dowels at their tips were recorded by TCs 4, 5 and 6. The temperature of the dowel tips followed the same fluctuation pattern as the beam and burner and reached a maximum temperature of 700 °F. TCs 1, 2 and 3 recorded the temperature at the bottom, middle and top of the steel connection. After 30 minutes of fire exposure the maximum temperature in the bottom of the connection was 975 °F and the

difference between bottom, middle and top of the connection was approximately 285 °F. According to the former studies [28, 29] the post-fire mechanical properties of ASTM A572 Gr 50 remains unaffected after exposure to temperatures up to 1112 °F (600 °C). Therefore, no reduction in residual strength of the steel connection is expected.

Figure 5.14. CLT beam ignited in the beginning of the fire test.

According to Figure 5.15, the load-carrying capacity of the assembly after 30 minutes of fire exposure was reduced to 18.4 kips, 55.8% of the ambient temperature capacity. Since the steel connection itself is expected to maintain its ambient temperature strength, this reduction in capacity is attributed to a gross loss of wood cross-section due to charring and loss of strength in the thermal penetration zone behind the char layer.

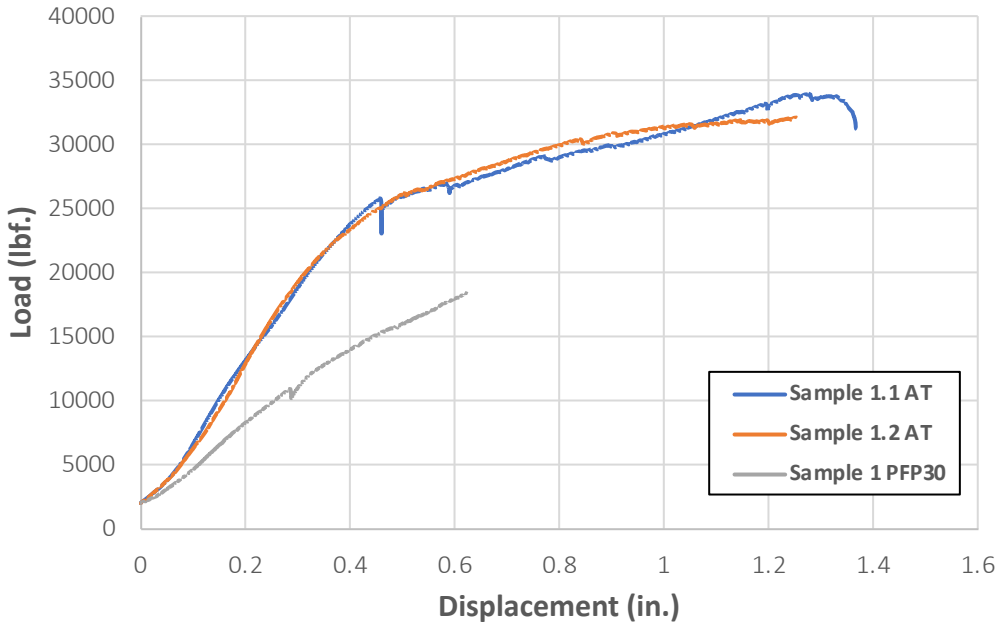

Figure 5.15. Load-displacement of CLT beam-to-girder assembly loaded after 30 minutes fire exposure.

Figure 5.16 shows the failure modes in the post-fire performance test replica. The embedment failure of the dowels was the dominant failure mode followed by row shear of the mid-layer of the CLT beam and plug shear of the CLT girder.

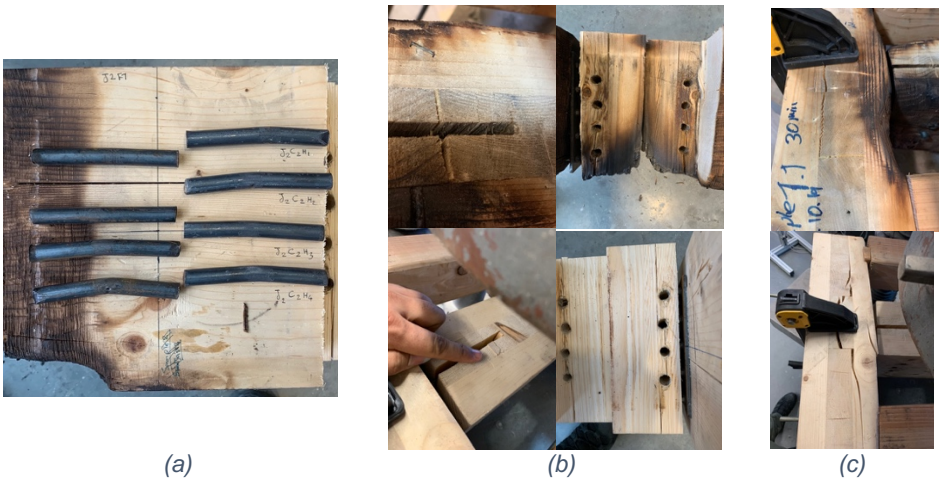

(a) (b) (c)

Figure 5.16. Post-fire performance failure modes sequence (a) embedment failure, (b) row shear in the mid-layer, (c) tear-out of the header sides.

5.3.3. Fire-Performance Test Results

The fire resistance (FR) of the CLT beam-to-girder assembly was studied through the coupled application of thermal and mechanical loading. A constant load equal to 22 kips (approximately 67% of the expected load-carrying capacity of the assembly at ambient temperature) was imposed while a nonstandard fire of approximately 900 °F was applied until failure.

Figure 5.17 shows the heat distribution along the exposed area during the FP test. According to the recorded heat distribution, the bottom of the CLT beam ignited after 2 minutes. This statement is confirmed by the visual observations and recorded videos. The beam bottom temperature increased until the 9th minute and then decayed for the remained for the fire loading. The connection temperature reached its maximum temperature of 1400 °F after 40 minutes in the bottom (at the middle and along the edge of the weld). Between minutes 40 and 75 the temperature of the middle and top of the connection increased significantly, and the steel connection reached nearly 1100 °F at the end of the test. At these temperatures, a reduction in strength and stiffness of the steel connection is expected. However, due to the reserve strength of the capacity during design, the steel connection itself does not experience failure.

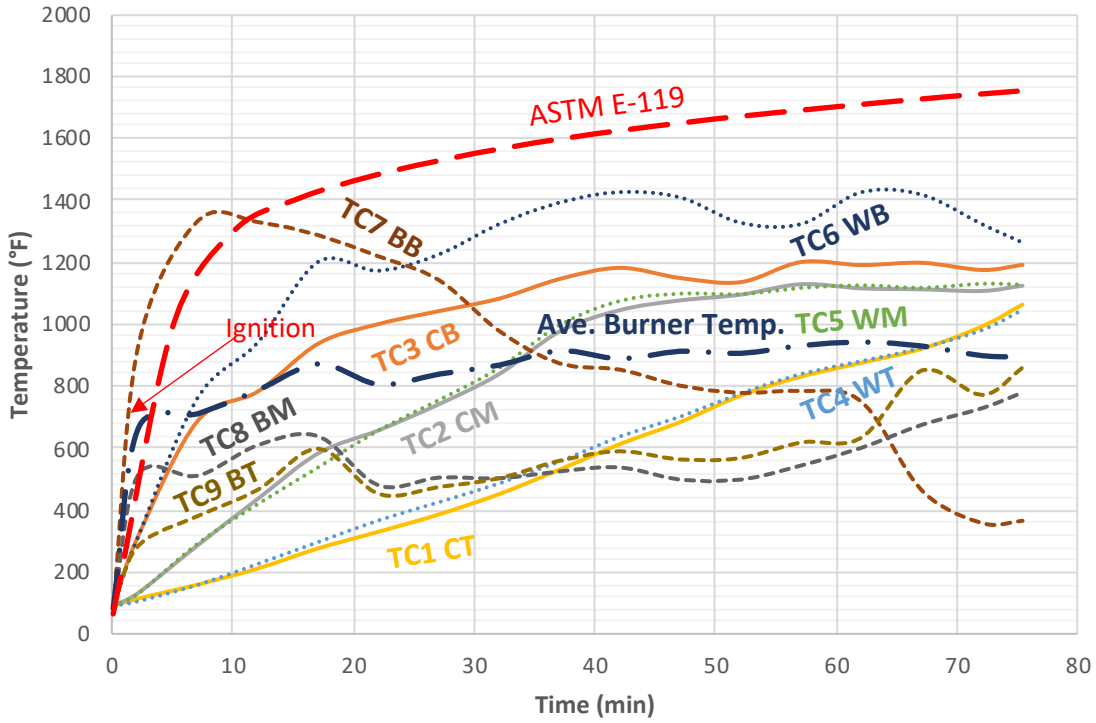

Figure 5.17. Heat distribution along the exposed area during the fire-performance test.

Figure 5.18 shows the deflection of the CLT beam at the mid-span recorded during the FP test. According to this figure, the sample failed after 55 minutes of non-standard fire exposure. The maximum displacement ratio occurred at this point and it was 0.01 (in/min).

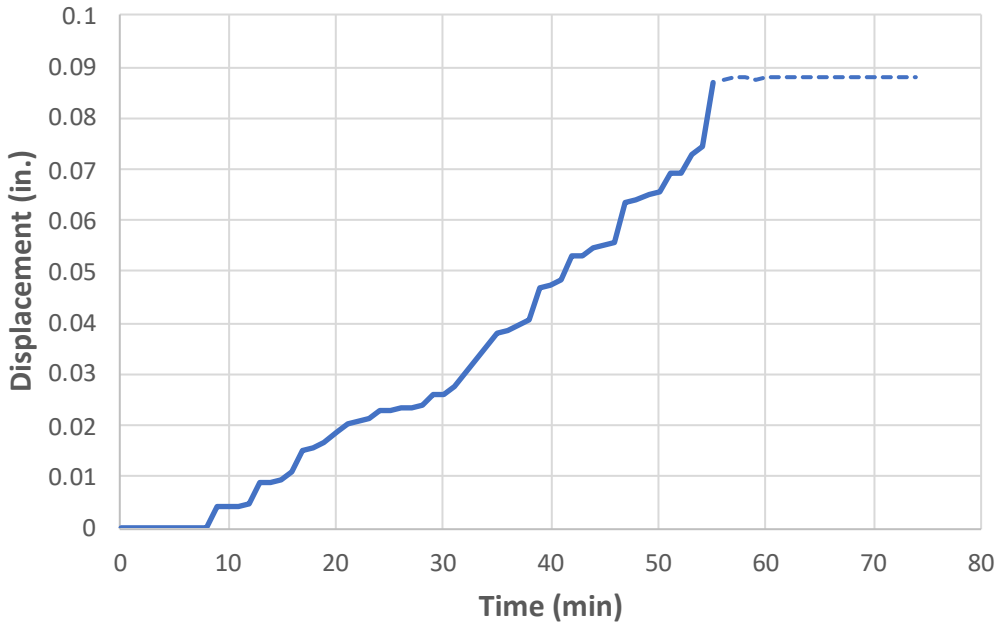

Figure 5.18. Displacement vs time at the mid-span of the CLT beam during the fire-performance test.

Figure 5.19 shows a series of video captures taken from the videos recorded during fire-performance test. Onset of ignition at the beam bottom can be seen at 2 minutes. The charring development around the connection is obvious in these pictures. The CLT beam started charring from the bottom corner and the lowest dowel was exposed after 30 minutes to the fire. This was where the embedment failure of the CLT beam was captured for the first time. By the end of the test, the lowest dowel was only surrounded with char.

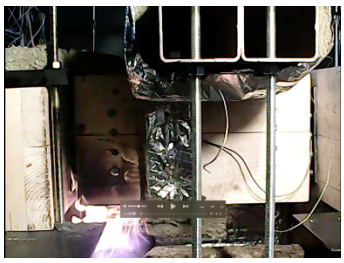

t=2 min.

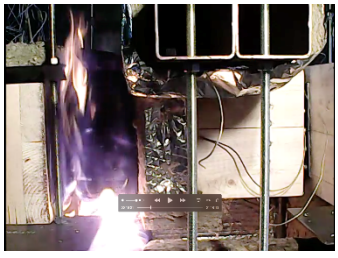

t=15 min.

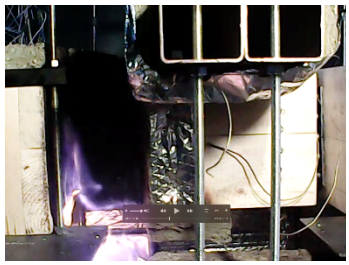

t=30 min.

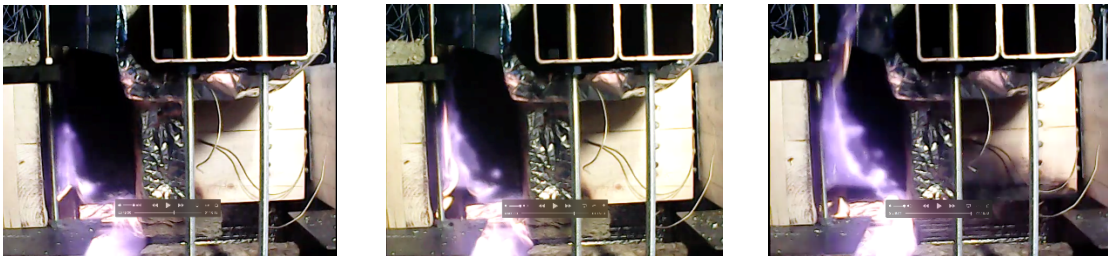

t=45 min. t=60 min. t=75 min.

Figure 5.19. Video shots recorded during fire-performance test.

Figure 5.20 shows the failure modes captured during the FP test. The failure initiated by embedment failure around the lower dowels (Figure 5.20.a) and followed by bending in the top dowel (Figure 5.20.b).

(a) (b)

Figure 5.20. FP test images: (a) embedment failure of the beam at the lower dowel location, (b) bending of the dowel 1 (D1) at the end of FP test.

Returning to Figure 5.17, the temperature of the connection at the time of failure at 55 minutes was nearly 1200°F at the bottom of the connection. At 1200°F the steel is expected to maintain only 35% of its ambient temperature yield strength. Failure, however, was not observed in the steel connection itself, but instead in the timber elements. This is

attributed to the extensive charring that occurred in the timber which in turn weakened the timber and led to the embedment failure in the beam.

Figure 5.21 shows the residual section of the CLT beam to girder assembly after the fire-performance test. Extensive charring occurred around the steel connection. The maximum char depth in the girder side occurred at the bottom and was equal to 1.6-in. The charring progress happened faster in the mid-layer of the CLT-beam in comparison with the exterior layers. In the assembly, changes in the geometry and boundary condition caused a rotation in the steel connection. However, as there was no contact between beam and girder, this rotation followed by a plastic deformation in the lower edge of the steel connection.

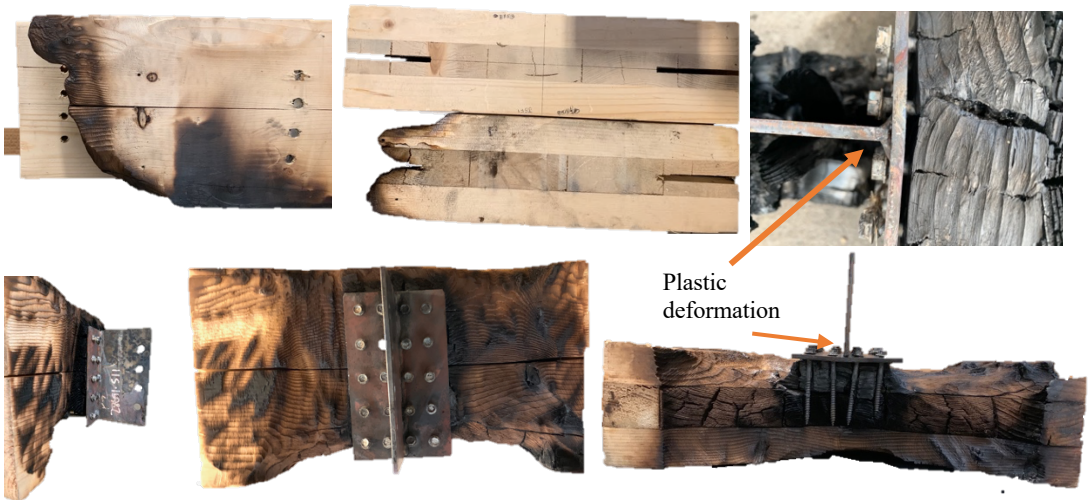

Figure 5.21. Residual section of the CLT beam to girder assembly after the fire-performance test.

5.4. Conclusions

This experimental study demonstrated the performance of a CLT beam-to-girder assembly connected with T-shaped connections subject to vertical load before, during and after non-standard fire.

For the assemblies tested at ambient temperature, ductile embedment failure of the CLT-beam around the dowels and plastic bending of dowels were the dominant failure modes This is significant inasmuch that brittle, splitting failure of the beam was not the controlling failure mechanism as is often seen in similar connections with timber elements loaded perpendicular to the grain. The samples also experienced secondary failures due to row shear failure in the mid-layer of the CLT-beam and splitting failure between the screws and finally at the outside layers of the CLT-beam.

For the assembly loaded after 30 minutes non-standard fire exposure (Post-fire performance test) embedment failure, bending of the dowels, row shear failure of the beam, and plug shear of the headers occurred, but importantly, no splitting occurred in the CLT members. The load carrying capacity of the assembly was reduced by 44% compared to the ambient capacity. The maximum recorded temperature of the steel connection during the PFP test was 975 °F. Therefore, the reduction in load-carrying capacity of the assembly is attributed to the gross loss of wood cross-section due to charring and loss of strength in the thermal penetration zone behind the char layer.

For the loaded assembly tested during the non-standard fire (Fire-performance test), ductile embedment failure and bending of the top dowel were the only failure modes observed when the specimen failed after 55 minutes of coupled fire and mechanical loading, with an imposed load of 67% of ambient capacity. In this case, the steel connection deformed slightly in the lower edge.

In both the post-fire and fire performance tests, extensive charring in the assemblies caused a degradation of timber strength and gross loss of section. The presence of the steel

connection promoted the charring process and facilitated the failure of the wooden beam at the connection area.

5.5. REFERENCES

[1] Barber, D., *Fire Safety of Mass timber Buildings with CLT in USA.* Wood and Fiber Science, 2018: p. 83-95.

[2] Smith, I. and A. Frangi, *Use of timber in tall multi-storey buildings*. 2014: International Association for Bridge and Structural Engineering (IABSE).

[3] Gagnon, S. and C. Pirvu, *CLT handbook: cross-laminated timber*. 2011: FPInnovations.

[4] Institute, A.N.S., *Standard for performance-rated cross-laminated timber. ANSI/APA PRG 320-2012*. 2012, APA-The Engineered Wood Association Tacoma, Washington.

[5]. Tuhkanen, E., J. Mölder, and G. Schickhofer, *Influence of number of layers on embedment strength of dowel-type connections for glulam and cross-laminated timber.* Engineering structures, 2018. **176**: p. 361-368.

[6] Gilfillan, J., S. Gilbert, and G. Patrick, *The use of FRP composites in enhancing the structural behavior of timber beams.* Journal of reinforced plastics and composites, 2003. **22**(15): p. 1373-1388.

[7] Dempsey, D.D. and D.W. Scott, *Wood members strengthened with mechanically fastened FRP strips.* Journal of Composites for Construction, 2006. **10**(5): p. 392-398.

[8] Li, Y.-F., et al., *A study on wood beams strengthened by FRP composite materials.* Construction and Building Materials, 2014. **62**: p. 118-125.

[9]. Solarov, R. and M. Glišić, *Glulam beams reinforced with frp strips and their application in architecture.* Spatium, 2014: p. 1-6.

[10] Franke, S., B. Franke, and A.M. Harte, *Failure modes and reinforcement techniques for timber beams–State of the art.* Construction and Building Materials, 2015. **97**: p. 2-13.

[11] Palma, P., et al. *Fire resistance tests on steel-to-timber dowelled connections reinforced with self-drilling screws*. in *2nd CILASCI–Ibero-Latin-American Congress on Fire Safety Engineering*. 2013. Eidgenösische Technische Hochschule Zürich.

[12] BlaB, H.J. and M. Schmid, *Self-tapping screws as reinforcement perpendicular to the grain in timber connections.* Joints in Timber Structures: Stuttgart, Germany, 12-14 September 2001, 2001: p. 163.

[13] Martin, Z. and D.A. Tingley. *Fire resistance of FRP reinforced glulam beams*. in *World Conference on Timber Engineering, Whistler Resort, British Columbia, Canada*. 2000.

[14] Palma, P. and A. Frangi, *Modelling the fire resistance of steel-to-timber dowelled connections loaded perpendicularly to the grain.* Fire Safety Journal, 2017.

[15] Hofmann, V., et al., *Fire resistance of primary beam–secondary beam connections in timber structures.* Journal of Structural Fire Engineering, 2016. **7**(2): p. 126-141.

[16] Khelifa, M., et al., *Analysis of the behavior of multiple dowel timber connections in fire.* Fire Safety Journal, 2014. **68**: p. 119-128.

[17] Audebert, M., et al., *Experimental and numerical analysis of timber connections in tension perpendicular to grain in fire.* Fire Safety Journal, 2014. **63**: p. 125-137.

[18] Peng, L., et al., *Fire Performance of Timber Connections, Part 1: Fire Resistance Tests on Bolted Wood-Steel-Wood and Steel-Wood-Steel Connections.* Journal of Structural Fire Engineering, 2012. **3**(2): p. 107-132.

[19] Audebert, M., et al., *Behavior of dowelled and bolted steel-to-timber connections exposed to fire.* Engineering Structures, 2012. **39**: p. 116-125.

[20] Audebert, M., et al., *Numerical investigations on the thermo-mechanical behavior of steel-to-timber joints exposed to fire.* Engineering Structures, 2011. **33**(12): p. 3257-3268.

[21] Moss, P., et al., *Experimental testing and analytical prediction of the behaviour of timber bolted connections subjected to fire.* Fire Technology, 2010. **46**(1): p. 129.

[22] Erchinger, C., A. Frangi, and M. Fontana, *Fire design of steel-to-timber dowelled connections.* Engineering Structures, 2010. **32**(2): p. 580-589.

[23] Erchinger, C., A. Frangi, and A. Mischler. *Thermal investigations on multiple shear steel-to-timber connections*. in *9th World Conference on Timber Engineering*. 2006. Citeseer.

[24] Palma, Pedro. *Fire behaviour of timber connections*. Diss. ETH Zurich, 2016.

[25] Gales, J., B. Chorlton, and C. Jeanneret, *The Historical Narrative of the Standard Temperature–Time Heating Curve for Structures.* Fire Technology, 2020: p. 1-30.

[26] ASTM A572 / A572M-18, *Standard Specification for High-Strength Low-Alloy Columbium-Vanadium Structural Steel*, ASTM International, West Conshohocken, PA, 2018, www.astm.org.

[27] ASTM D7147-11(2018), *Standard Specification for Testing and Establishing Allowable Loads of Joist Hangers*, ASTM International, West Conshohocken, PA, 2018, www.astm.org.

[28] Sajid, H.U. and R. Kiran, *Post-fire mechanical behavior of ASTM A572 steels subjected to high stress triaxialities.* Engineering Structures, 2019. **191**: p. 323-342.

[29] Lee, J., M.D. Engelhardt, and E.M. Taleff, *Mechanical properties of ASTM A992 steel after fire.* 2012.

6. NUMERICAL STUDIES ON THERMO-MECHANICAL PERFORMANCE OF STEEL DOWELED CONNECTIONS USED IN HEAVY TIMBER ASSEMBLIES.

Milad Shabanian [a], Nicole Leo Braxtan [a]

[a] University of North Carolina at Charlotte, Department of Civil and Environmental Engineering, 9201 University City Blvd, Charlotte, NC, 28223, United States

Highlights

- A coupled temperature-displacement finite element model capable of simulating the thermo-mechanical behavior of steel connection developed.
- Thermal performance of the steel connection in PFP tests validated by the developed model.
- The mechanical performance of the steel connection studied numerically at ambient temperature.
- The thermo-mechanical performance of the connection during non-standard and standard fire investigated numerically.

Abstract

A coupled temperature-displacement finite element model was developed in ABAQUS/CAE to study the thermo-mechanical behavior of T-shape steel connections at ambient temperature, during and after fire exposure. The FE model was validated through comparison with the experimental data gathered during post-fire-performance tests conducted on the intermediate assemblies with ASTM A572 Gr50 steel connections presented in chapters 4, 5 and 6. The validated model was then used to study the thermo-

mechanical performance of the steel connections at ambient temperature and during non-standard and standard fire exposure.

Keywords: Finite Element analysis; T-shape Steel Connection; Fire-performance; Coupled temperature-displacement model

6.1. Introduction

Recent developments in engineered wood products and construction standards have increased the demand for heavy timber construction. Considering the vital role of connections in transferring load in the structural load path and the increased attention given to the performance of structures during fire, it is essential to improve the overall knowledge of thermo-mechanical behavior of the connections in timber structures. As the history of heavy timber construction spans many centuries [1], the mechanical performance of connections in heavy timber structures has been well studied at the ambient temperature [2]. However, the design recommendations related to the performance of connections at elevated temperatures are based on a limited number of experiments, mostly performed on timber assemblies loaded in tension [3-5]. Considering the difficulties and expenses of conducting fire experiments on combustible heavy timber assemblies, numerical simulation offers a cost-effective, alternative solution. Existing literature presents experimental studies and numerical simulations investigating the fire-performance of timber connections [6-10]. These studies are all performed on timber elements connected with bolts and loaded in tension. There are also limited studies validating the fire-performance and load-carrying capacity of assemblies loaded perpendicular to the grain

with finite element simulations [11-13]. The experiments conducted for these studies were all under standard fire condition and in closed furnaces with limited access to the connections. Finite element simulation of heavy timber assemblies connected with steel connections loaded perpendicular to the grain and exposed to fire is a complex problem. This model should include temperature-dependent thermal and mechanical material properties and would require simulating the change in geometry and boundary condition.

Due to the complexity in modeling the change in geometry of the combustible timber material, this research focused only on the steel connection as an initial solution. This paper presents the numerical studies conducted on the T-shape steel connection tested before, during and after non-standard fire exposure. For this purpose, a three-dimensional, coupled thermal-stress finite element model was developed using ABAQUS/CAE software. The model was used to conduct three sets of numerical studies on the T-shape steel connection: (1) analyzing the steel connection at ambient temperature; (2) validating the coupled heat-transfer FE model with post-fire performance (PFP) test results; and (3) coupled thermo-mechanical FP analyses. These finite element model will also serve as a tool for future expanded numerical studies investigating the fire-performance of T-shape steel connections used in timber structures.

6.2. Finite Element Simulation

The finite element model of the steel connection was generated using ABAQUS/CAE, hosted on a UNC Charlotte Linux server with a 64 core AMD CPU and 1 TB memory. Then, the analyses were submitted to the ABAQUS software solver in the

UNC Charlotte COPPERHEAD cluster. The Redhat Linux based high-performance computing environment permitted submitting multiple simulations simultaneously.

6.2.1. Finite Element Model

A unique finite element model was developed to study the thermo-mechanical behavior of the T-shape steel connections exposed to different thermal conditions. This model can be used in heat-transfer, stress, and coupled thermal-displacement simulations. However, to follow a consistent methodology in this study, only coupled thermal-displacement analyses were conducted. The focus of this research was on performance of steel connections in timber structures. Therefore, only the steel connection was modeled.

Figure 6.1 shows the T-shaped steel connection utilized in intermediate size assemblies and the 3D deformable part created for this study in accordance with the dimension of the steel connection (Figure 3.2). SI units consistent with mm, kg, seconds, and ˚C were used throughout the model.

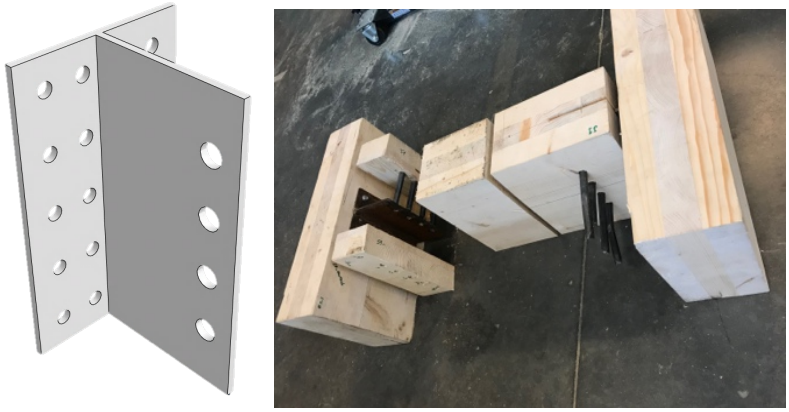

Figure 6.1. T-shape steel connection utilized in intermediate size assemblies.

6.2.2. Material Properties

The T-shape steel connection was fabricated from ASTM A572 Grade 50 structural steel [14]. Figure 6.2 shows the temperature-dependent thermo-mechanical properties defined in the model, prescribed by Eurocode, EN 1993-1-2:2005 [15].

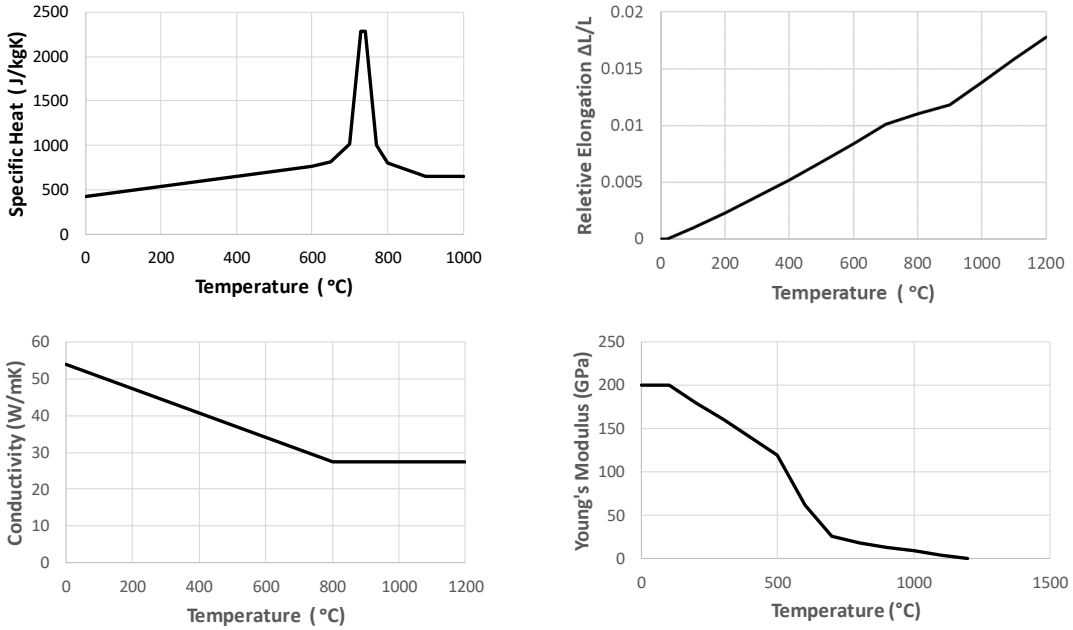

Figure 6.2. Temperature-dependent thermo-mechanical material properties [15].

The Johnson-Cook (JC) plasticity model was used to simulate the plastic hardening behavior of the steel material [16]. Table 6.1 describes the mechanical material properties and JC model constants used in finite element simulations [17]. Parameters A, B, C, n, and m are material constants.

The JC plastic hardening model is an isotropic hardening model defining the yield stress as a function of equivalent plastic strain and temperature (Eq. 6.1).

$$\sigma = [A + B(\bar{\varepsilon}^{pl})^n](1 - \hat{\theta}^m) \qquad \text{Eq. 6.1}$$

Table 6.1. Material properties and JC model constants for use in FE simulation [17].

Young's modulus	***Poisson's ratio***	***Density***	***Melting Temperature***	***Transition Temperature***
200 GPa	0.3	7850 kg/m^3	1500 ^{o}C	20 ^{o}C
A	*B*	*C*	*n*	*m*
348 MPa	900 MPa	*0.032*	*0.434*	*1*

In this equation $\bar{\varepsilon}^{pl}$ is the equivalent plastic strain, and A is a constant JC plasticity parameter equal to yield stress at transition temperature (ambient temperature in this case). B, n and M are also JC plasticity parameters measured form material calibration at or below transition temperature ($\theta_{transition}$). $\hat{\theta}$ is the nondimensional temperature measured using equation 6.2.

$$\hat{\theta} \equiv \begin{cases} 0 & for \quad \theta < \theta_{transition} \\ \dfrac{(\theta - \theta_{transition})}{(\theta_{melt} - \theta_{transition})} & for \quad \theta_{transition} \leq \theta \leq \theta_{melt} \\ 1 & for \quad \theta > \theta_{melt} \end{cases} \qquad \text{Eq. 6.2}$$

6.2.3. Finite Element Mesh

An independent instance of the connection part was created in the assembly module. The instance was partitioned precisely to allow for structured meshing. Figure 6.3.a shows the partitioned instance and the partitioning pattern. Figure 6.3.b shows the meshed assembly. The partitioned assembly was meshed with standard, coupled temperature-displacement hexahedral-shaped elements (C3D8T). The mesh size was controlled by setting the approximate global seed size equal to 1.

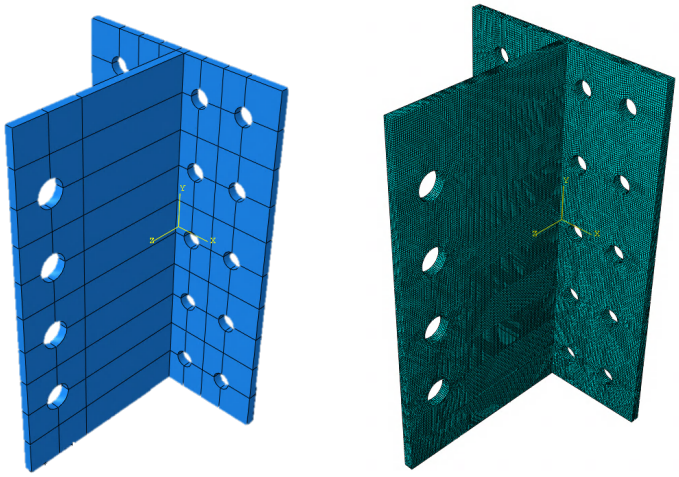

(a) *(b)*

Figure 6.3. (a) Partitioned instance and (b) fine structured mesh.

6.2.4. Model Validation

The FE model was validated against the results from the post-fire performance experiments presented in Figures 4.12, 4.14, and 5.13. Nodal temperatures were calculated through the coupled temperature-displacement finite element analysis and compared to the experimental test results. The model was then used to compare the performance of the connection at ambient temperature and during non-standard and standard fire.

6.2.4.1. Thermal Validation

The finite element model was validated by comparing temperature data output from thermocouples during experimental PFP testing with nodal temperatures calculated in Abaqus. FE model thermal boundary conditions were prescribed along the bottom surface of the connection simulating the heat input at the exposed lower surface of the connection; recall that the remainder of the connection surface was enclosed within the timber components and thus not directly exposed to the fire. Specifically, the temperatures

recorded during the PFP experiments at the bottom of the connections (TC1-CB) and dowel locations (TC4-D2, TC5-D3, TC6-D4) were used as the imposed thermal boundary condition for the FE model. Temperatures across the entire connection were then calculated by Abaqus through a nonlinear, transient heat transfer analysis. Figure 6.4, 6.5 and 6.6 compare the nodal temperatures calculated at top and middle of the connections during the FE simulations with the temperatures measured during the PFP experiments. The finite element analysis heat distribution output along the connection appears to be a good approximation of the experimental results. Temperatures of the connection increased more gradually in the beginning of the FE simulations in comparison to the PFP experiments, while this condition changed as time progressed and the FE model ultimately estimated higher temperature at the end of the simulation.

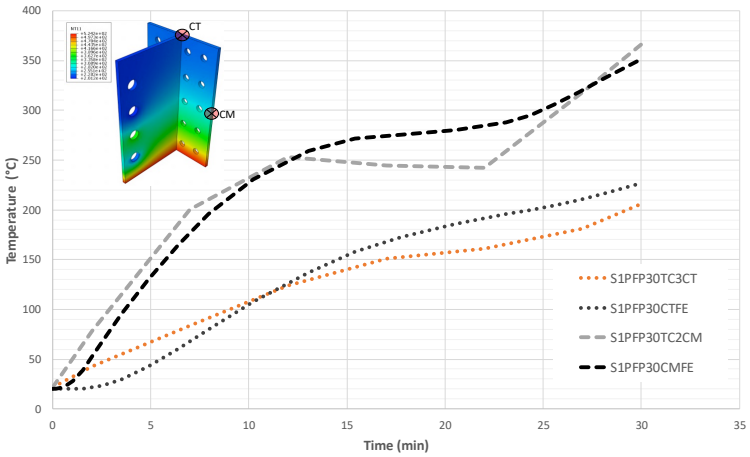

Figure 6.4. PFP30 experimental and simulated temperature of steel connection in CLT beam-to-girder assembly.

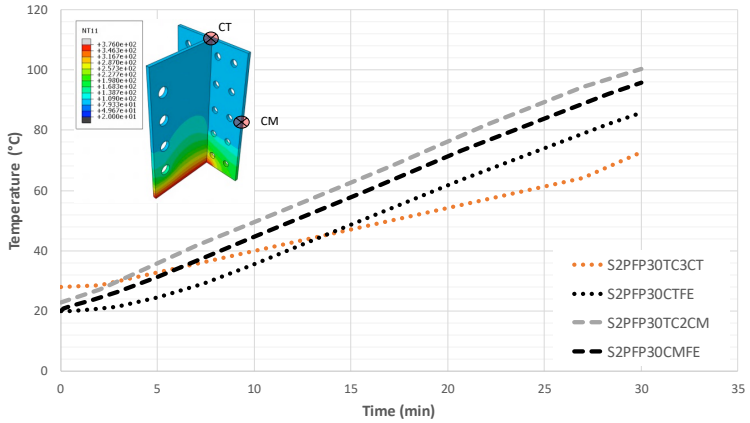

Figure 6.5. PFP30 experimental and simulated temperature of steel connection in glulam-beam to CLT-wall assembly.

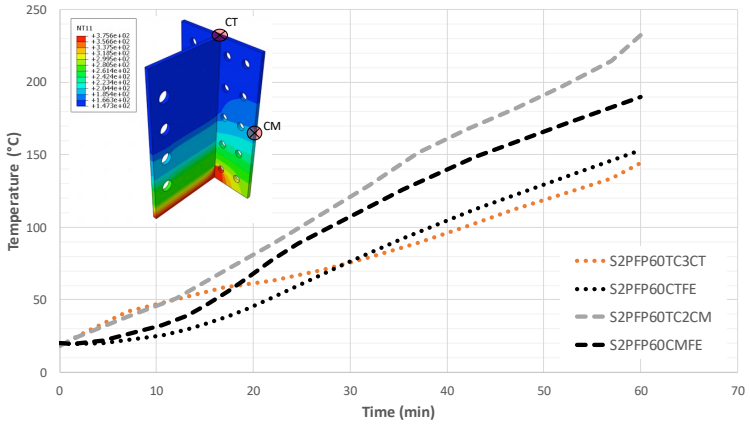

Figure 6.6. PFP60 experimental and simulated temperature of steel connection in glulam-beam to CLT-wall assembly.

The small temperature differential between the FE simulations and experimental test results, is attributed to three factors when approximating the post fire experiments with the FE model. The primary factors are related to the complex and evolving boundary conditions over the duration of fire exposure. First, the heat transfer through the timber elements was neglected in the FE simulations to simplify the model. As the fire progresses, the timber elements transform to char. The low conductivity of the char layer in contact with the steel connections changed the boundary condition of the contact surfaces and the

resulting heat transfer between the steel and timber elements. Figure 6.7 shows the surface area of the connection in contact with timber.

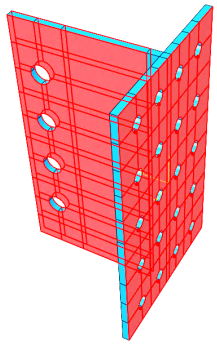

Figure 6.7. Neglected surfaces of steel connection in contact with timber.

Second, the thermal boundary conditions prescribed to simulate the fire exposure were not identical to the experiments. In the finite element model, it was assumed that the connection was exposed to the fire only on the bottom surface. This is while in CLT beam-to-girder assembly, there was a small gap between the connection and beam members, and the steel connections were also exposed, but to a lesser extent, to the fire on the surfaces parallel to the fire direction. Figure 6.8 shows the exposed surfaces parallel to the fire exposure direction.

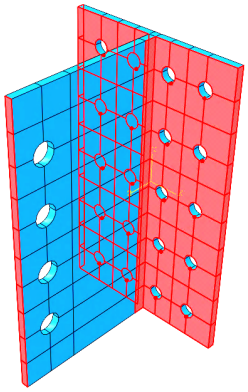

Figure 6.8. Neglected surfaces of steel connection parallel to the non-standard fire exposure.

Lastly, the thermal properties of the structural steel were prescribed from Eurocode, EN 1993-1-2:2005 and were not the exact material properties of the ASTM A572 GR50 tested. They were selected as the closest approximation in absence of actual material tests and would not likely cause large discrepancies.

6.2.5. Thermo-Mechanical Performance

The validated model was then used to study (1) the thermo-mechanical behavior of the steel connection at ambient temperature and (2) the fire performance of the connection when the loaded and exposed to a non-standard and standard fire.

The ambient temperature models had only mechanical load prescribed while the assembly remained at room temperature. The average failure load of the assemblies at ambient temperature (as determined in the experimental tests) was instantaneously applied as a pressure type of load at the contact surfaces of the dowels on the steel connection, as shown in Figure 6.9.a.. The steel connection was fixed at the screw locations according to the Figure 6.9.b.

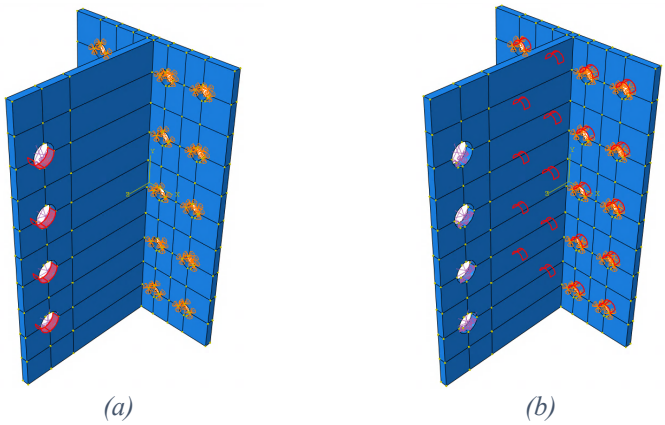

(a) *(b)*

Figure 6.9. (a) Loaded connection at the dowels contact with steel connection, (b) fixed on header side at ambient temperature.

The fire performance models included coupled thermal-mechanical loading where the mechanical load was applied and then held constant while fire conditions were prescribed. In this simulation, the applied load was reduced to approximately 60 percent of the average failure load, and again applied at the dowel contact surfaces. The heat distribution along the connections recorded during the fire tests were then applied as a thermal boundary condition. Figure 6.10 displays the steel connection simulated in accordance with the fire-performance test condition.

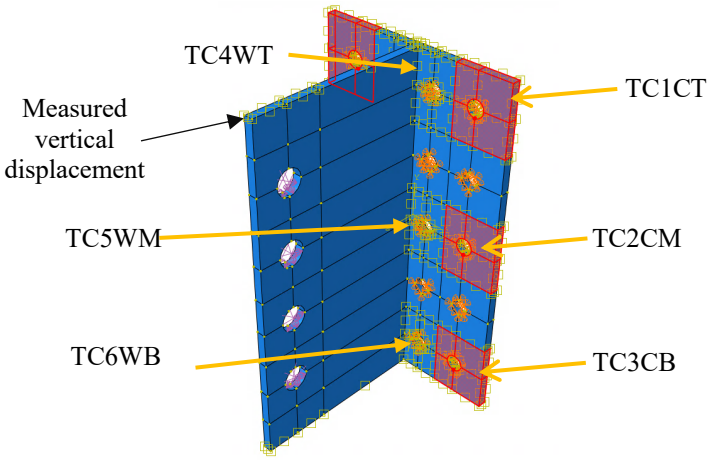

Figure 6.10. Steel connection modeled based on fire-performance thermal and loading condition.

Figure 6.11 illustrates the maximum vertical displacement of the steel connection (measured at the top left corner of the connection as shown in Figure 6.10) at ambient temperature (AT) versus during fire performance (FP) for three different tested assemblies. In the ambient tests, there is an initial, instantaneous deflection due to the applied load, but then the deflection remains constant for the duration of the test as the temperature remains constant. In the fire performance tests, there is again an initial, instantaneous downward deflection due to the applied load, but then the connection begins to deflect upward due to thermal expansion while the elevated temperatures are prescribed. Results show that the

maximum displacement of the connections occurred due to the thermal expansion in steel and not the imposed load.

The connection used in the glulam beam to CLT wall assembly (Figure 6.11.b) was the only connection that softened after 70 minutes of non-standard fire exposure and began to deflect downward. A comparison between maximum displacement of the connections resulted from FE simulations (Figure 6.11) and maximum displacement of the assemblies in the mid-span (Figures 3.18, 4.18, 5.18) during the fire-performance tests shows that the deformation in the assemblies mostly occurred due to the change in geometry and loss of gross area of timber elements and steel connection did not deform noticeably. According to the FE simulation results, the maximum displacement of the steel connection expanded was in range of 0.25-0.3 mm, while this value at the mid-span of the beam was 2.28-4.31 mm (0.09-0.17 in.).

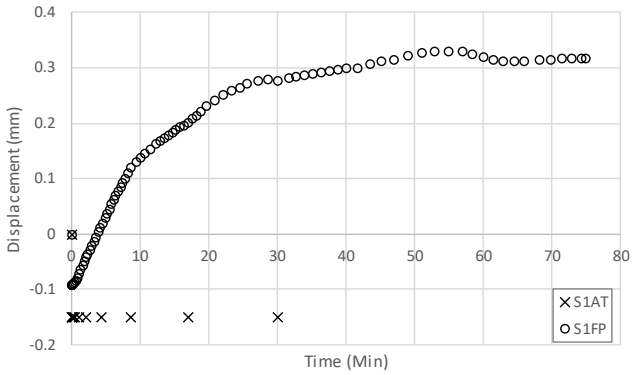

(a)

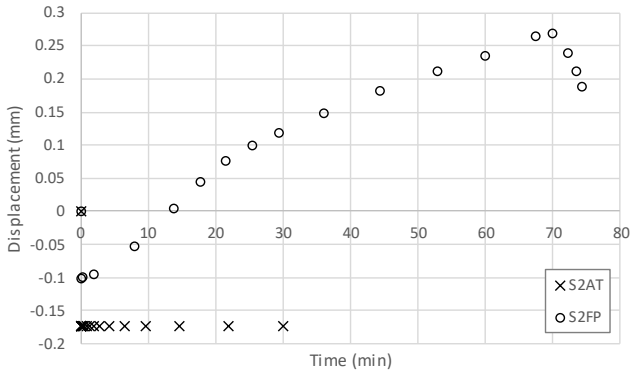

(b)

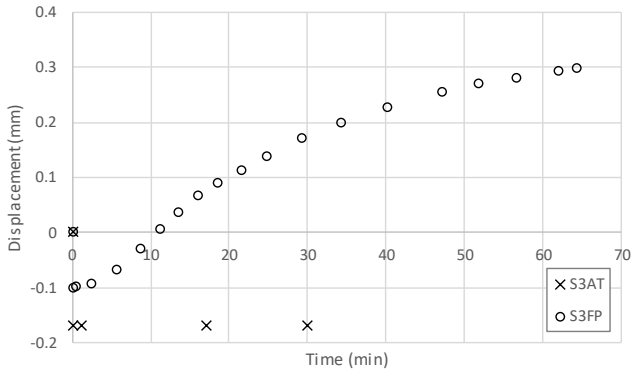

(c)

Figure 6.11. Maximum simulated displacement of the connections at ambient temperature vs. fire-performance. (a) CLT beam-to-girder, (b) glulam-beam to CLT-wall, (c) glulam beam-to-girder.

The validated FE model was also used to study the fire-performance of the steel connection exposed to the ASTM E119 standard fire curve. Figure 6.12 compares the FE results related to the maximum displacement of the connections exposed to the ASTM E-119 standard fire and the non-standard fires prescribed in the actual fire-performance tests for each of the three tested assemblies (S1: CLT beam-to-girder, S2: glulam beam to CLT wall, and S3: glulam beam-to-girder). The thermal load applied to each assembly is the same (E119 fire), however the mechanical load varies for each assembly (67% of the expected ambient temperature failure load). According to the FE results, the steel

connections would start losing strength at approximately 40 minutes if they were exposed to the ASTM E119 fire.

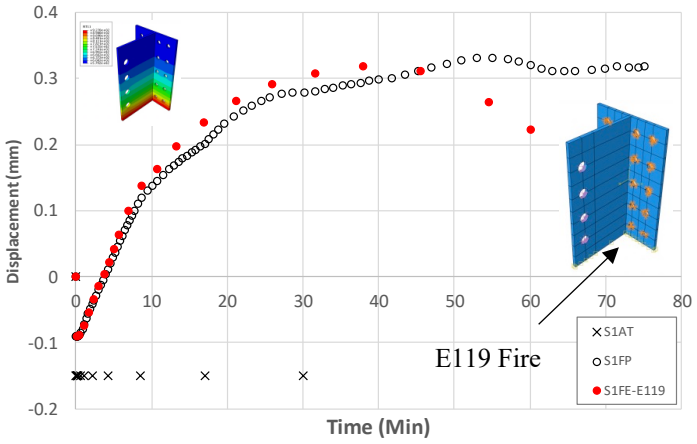

(a)

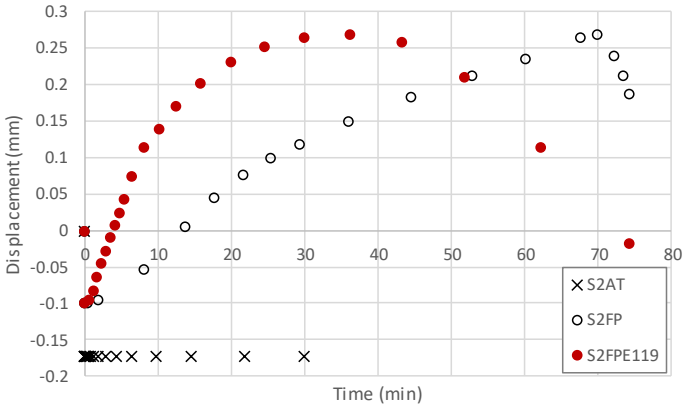

(b)

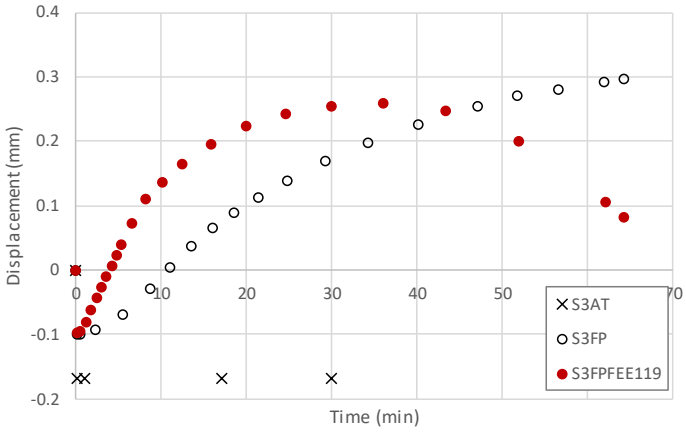

(c)

Figure 6.12. Maximum simulated displacement of the connections at ambient temperature vs. fire-performance. (a) CLT beam-to-girder, (b) glulam-beam to CLT-wall, (c) glulam beam-to-girder.

6.3. Conclusion

The FE model developed in this study coupled transient heat transfer with the Johnson-Cook (JC) temperature-dependent plastic hardening model. This unique model was utilized as a numerical tool to simulate the behavior of the steel connection before, during (FP) and after (PFP) non-standard fire exposure. In addition, the model was used to evaluate the thermo-mechanical performance of the connections exposed to the ASTM E119 standard fire. A validation study confirmed that the model provides a good estimation of heat distribution along the steel connection during fire exposure. Therefore, the validated FE model can be used to conduct a parametric study on the fire-performance of different metal connections with various loading and fire scenarios.

The thermo-mechanical FE results confirmed that the steel dowels and timber elements failed in ambient temperature and fire-performance tests before the steel connection developed any considerable plastic deformation. During the fire-performance

tests, change in residual section and boundary conditions were the significant cause of displacement.

6.4. REFERENCES

[1] Smith, I. and A. Frangi, *Use of timber in tall multi-storey buildings*. 2014: International Association for Bridge and Structural Engineering (IABSE).

[2] Perkins, N.S., P. Landsem, and G.W. Trayer, *Modern connectors for timber construction*. Vol. 1. 1933: US Government Printing Office.

[3] Norén, J., *Load-bearing Capacity of Nailed Joints Exposed to Fire.* Fire and materials, 1996. **20**(3): p. 133-143.

[4] Buchanan, A.H., *Fire performance of timber construction.* Progress in structural engineering and materials, 2000. **2**(3): p. 278-289.

[5] König J., Fontana M., *The performance of timber connections in fire-test results and rules of Eurocode 5*. Proceedings of the International RILEM Symposium 2001; Aicher A, Reinhardt HW. RILEM publications: 639–648.

[6] Cachim PB, Franssen JM. *Numerical modelling of timber connections under fire loading using a component model*. Fire Safety Journal. 2009 Aug 1;44(6):840-53.

[7] Moss P, Buchanan A, Fragiacomo M, Austruy C. Experimental testing and analytical prediction of the behaviour of timber bolted connections subjected to fire. Fire Technology. 2010 Jan 1;46(1):129.

[8] Racher P, Laplanche K, Dhima D, Bouchaïr A. *Thermo-mechanical analysis of the fire performance of dowelled timber connection*. Engineering Structures. 2010 Apr 1;32(4):1148-57.

[9] Erchinger C, Frangi A, Fontana M. *Fire design of steel-to-timber dowelled connections. Engineering Structures.* 2010 Feb 1;32(2):580-9.

[10] Moss PJ, Buchanan AH, Fragiacomo M, Lau PH, Chuo T. Fire performance of bolted connections in laminated veneer lumber. Fire and Materials: An International Journal. 2009 Aug;33(5):223-43.

[11] Akotuah Ohene A. *Modelling the fire performance of hybrid steel-timber connections,* 2014 (Doctoral dissertation, Carleton University).

[12] Palma, P. and Frangi, A., 2016. *A framework for finite element modelling of timber connections in fire*. Structures in Fire.

[13] Palma P, Frangi A. *Modelling the fire resistance of steel-to-timber dowelled connections loaded perpendicularly to the grain*. Fire Safety Journal. 2019 Jul 1;107:54-74.

[14] ASTM A572 / A572M-18, *Standard Specification for High-Strength Low-Alloy Columbium-Vanadium Structural Steel*, ASTM International, West Conshohocken, PA, 2018, www.astm.org.

[15] EN 1993-1-2: 2005, *Eurocode 3—design of steel structures—part 1-2: general rules—structural fire design,* (2005).

[16] Johnson, Gordon R., and William H. Cook, *Fracture characteristics of three metals subjected to various strains, strain rates, temperatures and pressures,* Engineering fracture mechanics 21.1 (1985): 31-48.

[17] Visser, W., et al., *Deformation characteristics of low carbon steel subjected to dynamic impact loading*, Materials Science and Engineering: A 528.27 (2011): 7857-7866.

7. CONCLUSION

7.1. Introduction

The advancement of timber structures and high demand for construction with heavy timber products increased the interest in the fire-performance of tall timber buildings. This research was motivated by contribution to a case study issued by SFPE on Performance-Base-Design (PBD) of a 30 story CLT building. Inspired by the case study and considering the key role of connections in the survival time of a building during fire incidents, this research aimed to study the thermo-mechanical performance of steel connections in tall timber structures. The research objectives were achieved through a combination of experimental and numerical studies. Conclusions of the research program are summarized in this chapter. Challenges and limitations within this research are presented to provide insight into future studies. Finally, based on the experiences, challenges and limitations confronted during this research recommendations are provided for continued future studies.

7.2. Case Study

A 30-story hybrid timber-reinforced concrete structure was designed for the purpose of the 12th International Conference on Performance-Based Codes and Fire Safety Design Methods. The author's specific contributions to the case study include: the architectural design, structural system adoption and providing the final architectural and structural drawings. In designing this structure, Glulam was utilized for the columns and beams, CLT panels were used for load bearing walls and in decking systems, and

reinforced concrete was used for the core shear walls. Steel connections joined Glulam beams to CLT walls, Glulam columns and Glulam beams. The fire-performance of Glulam beam-to-columns was addressed previously in literature, although there was a gap in knowledge on the fire-performance of Glulam beam-to-girder and Glulam-beam to CLT-walls. Therefore, this research was developed to address the performance of T-shape (slotted-in) steel connections used in the aforementioned configurations. On the other hand, T-shape doweled connections increase the tendency of undesirable brittle splitting failure. Reinforcement with self-drilling screws is a common retrofitting method to avoid this failure. However, this method showed a negative effect on fire-performance of the assembly. The concern with brittle splitting failure of Glulam beams loaded perpendicular to the grain led to designing an additional assembly with CLT-beams. In this assembly T-shape doweled steel connections connect the CLT-beams to CLT girders.

7.3. Experimental Studies

In this research thermo-mechanical performance of three sets of intermediate-size assemblies were investigated at ambient temperature (AT), during non-standard fire exposure (FP) and after non-standard fire exposure (PFP): (1) Glulam beam-to-girders, (2) Glulam-beam to CLT-walls and (3) CLT beam-to-girders. The experimental results are summarized in the following.

7.3.1. Ambient Temperature

Experimental studies performed at ambient temperature on the assemblies that included a Glulam beam, identified that the Glulam beams loaded perpendicular to the

grain experienced embedment failure, plastic bending of dowels and splitting failure. The splitting failure in these experiments was attributed to the friction between the beam and headers. This friction could be eliminated by adding a gap between beam and headers. It is important to note that the ductility of dowels played an important role in ductility of the assembly, allowing for larger deformations in the connection prior to the splitting failure in the beam.

Ambient temperature tests conducted on the CLT beam-to-girder assembly confirmed that utilizing CLT as a beam member can improve the ductility of beam. The CLT-beam failure started with embedment failure of the CLT-beam and plastic bending of the dowels, continued with row shear failure in the CLT mid-layer and then stopped after splitting failure occurred at the outermost layers of the CLT beam. Splitting did not progress to the next layer of CLT which was orthogonally oriented to the outer layer.

The CLT-walls and Glulam-girders (headers) failed in different manners. The CLT-wall headers failed due to tensile plug-out from a force couple resisting the moment transferred to the wall while the Glulam girders split by transferred shear force perpendicular to the grains through the screws. The cracks formed by the splitting failure in the Glulam girder headers propagated along the girder's width while the cracks formed in the tensile zone of the CLT-headers were limited to the first layer of the CLT where the grains were perpendicular to the shear force.

7.3.2. Post-Fire performance

In comparison to the AT tests, the failure modes of assemblies after fire exposure had one significant change. No splitting failure occurred in the beam members on the fire

exposed connection. This was due to the change in geometry and boundary condition of the header sides exposed to the fire where the degradation of the wood due to charring decreased the contact between connecting elements.

Glulam-beam to CLT-wall assemblies with minimum exposed surfaces (CLT-wall was exposed only on one-side) during the fire tests had the highest residual strength while the CLT beam-to-girder assembly showed the lowest residual strength. The post-fire-performance test results show that the maximum load carrying capacity reduction of Glulam beams exposed 30 minutes to non-standard fire was equal to 24% while for the CLT beam this reduction was around 45%. The maximum reduction in load carrying capacity of Glulam beams exposed 60 minutes to non-standard fire was 48%. In all PFP tests, the temperatures in the connections remained below the threshold for reduction in residual mechanical properties of the steel. The failure was thereby attributed to gross loss of section due to charring.

7.3.3. Fire-Performance

The fire-performance tests conducted on the assemblies highlighted the importance of protecting the metal connections from fire exposure. In this research, the steel connection itself did not fail during the fire-performance tests. However, in the CLT beam-to-girder assembly that included a gap between the members, the steel connection was not concealed, and the charring and reduction in cross section of the CLT beam was considerable in comparison to the other two assemblies. In this case (CLT beam-to-girder) that the steel connection left totally exposed to fire, there was a plastic deformation in the bottom edge of the connection. It is also noted that the change in the geometry of the

headers at the contact location with the connection is critical to failure of the assembly. This boundary change promoted the embedment failure around the dowels.

In all fire-performance tests, embedment failure of the beam was the controlling failure mode observed. Unique to the CLT beam-to-girder assembly, charring progress far enough up the connection that the lower dowel fell out and the load was redistributed to the top dowel, causing unexpected, larger forces and bending in the dowel. Table 7.1 provides a summary of test result at different thermal condition.

Table 0.1. Test result summary

Assembly Description	Type of Test	Failure Load (lbf.)	Joist Failure Mode	Header Failure Modes
A1 CLT Beam-to -Girders	AT	33204	Embedment, Row Shear, Splitting of out-side layer	Splitting
	PFP30	18402	Embedment, Row Shear	Withdrawal
	FP	22400	Embedment, Dowel Bending	Connection Plastic Deformation
A2 GL-Beam to CLT-Walls	AT	37581	Embedment, Splitting	Withdrawal
	PFP30 PFP60	32557 23732	Embedment, Splitting	Withdrawal
	FP	24640	Embedment	Withdrawal
A3 GL-Beam-to--Girders	AT	36772	Embedment, Splitting	Withdrawal and Splitting
	PFP30 PFP60	28037 19175	Embedment	Withdrawal and Splitting
	FP	24640	Embedment	Withdrawal and Splitting

7.3.4. Numerical Studies

The unique, FE model generated for this research is a coupled temperature-displacement model, capable of simulating thermo-mechanical performance of the T-shape doweled steel connection in different thermal condition. This model was used for the purpose of thermal validation of PFP test results. Comparison with the PFP experimental results confirmed that the FE model provides a good estimation of recorded temperatures along the connection. Also, thermo-mechanical behavior of the loaded connection at ambient temperature and during non-standard fire was studied through the finite element simulations. Doing a parametric study on the steel connection is another capability of this model. Flexibility and applicability of this model for parametric studies was checked with performing a finite element simulation on fire-performance of the loaded connections exposed to the ASTM E119 fire curve. In comparison with the simplified models used in other studies to simulate the interaction between the timber, dowels and steel plates, the FE model developed in this study focused only the steel connection. It is also possible to extend this model with altered geometry, or more parts to simulate the whole assembly.

7.4. Research Challenges and Limitations

Due to the hazardous nature of fire experiments on combustible materials, this research presents several limitations. Familiarization with these challenges will aid in improving the future studies in this field.

7.4.1. Experimental Studies

Testing samples at ambient temperature included the following challenges:

- Sample preparation: Preparing the samples from scratch required specific carpentry tools such as CNC machine, milling tools and chain saw. The research would be simplified if samples could be prepared and ordered from an outside source.
- Instrumental and access limits: Testing samples with the Universal Testing Machine with limited access restricted the measurements to the mid-span of the beam. Consider additional image processing techniques, strain gauges, or other instrumentation.
- Physical activities: This type of experiments require teamwork. The intermediate-size assemblies were heavy enough to require at least a two-member team for performing the tests.

Conducting the fire tests safely had specific challenges:

- Testing combustible assemblies required a hooded lab with access to different fire safety measures. Finding a safe place for the fire test was one of the most time-consuming parts of this research.
- Fabricating a customized test set-up and burner.
- Restrictions in access to the required testing instruments such as heating panels, ICAL device, thermal camera, data acquisition devices that originally planned for and were no longer accessible due to issues beyond the research team control with the relocation of lab equipment.
- Using propane gas.
- Transferring samples between fire lab and material lab.
- Cleaning the samples.

7.5. Future Research

1. Adding CLT deck to the assembly.
2. Testing materials to find their temperature-dependent material properties or using materials with better defined properties.
3. Making the ambient temperature tests boundary condition more realistic. (Using the customized test frame for AT tests and using a jack connected to the reaction wall or even the same jack with automatic load controller).
4. Measuring connection displacement directly by strain gauges or image processing (which is not an easy task!).
5. For the fire tests using heating panels with uniform heat flux or ICAL will be interesting. Using thermal camera during the tests can be very useful.
6. Using the FE model and find critical geometry for connection.
7. Extending the FE model and perform parametric study on the connection.
8. Considering the load redistribution during the fire-performance tests.

7.6. Research Contribution and Novelty

- CLT beam-to-beam assembly tested for the first time before (AT), during (FP) and after fire exposure (PFP).
- The Glulam beam was tested before at different thermo-mechanical conditions (AT, PFP and FP), this was the first time that its performance in a beam-to-girder and beam-to-CLT wall assembly was tested.

APPENDIX A: CASE STUDY DRAWINGS

This research was inspired by contribution to a case study on performance base design of a 30-story CLT building. In this appendix, rendered models of the designed structure and more drawings are included. These drawings represent the author's contributions to the case study.


Fitness centers and Refuge areas

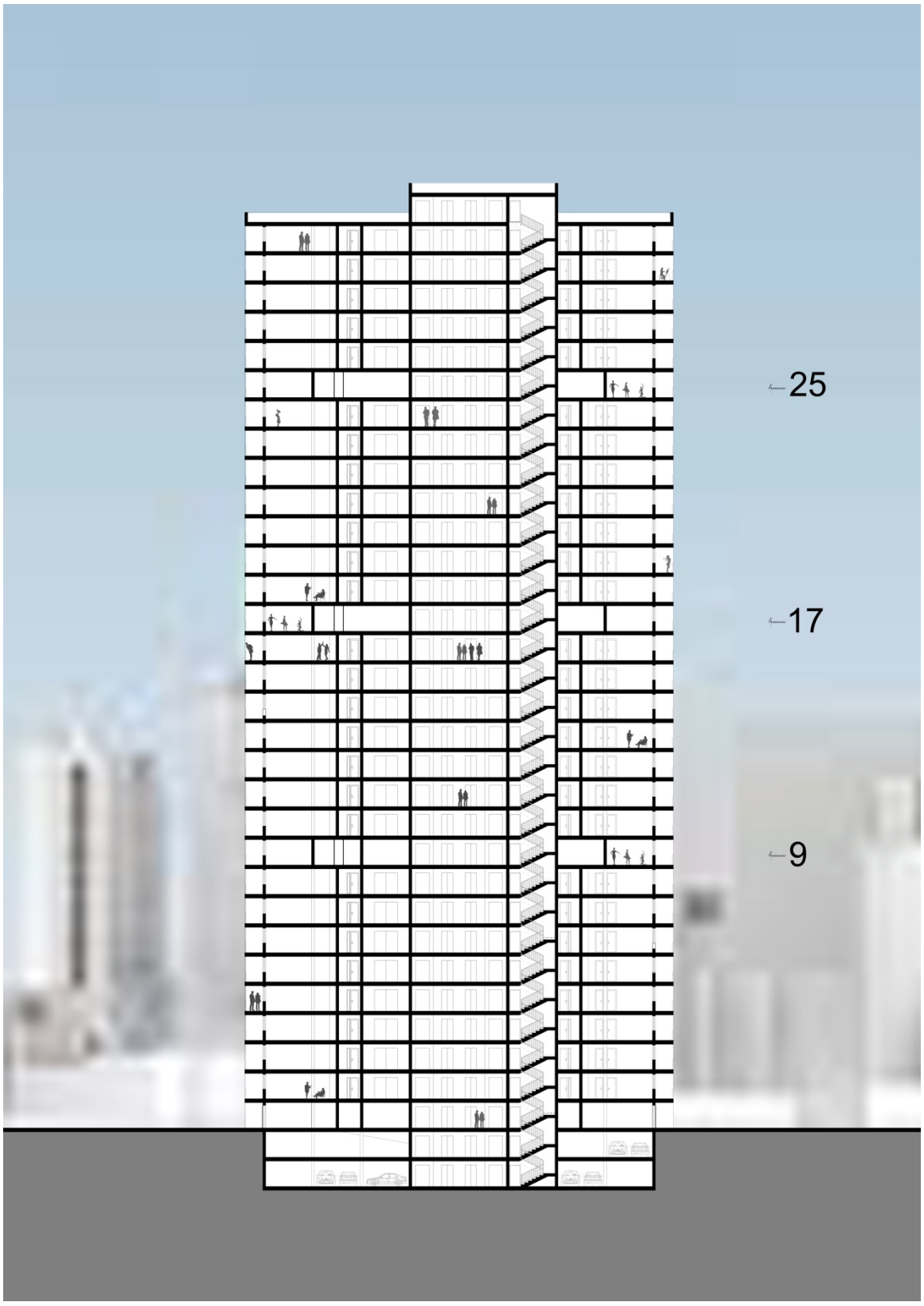
25
17
9

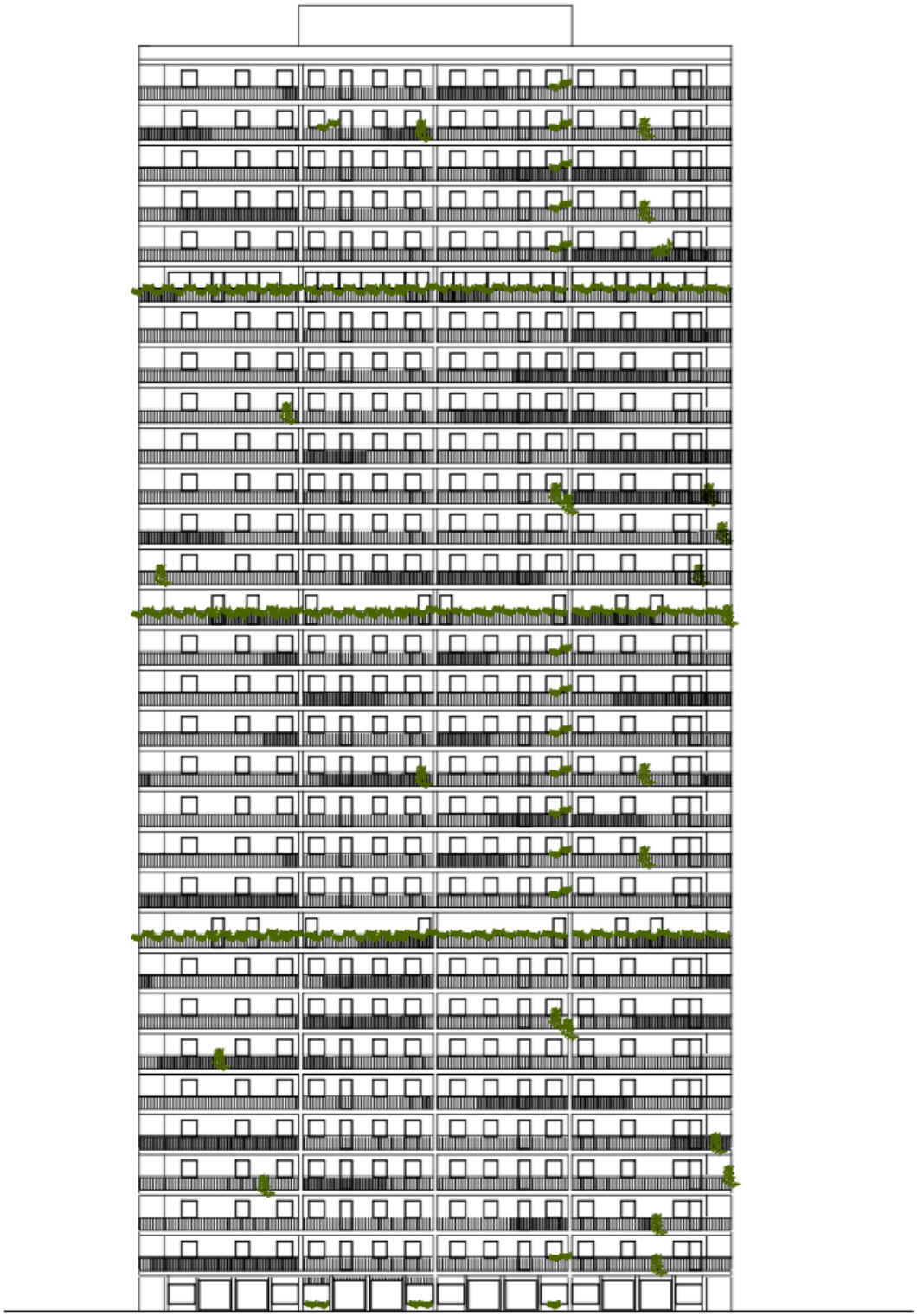

Side View (West View)

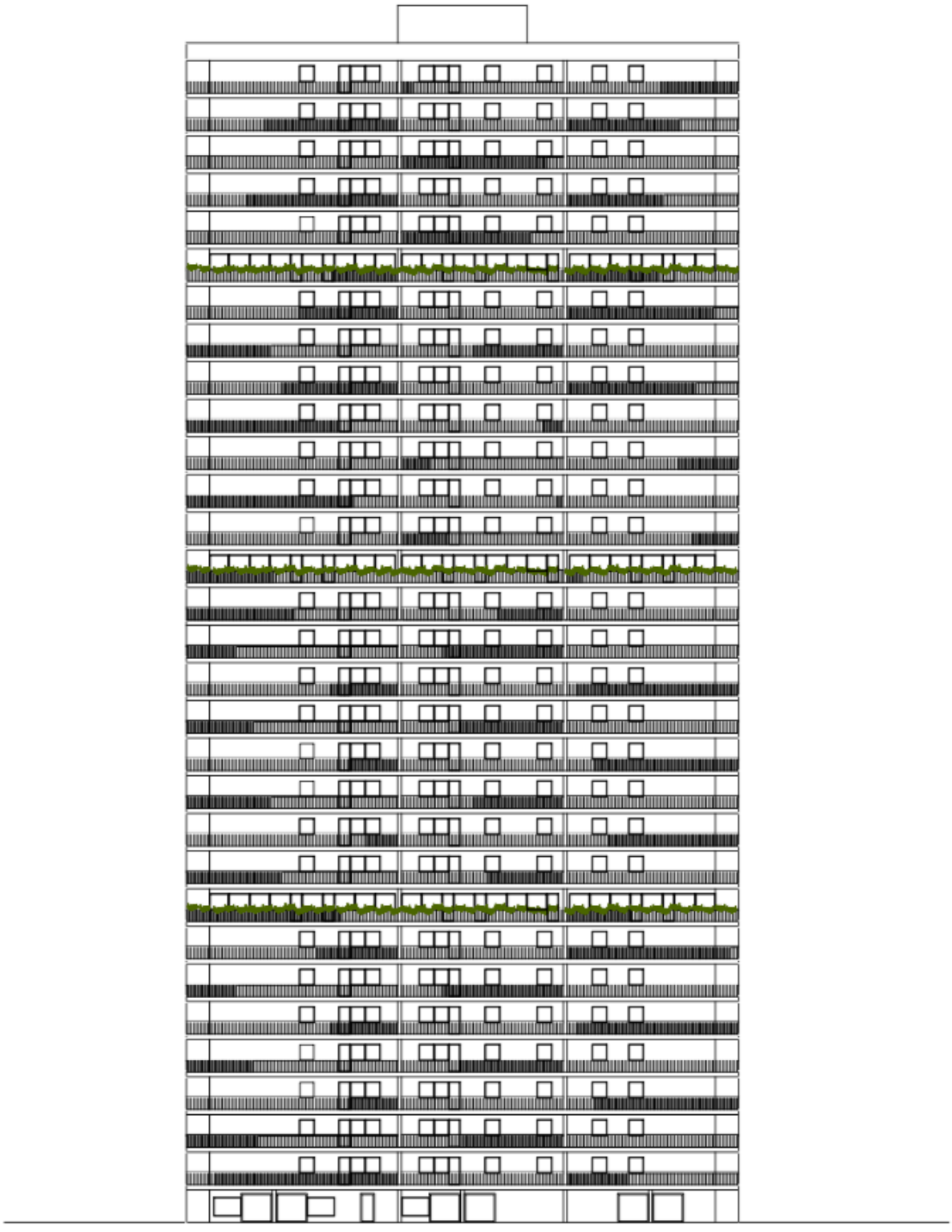

North Elevation (Front View)

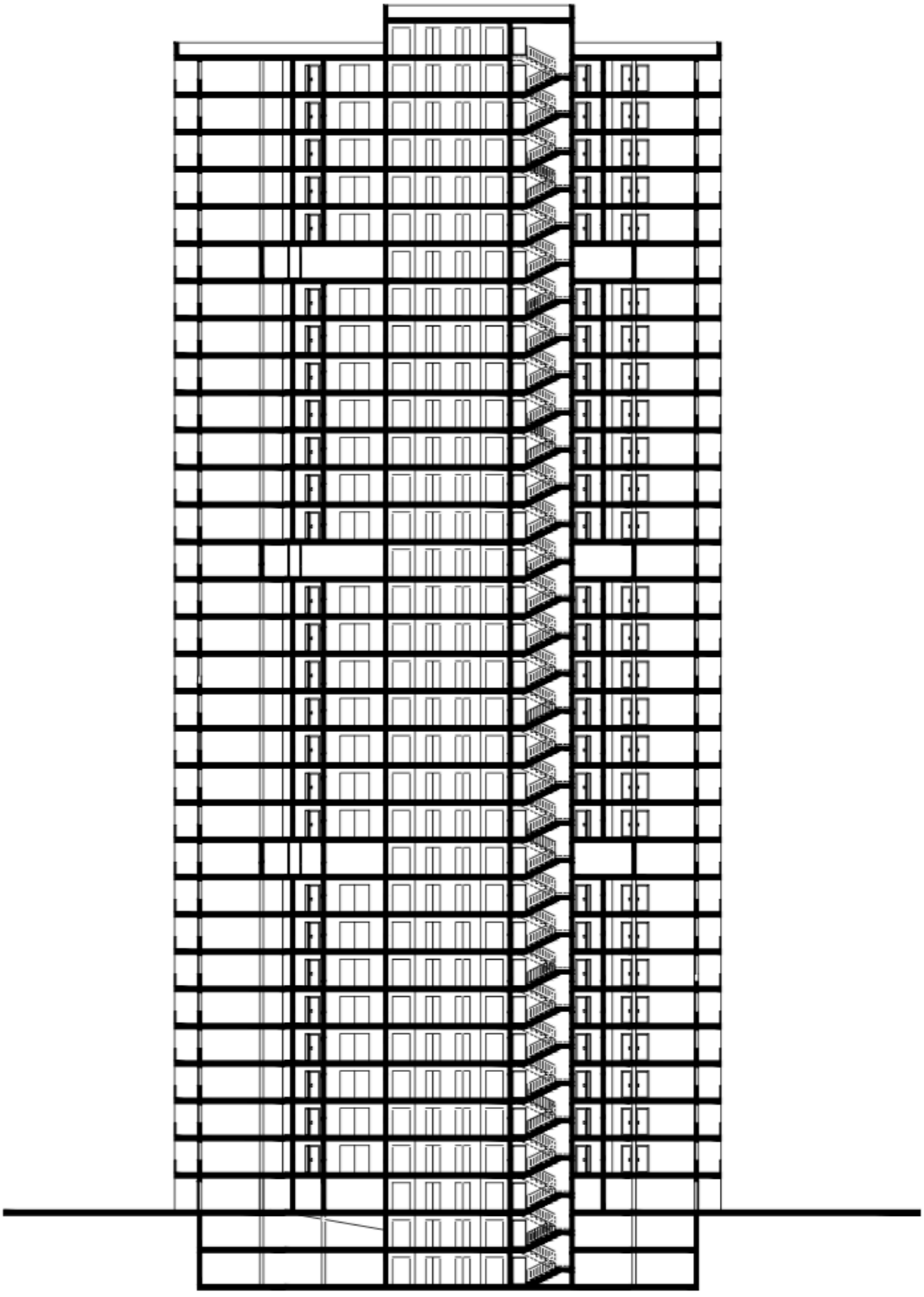

Floor Beam Plan

Horizontal Structural components

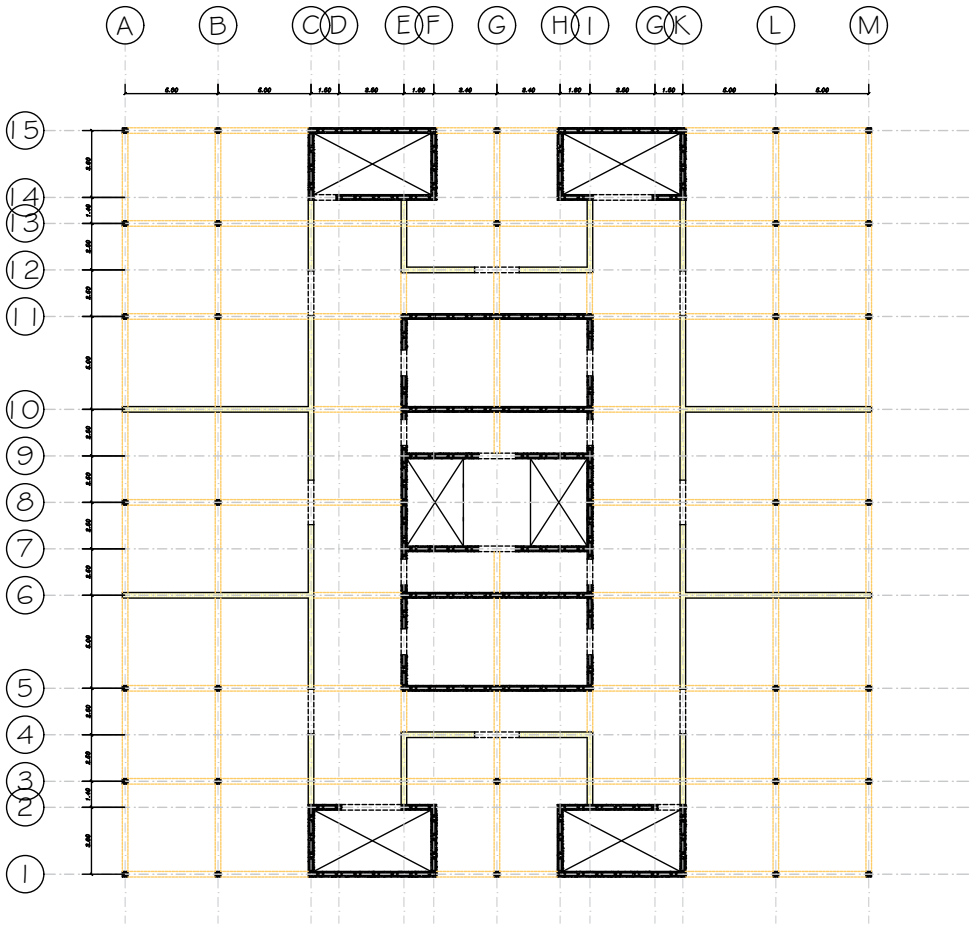

Ground Floor Structure

Vertical Structural Components

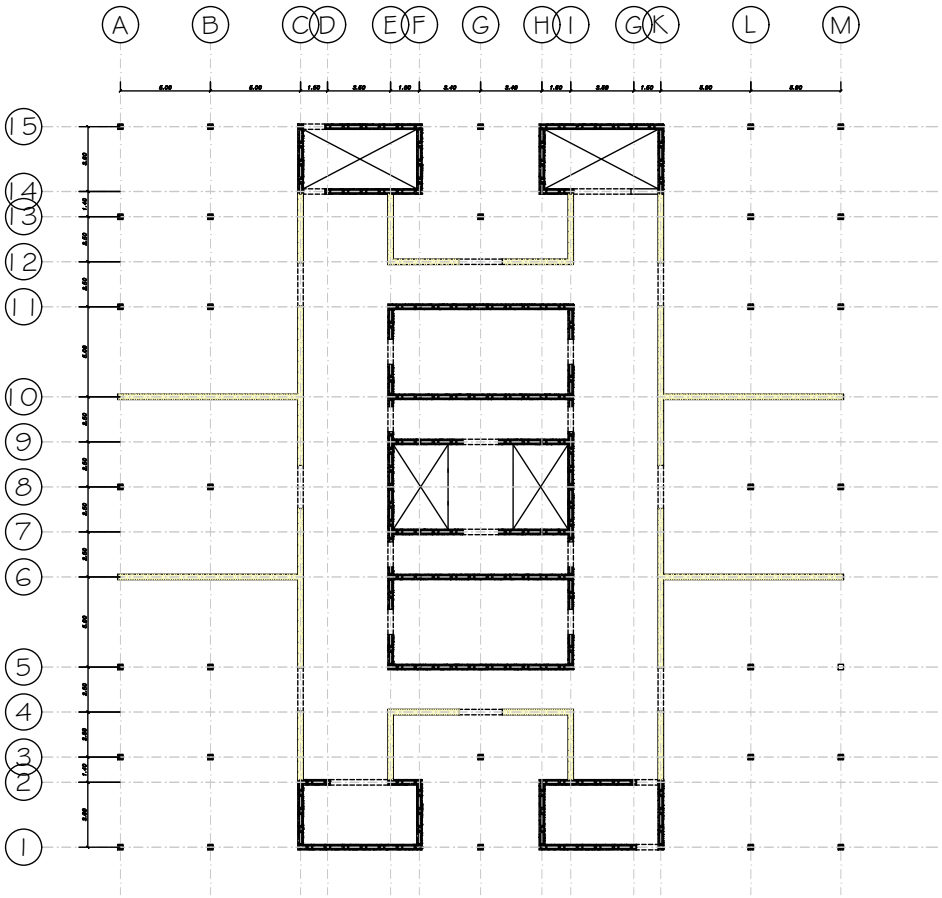

Ground Floor Beam Plan

Horizontal Structural components

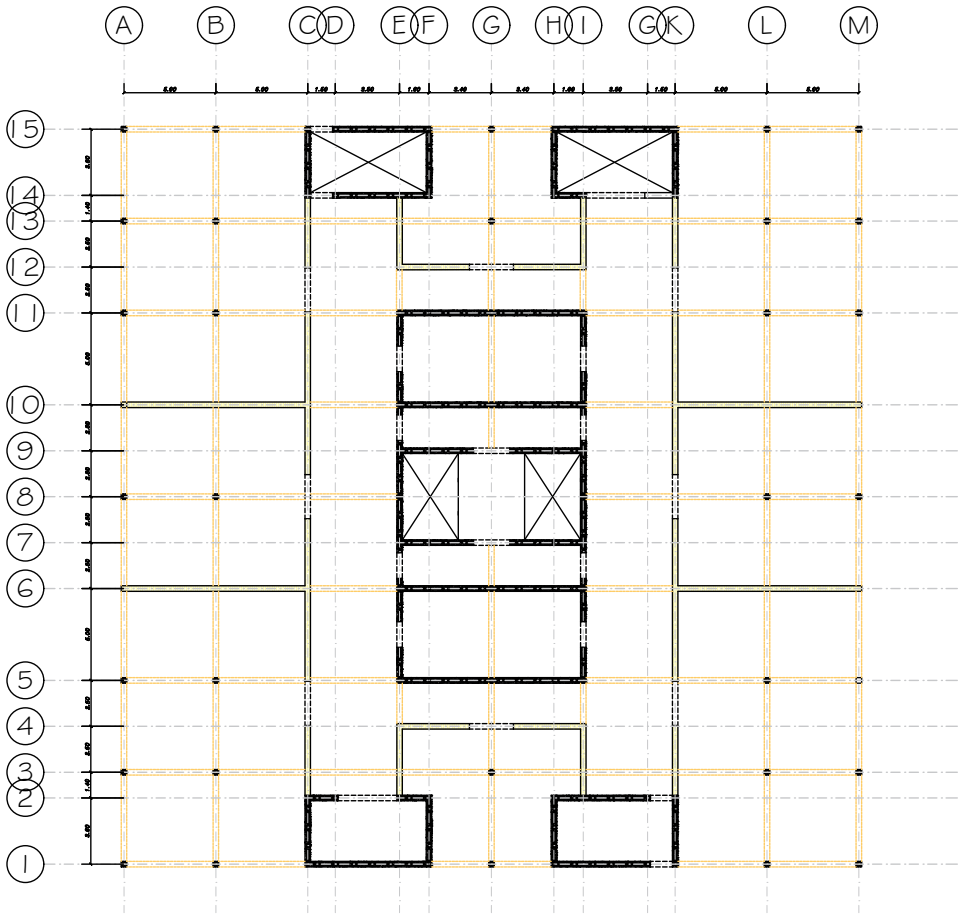

Floors Structure

Vertical Structural Components

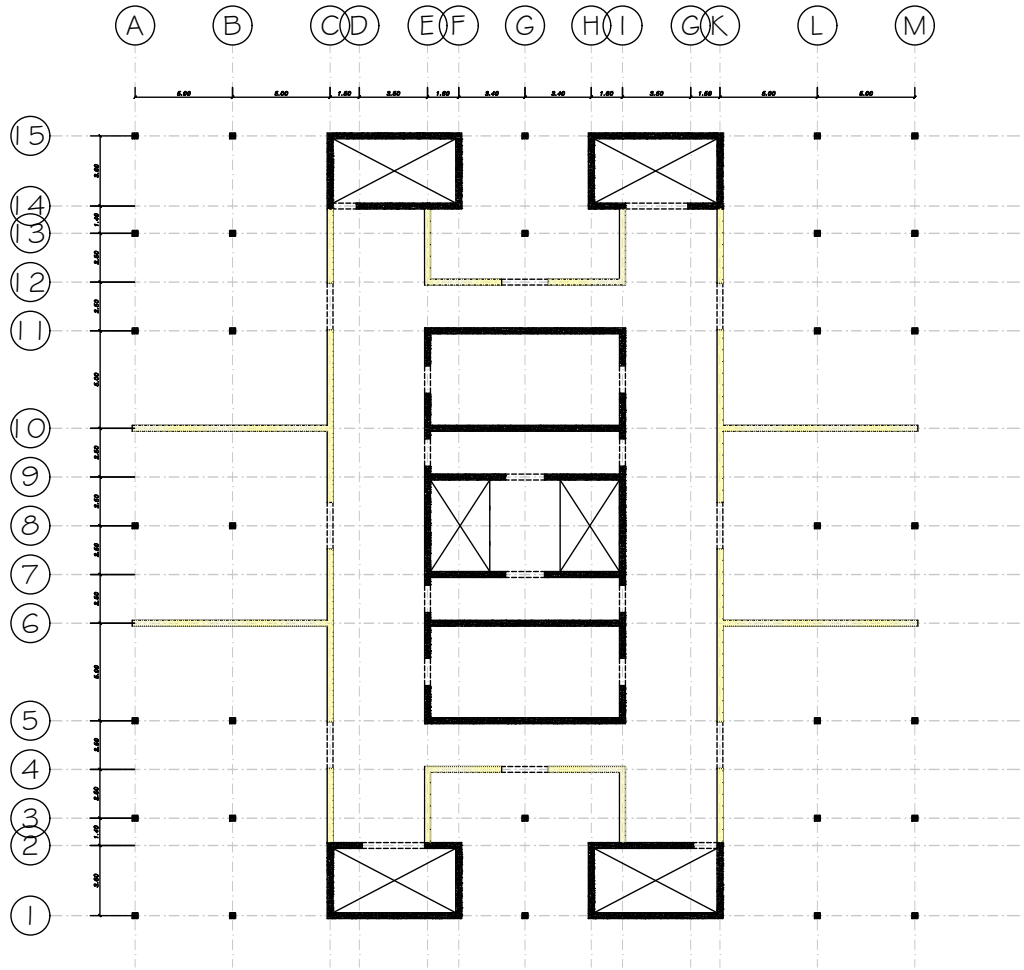

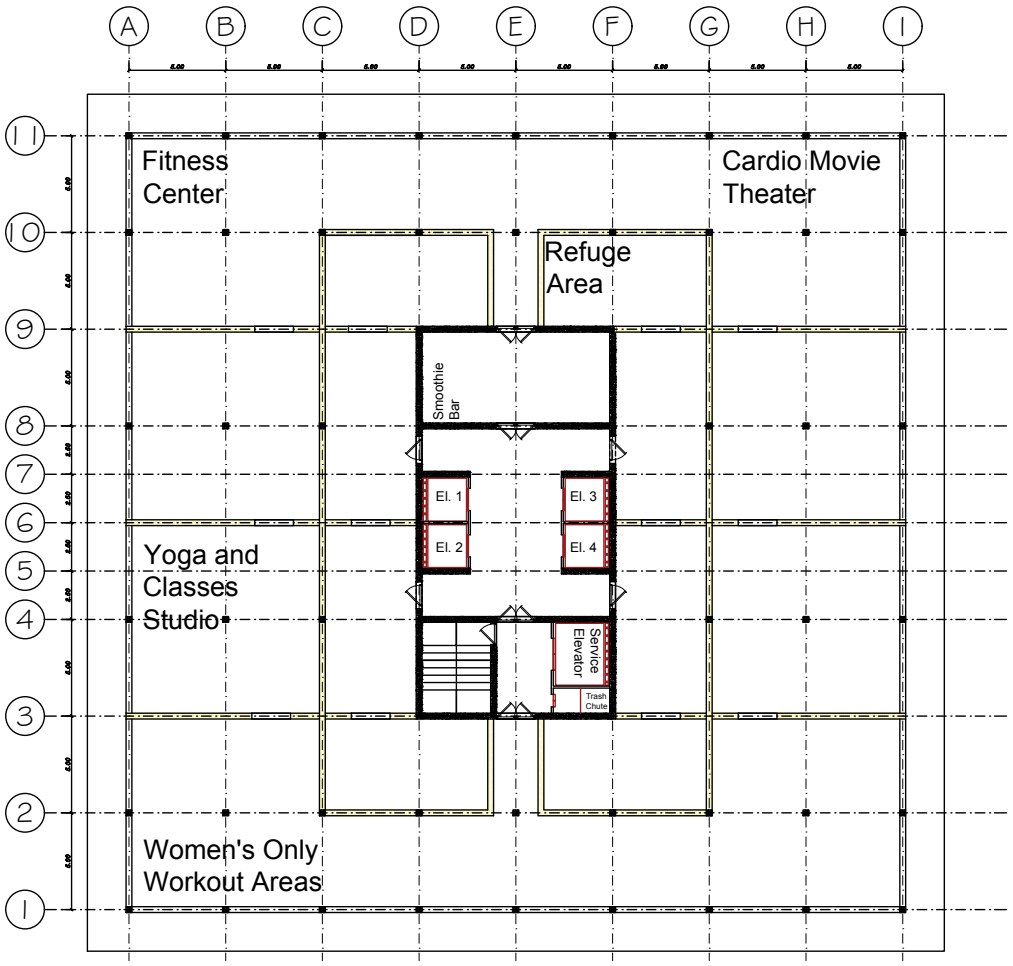

Floor 9th Plan (Dual Fitness Center, Refuge Area)

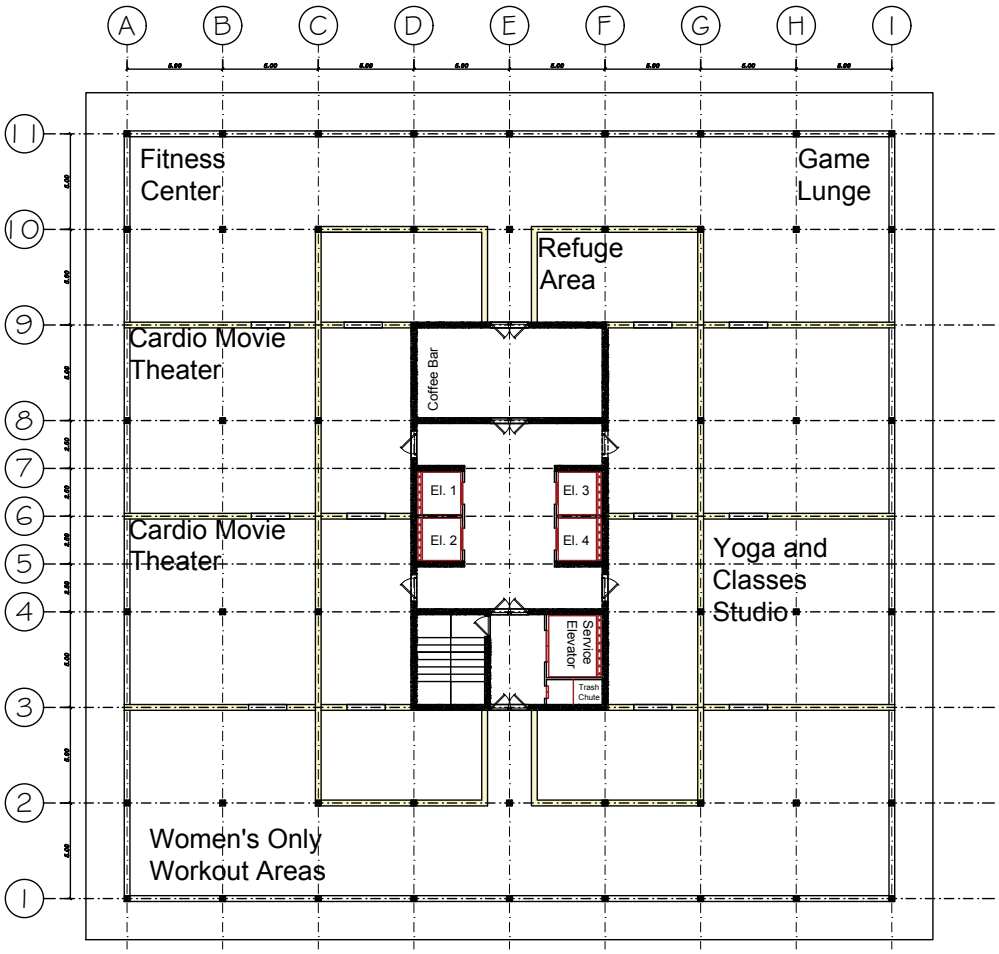

Floor 17th Plan (Fitness Center, Refuge Area, Game Lunge and Coffee bar)

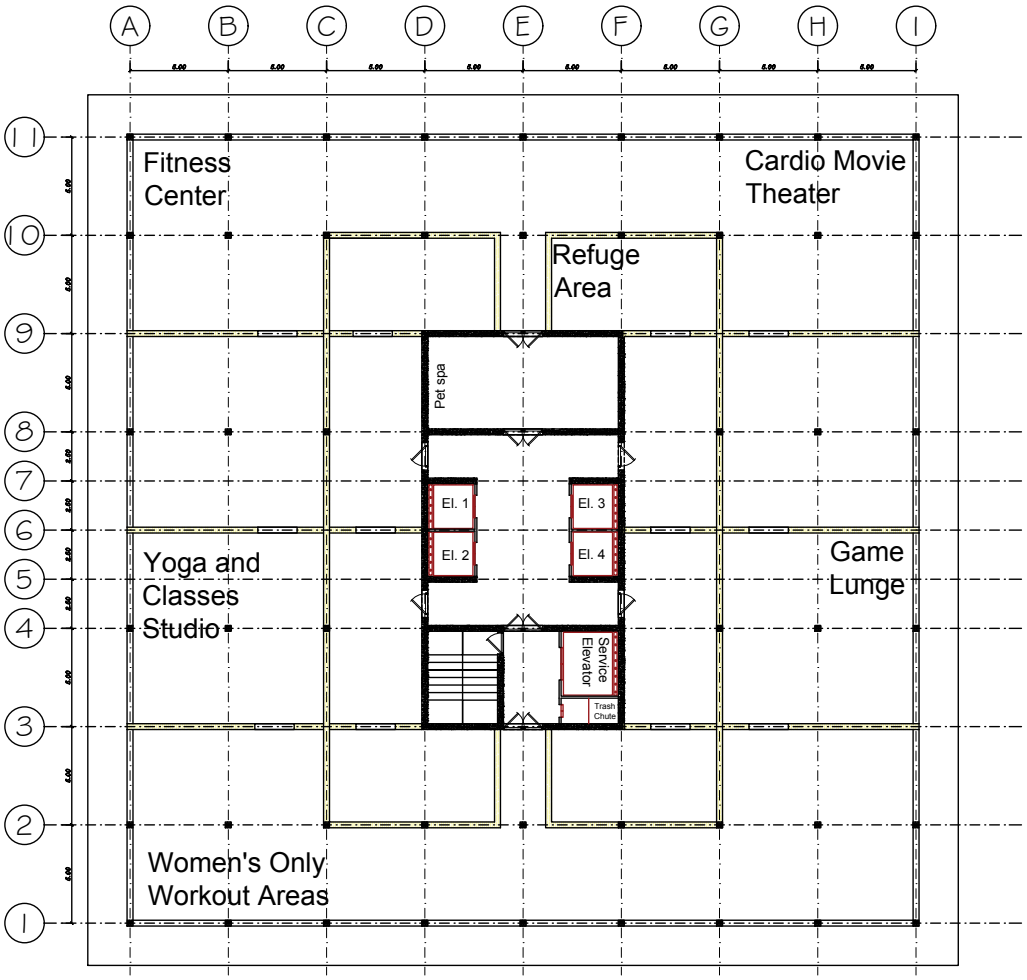

Floor 25th Plan (Fitness Center and Refuge Area)

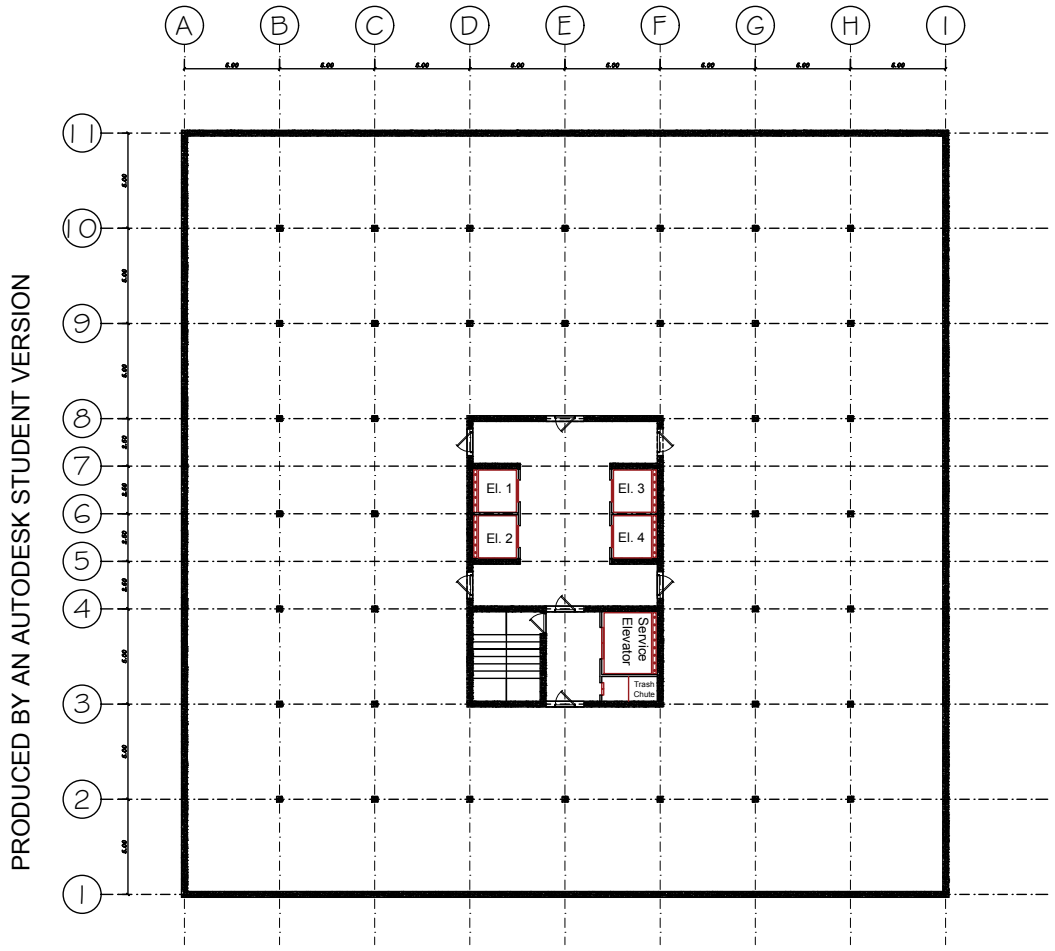

Car Parking 1 Plan (P1)

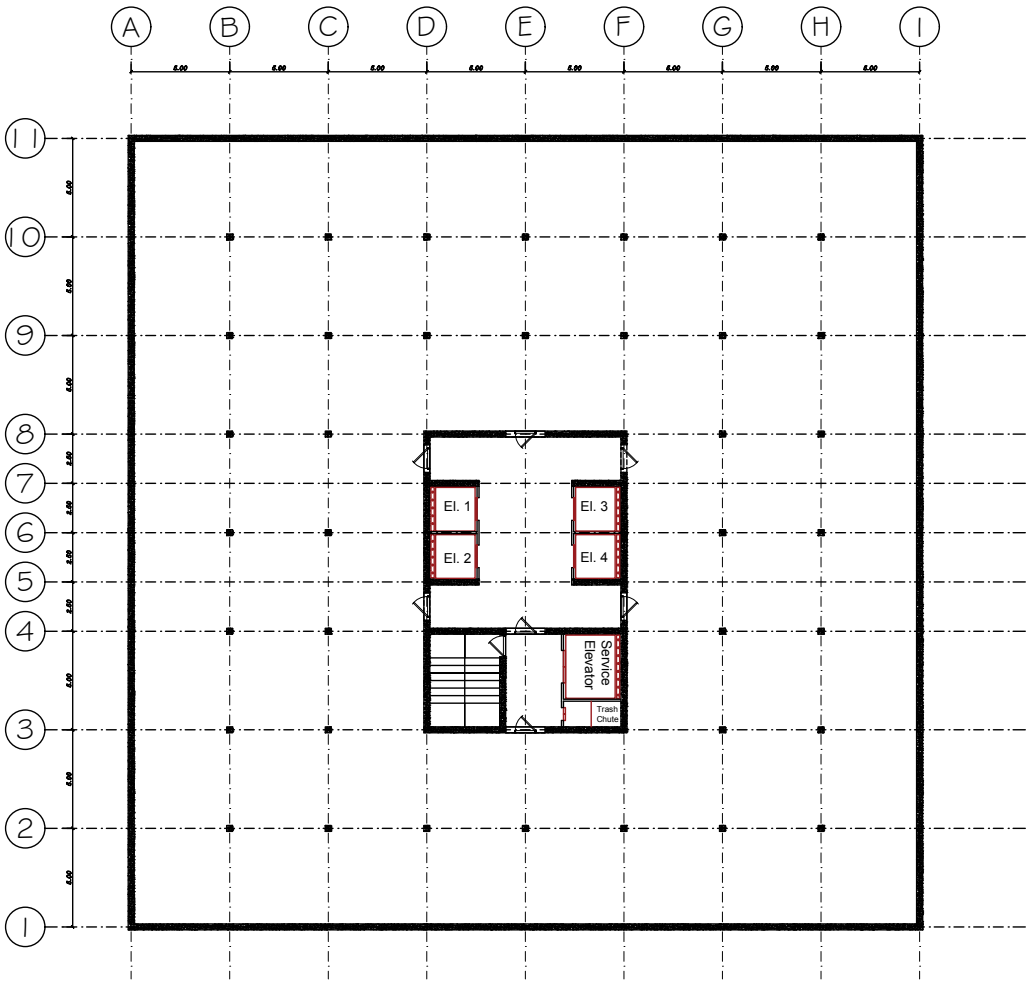

Car Parking 2 Plan (P2)

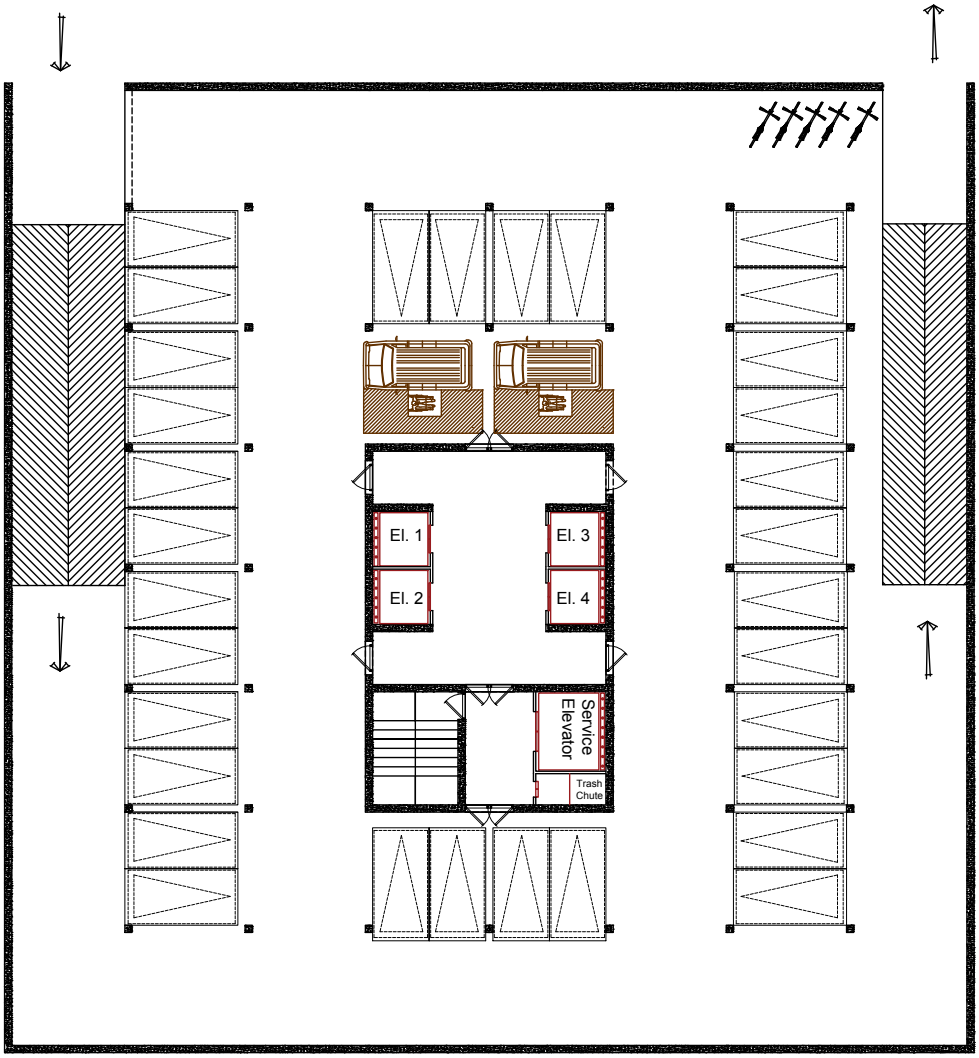

Car Parking 1 Plan (P1)

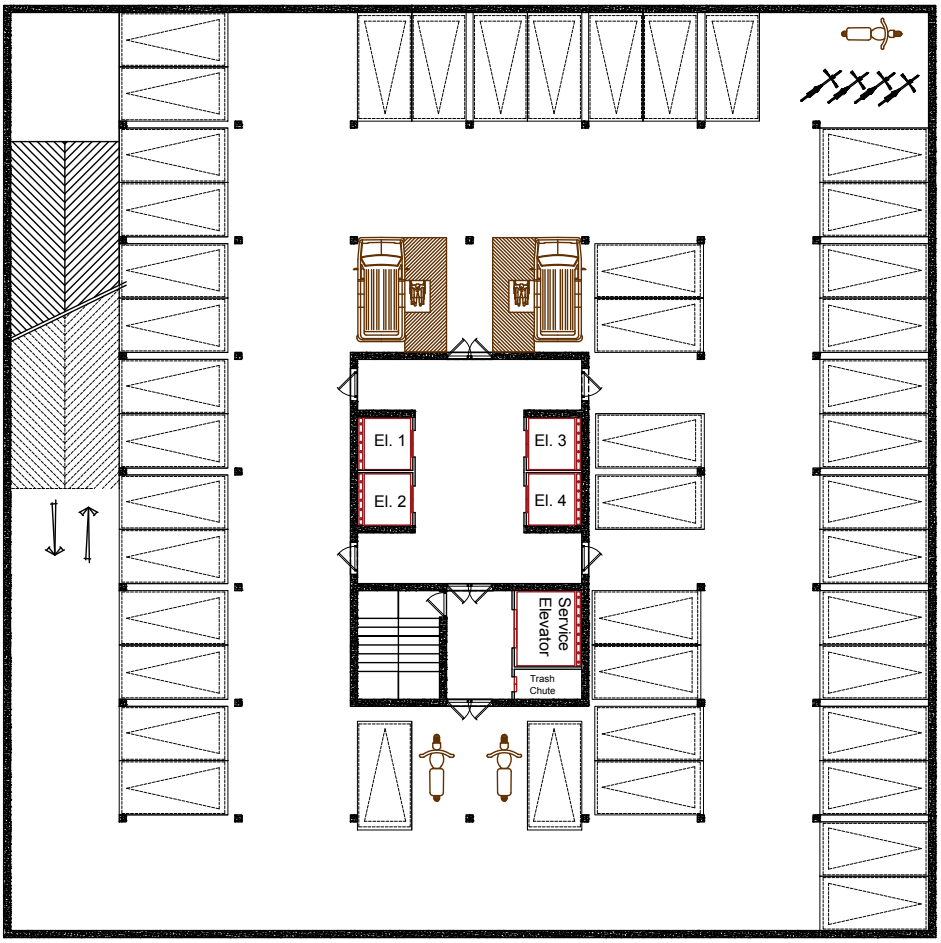

Car Parking 2 Plan (P2)

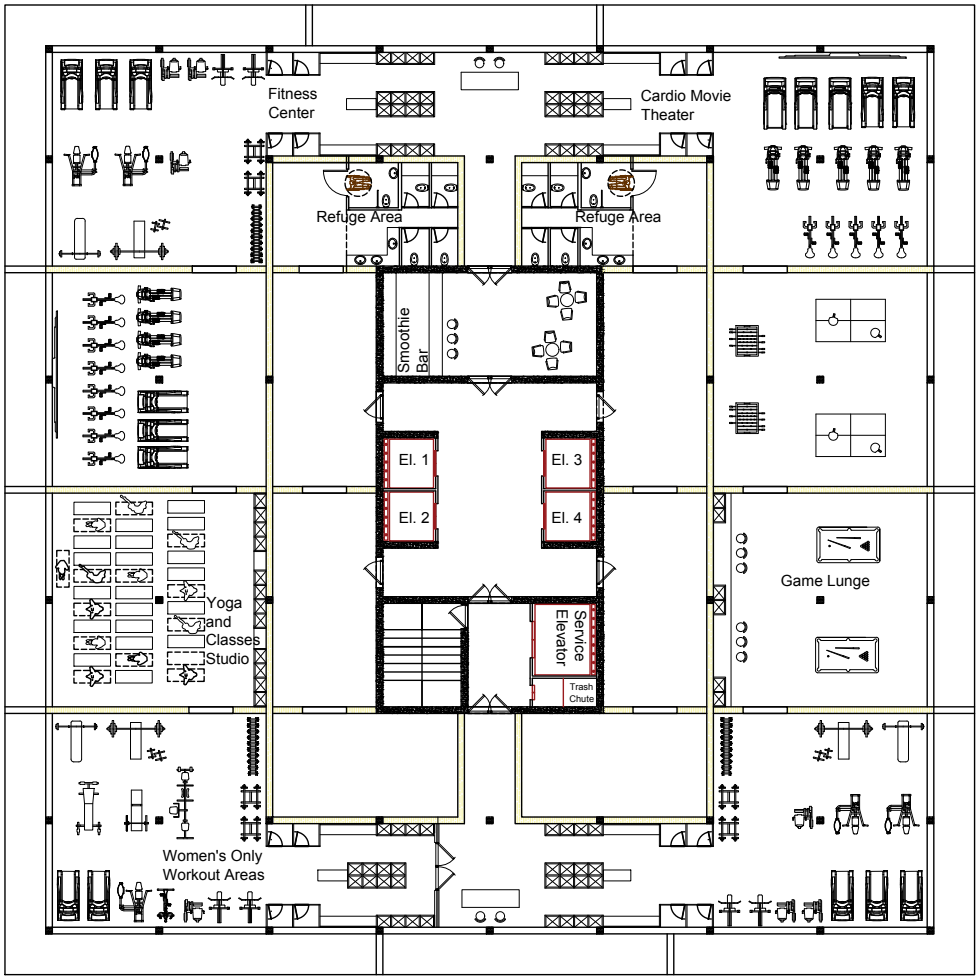

Floor 9th Plan (Dual Fitness Center, Refuge Area)

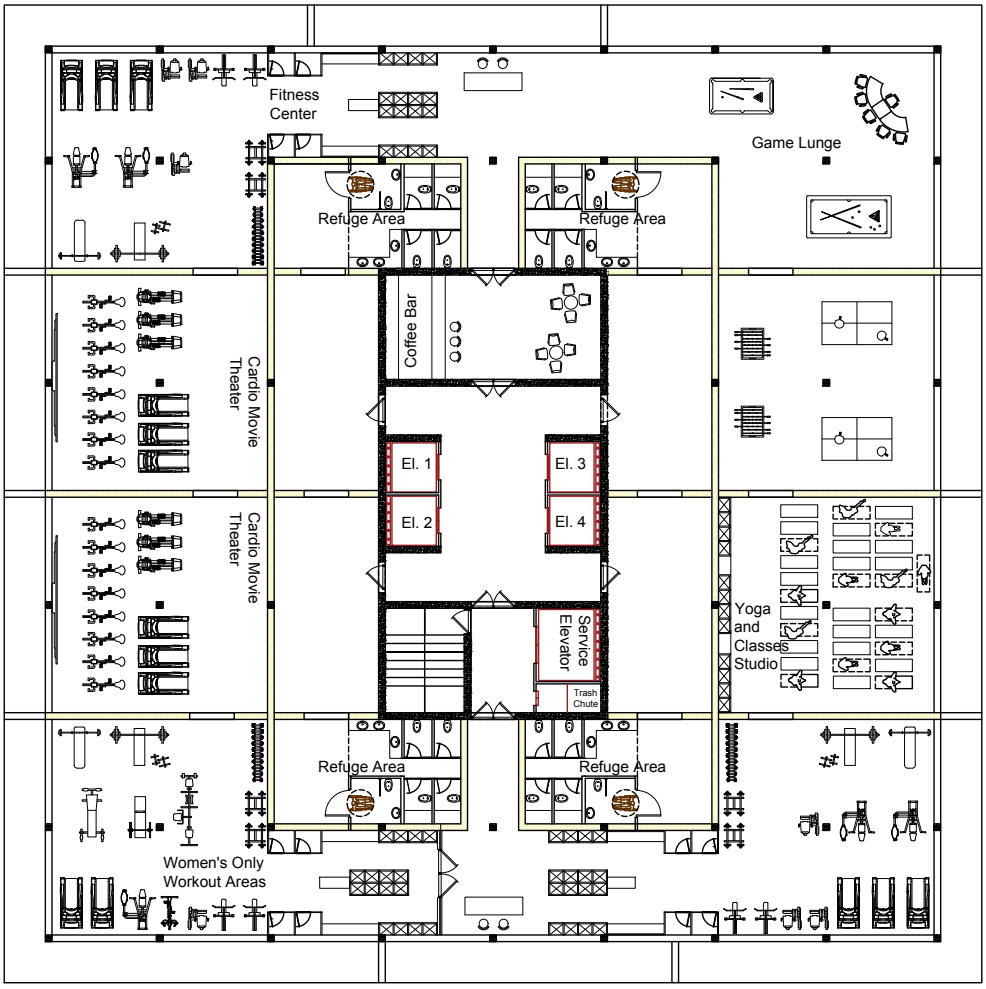

Floor 17th Plan

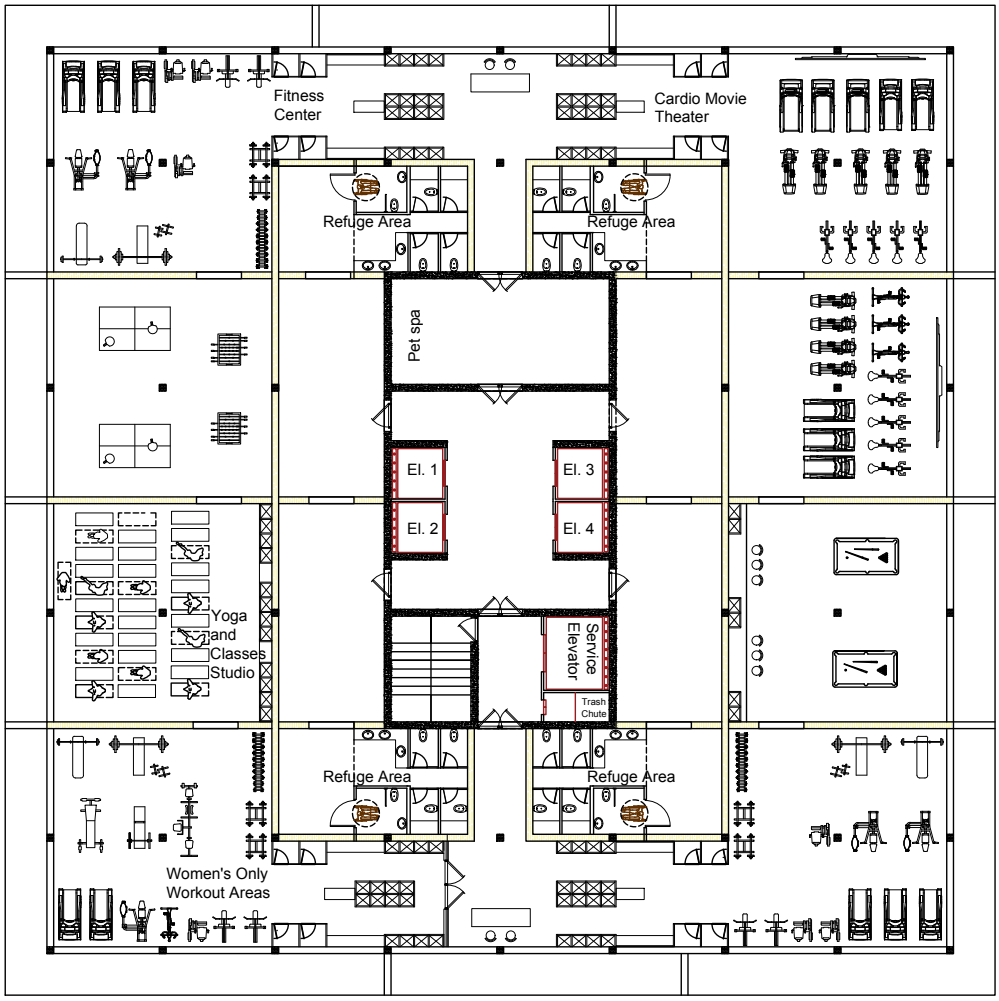

Floor 25th Plan

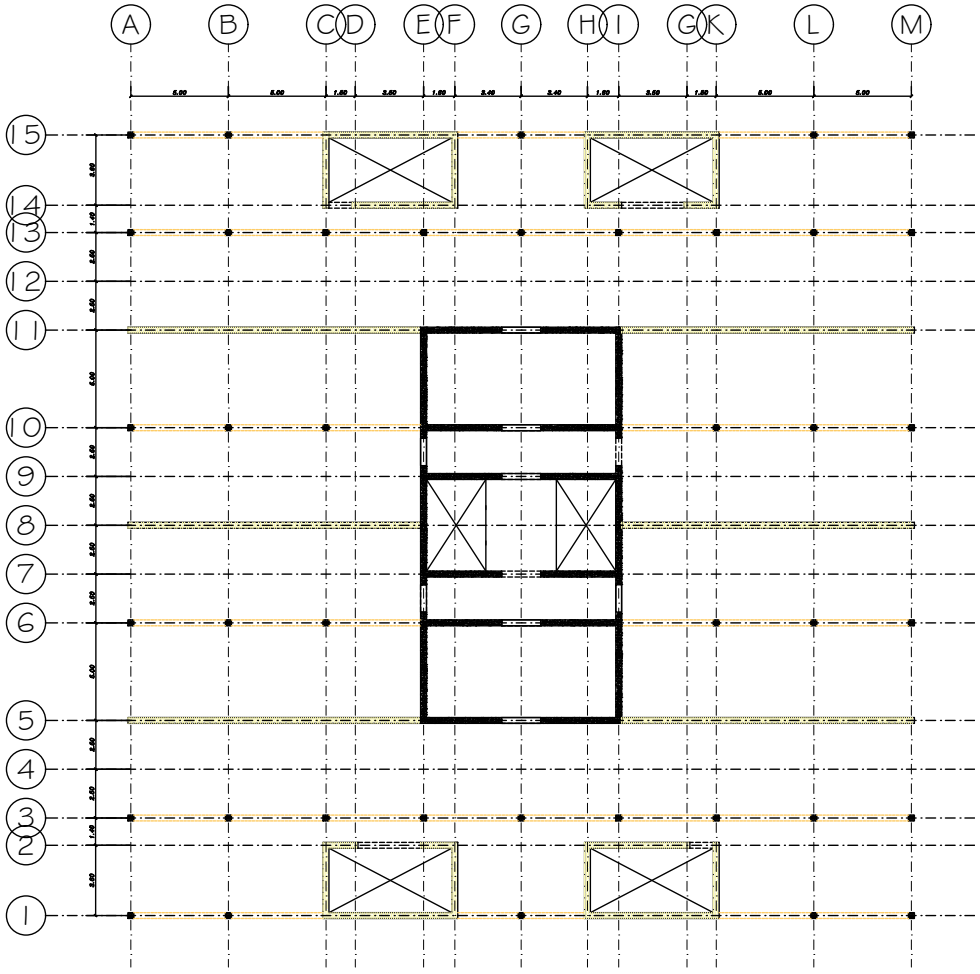

Floor Beam Plan

Horizontal Structural components

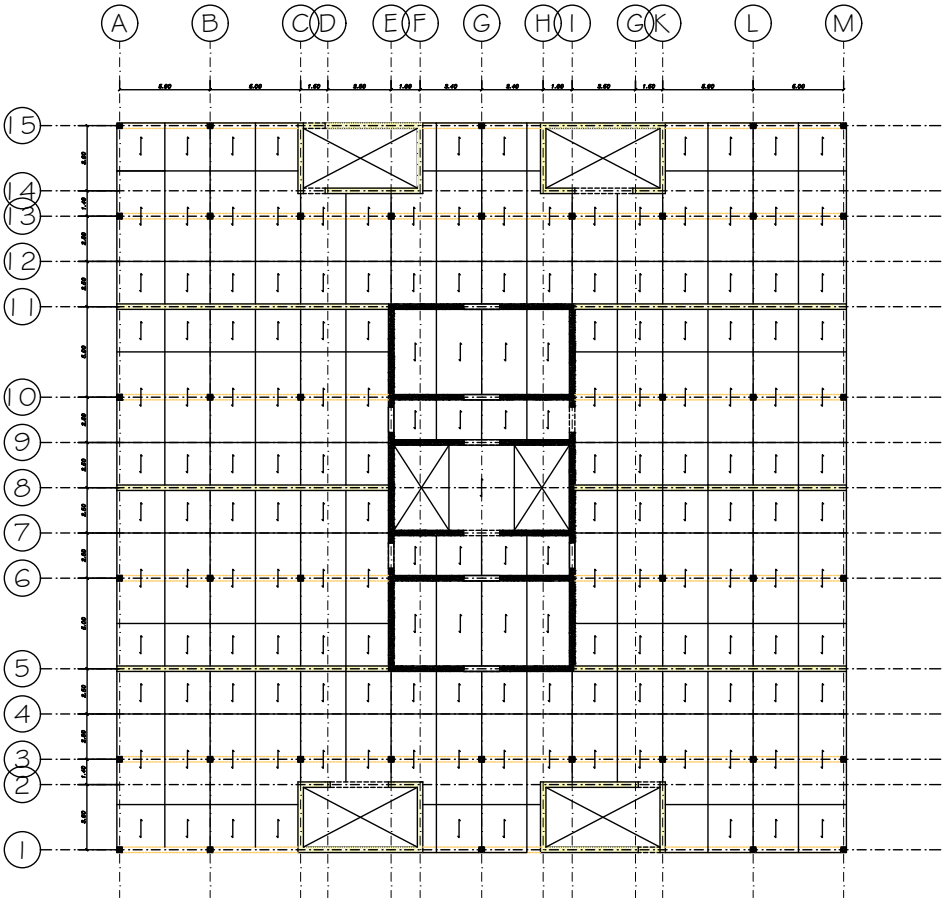

Floor Beam Plan

Horizontal Structural components

Floor Beam Plan

Horizontal Structural components

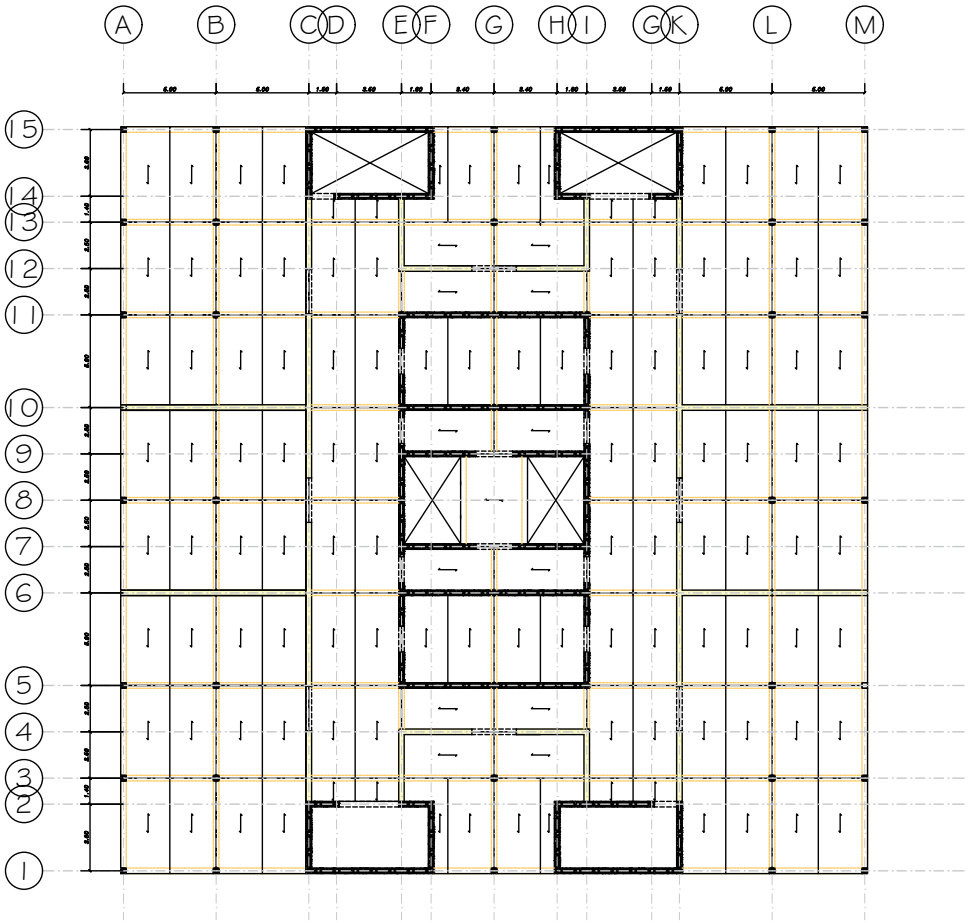

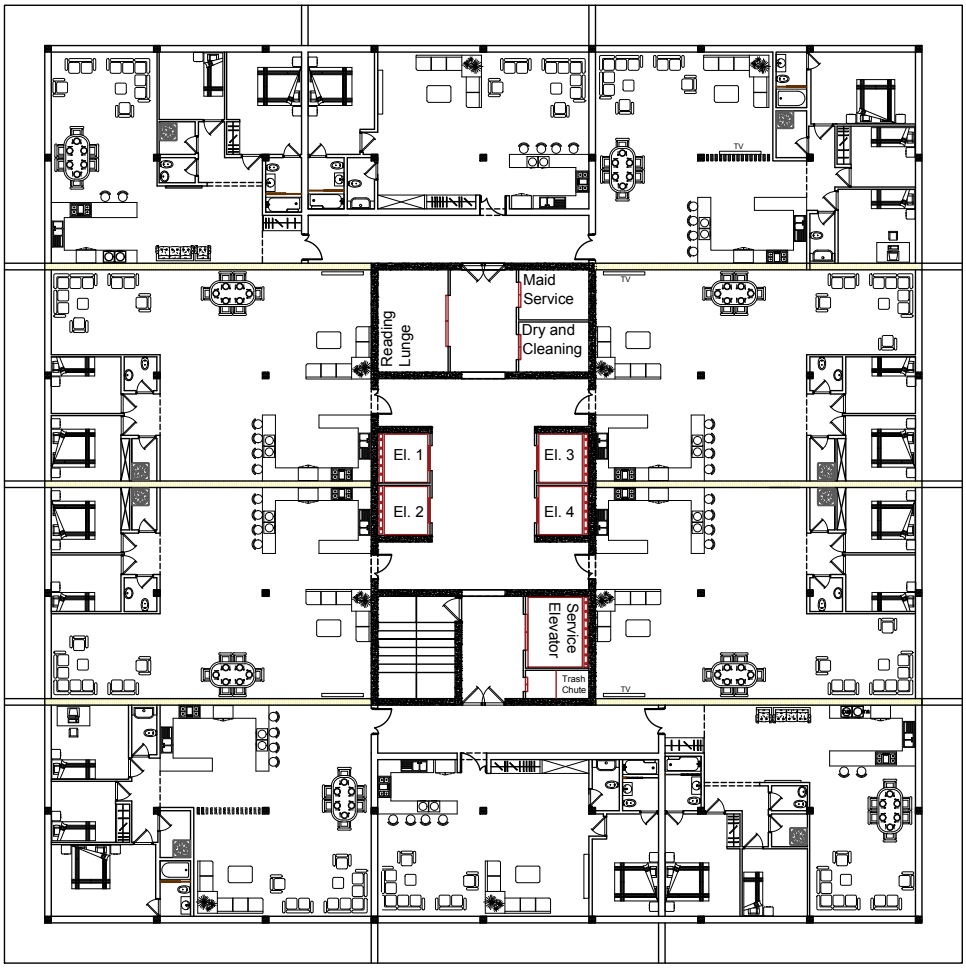
Maid
Service
Dry and
Cleaning
Reading
Lunge
El. 1
El. 2
El. 3
El. 4
Service
Elevator
Trash
Chute
TV

Floor Plan

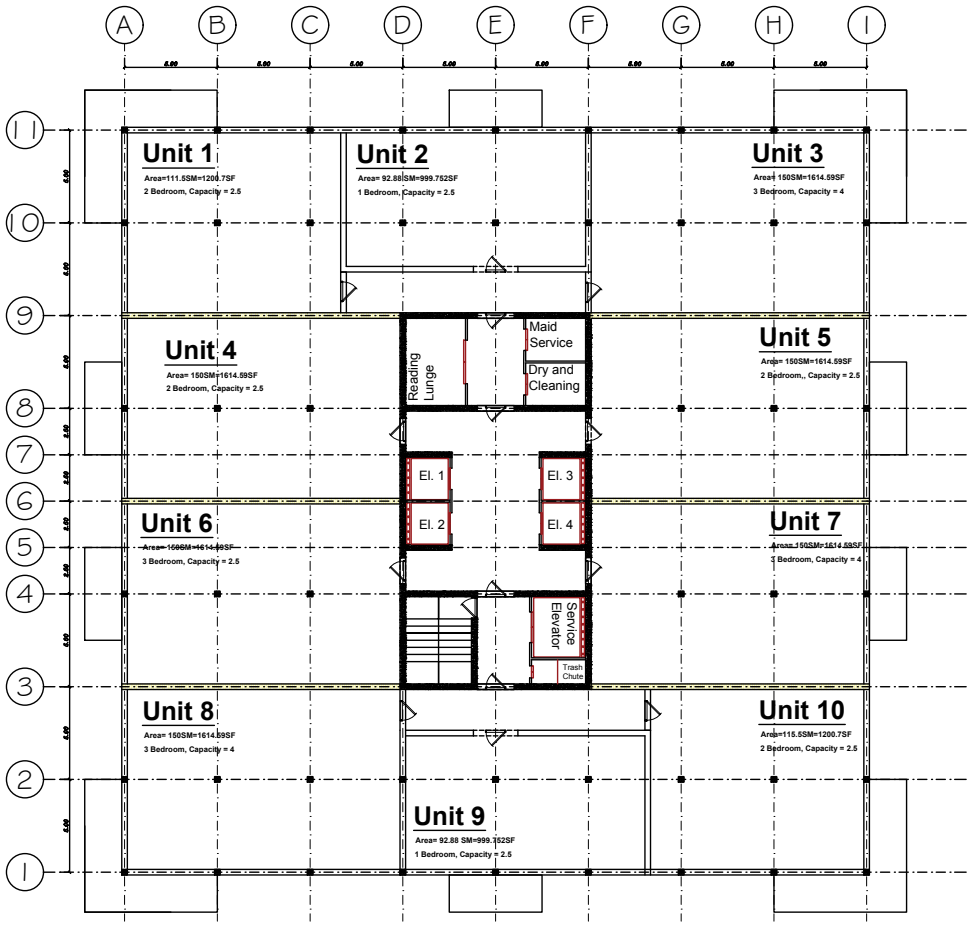
A
B
C
D
E
F
G
H
I
11
10
9
8
7
6
5
4
3
2
1
Unit 1
Area=111.5SM=1200.7SF
2 Bedroom, Capacity = 2.5
Unit 2
Area= 92.88SM=999.752SF
1 Bedroom, Capacity = 2.5
Unit 3
Area= 150SM=1614.59SF
3 Bedroom, Capacity = 4
Unit 4
Area= 150SM=1614.59SF
2 Bedroom, Capacity = 2.5
Reading Lunge
Maid Service
Dry and Cleaning
Unit 5
Area= 150SM=1614.59SF
2 Bedroom,, Capacity = 2.5
El. 1
El. 2
El. 3
El. 4
Unit 6
Area= 150SM=1614.59SF
3 Bedroom, Capacity = 2.5
Unit 7
Area= 150SM=1614.59SF
3 Bedroom, Capacity = 4
Service Elevator
Trash Chute
Unit 8
Area= 150SM=1614.59SF
3 Bedroom, Capacity = 4
Unit 10
Area=115.5SM=1200.7SF
2 Bedroom, Capacity = 2.5
Unit 9
Area= 92.88 SM=999.752SF
1 Bedroom, Capacity = 2.5

Floor Plan

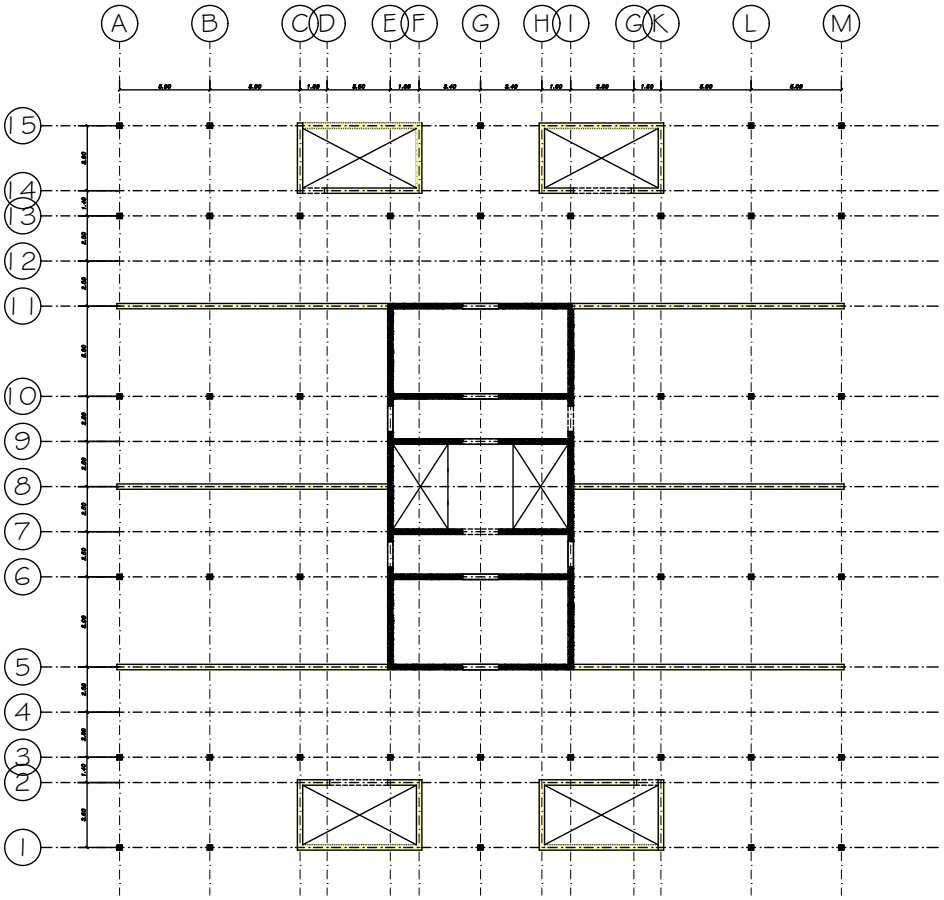

Floors Structure

Vertical Structural Components

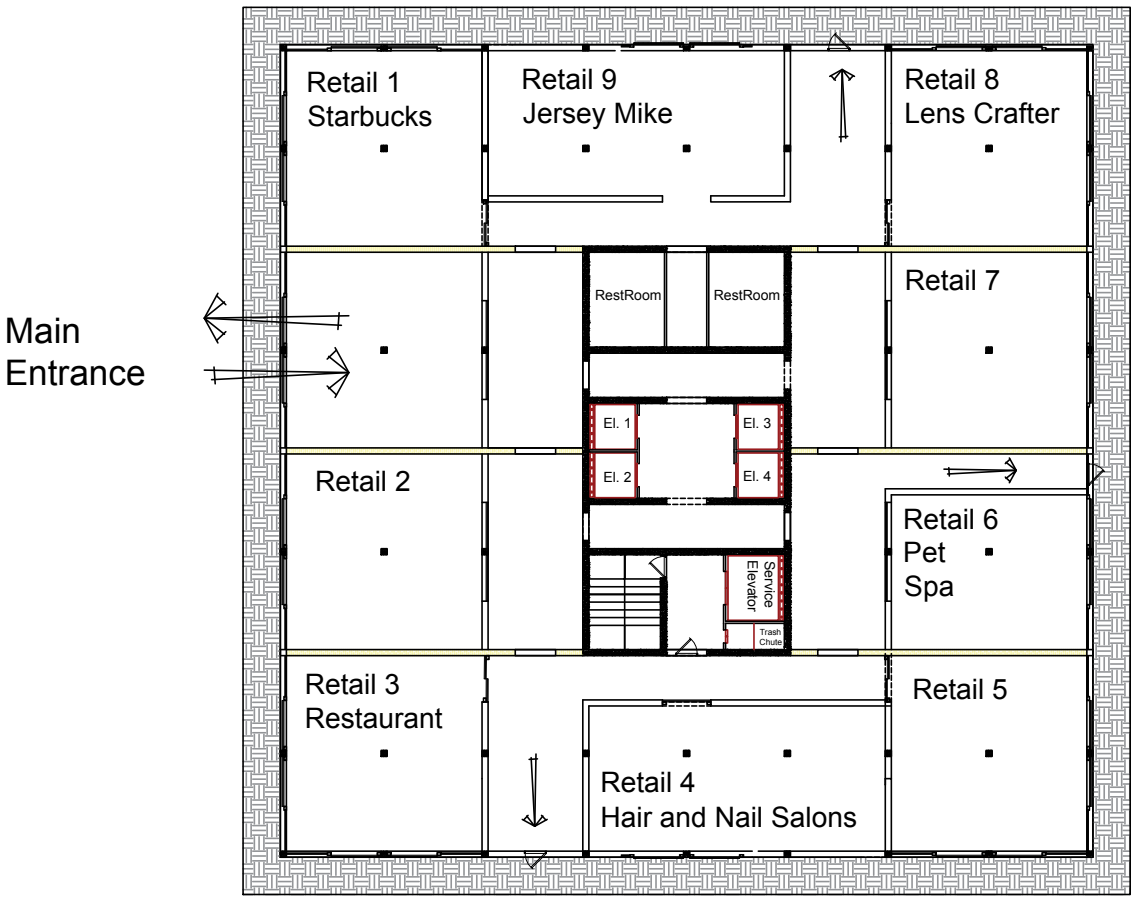

Ground Floor Plan

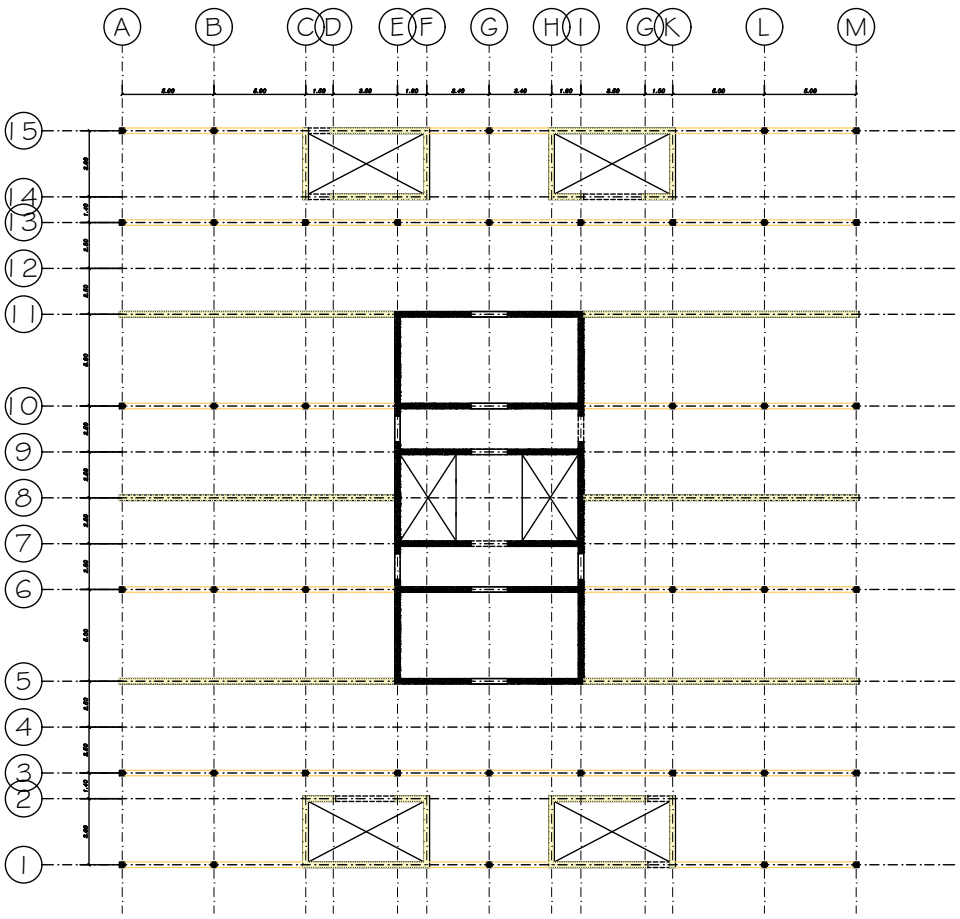

Ground Floor Beam Plan

Horizontal Structural components

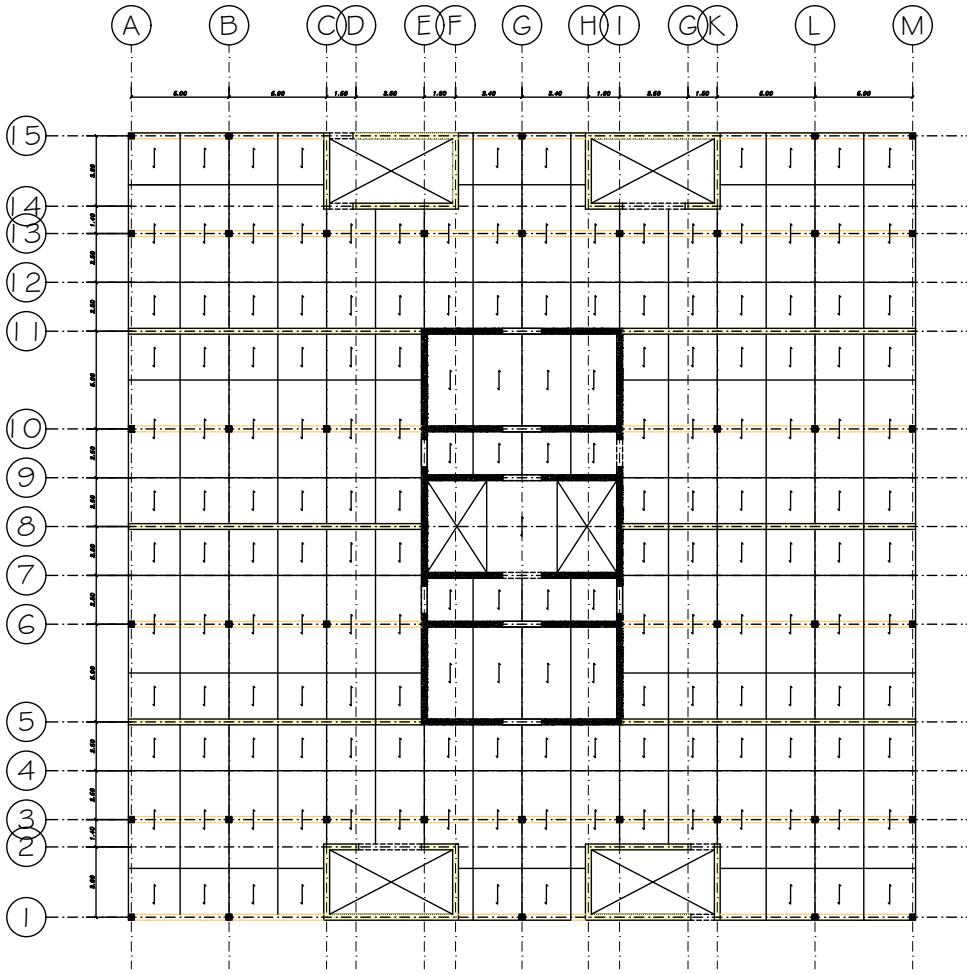

Ground Floor Beam Plan

Horizontal Structural components

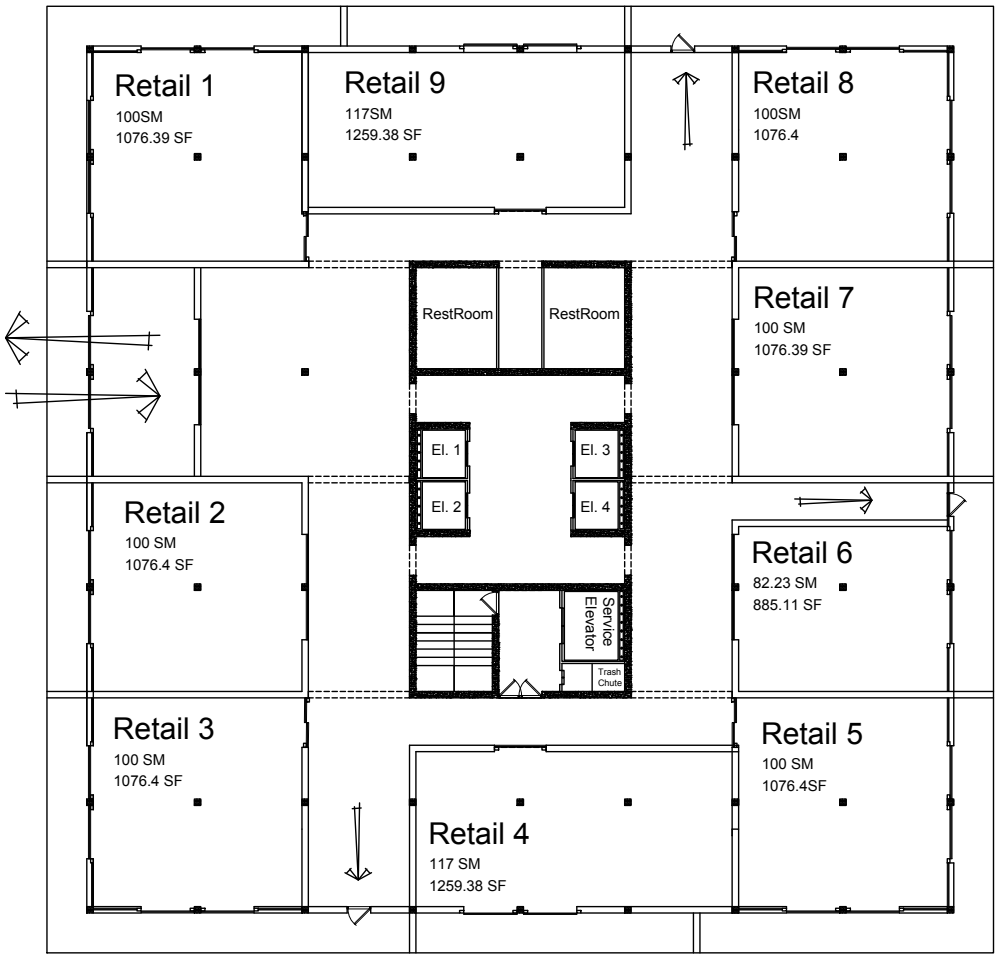

Ground Floor Plan

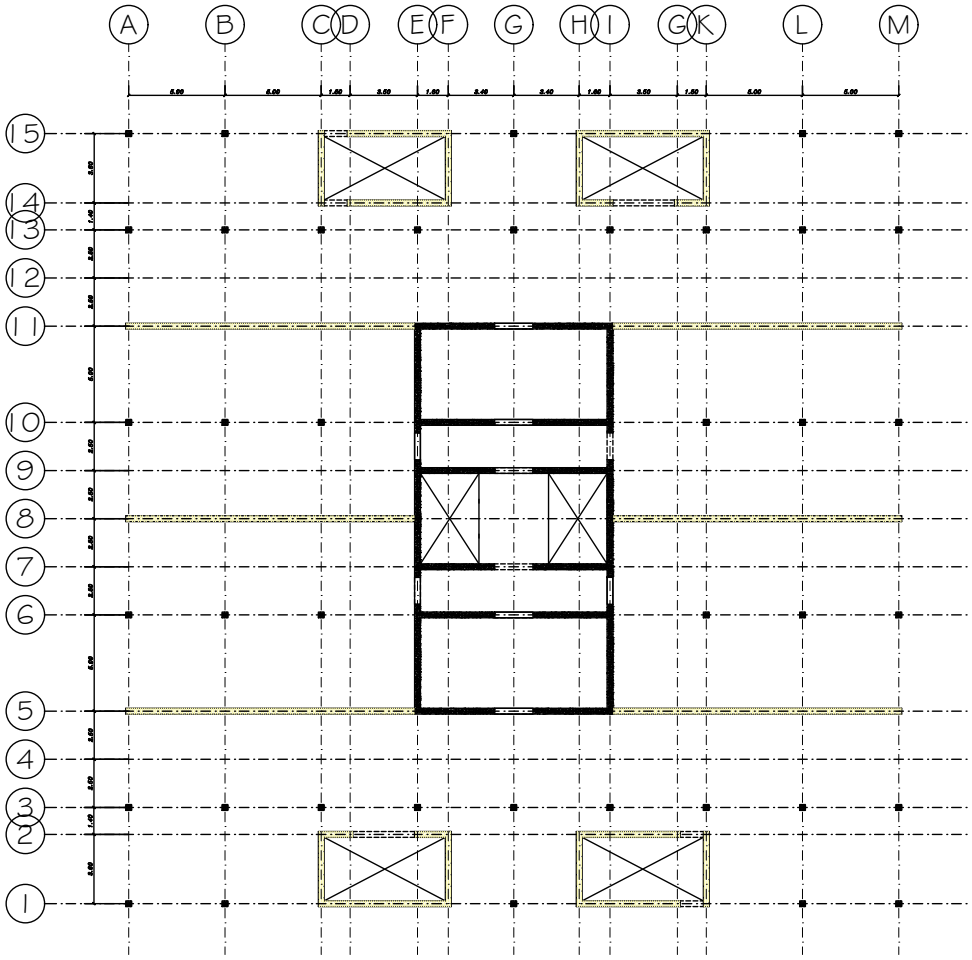

Ground Floor Structure

Vertical Structural Components

Each one of Assemblies 2 and 3 tested twice under fire-performance condition. However, for each assembly one of the experiments failed as the loading jack stopped acting. The experimental results related to these failed tests provided in the following.

Assembly 2: Glulam-beam to CLT-walls connected with T-shape steel connections

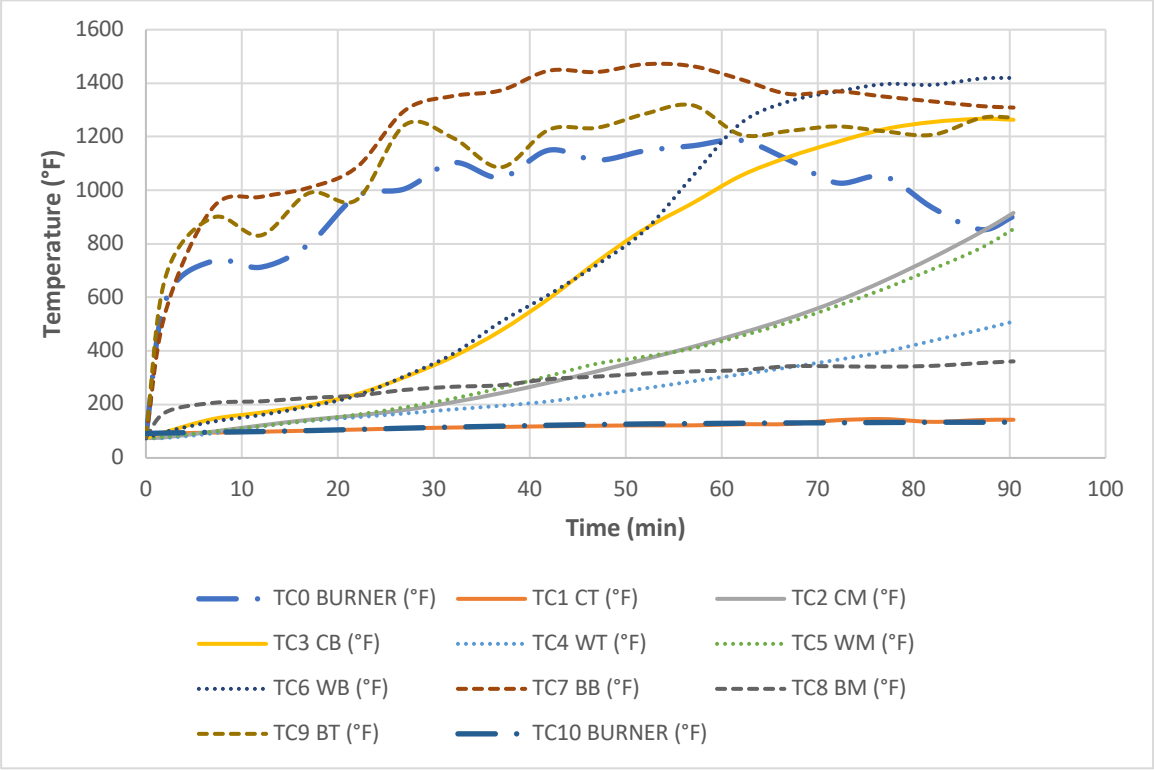

TC10 and TC1 were disconnected during this test. And loading jack did not work.

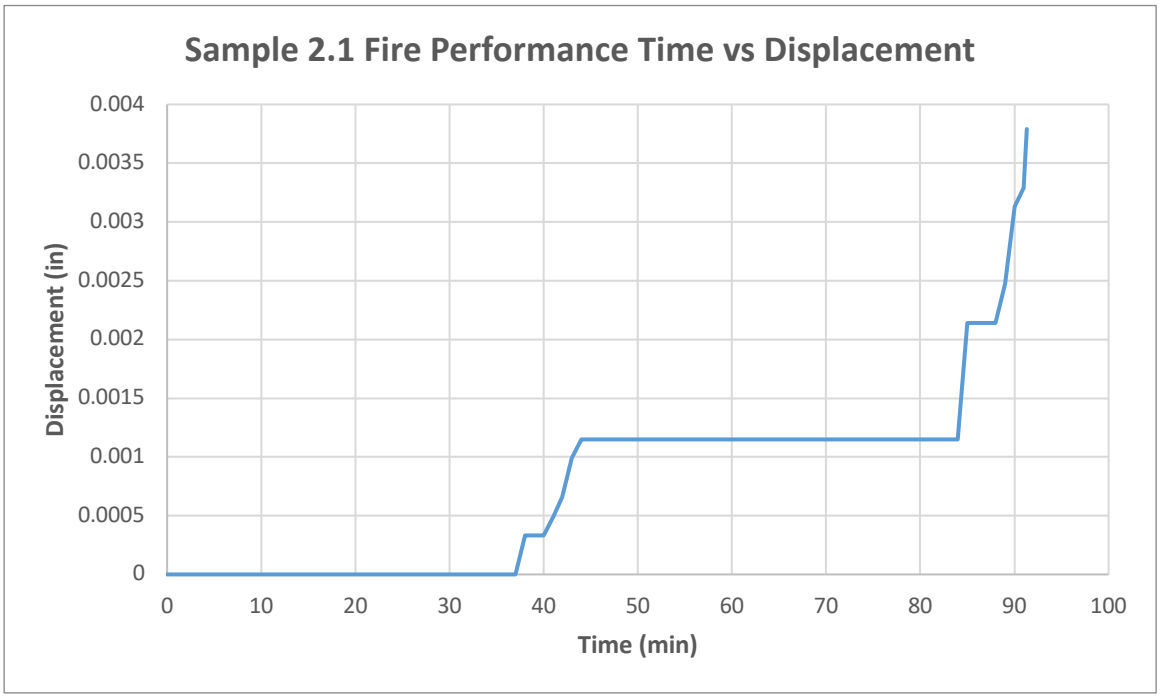

Assembly 3: Glulam beam-to-beam connected with T-shape steel connections

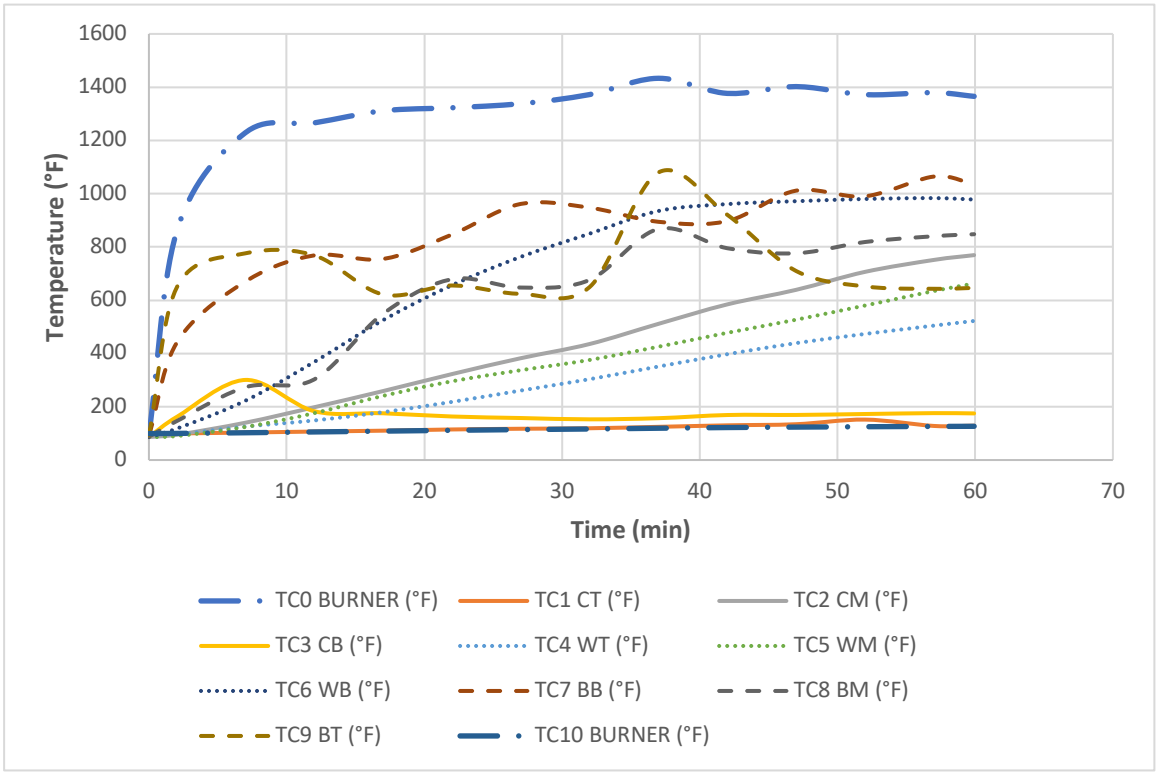

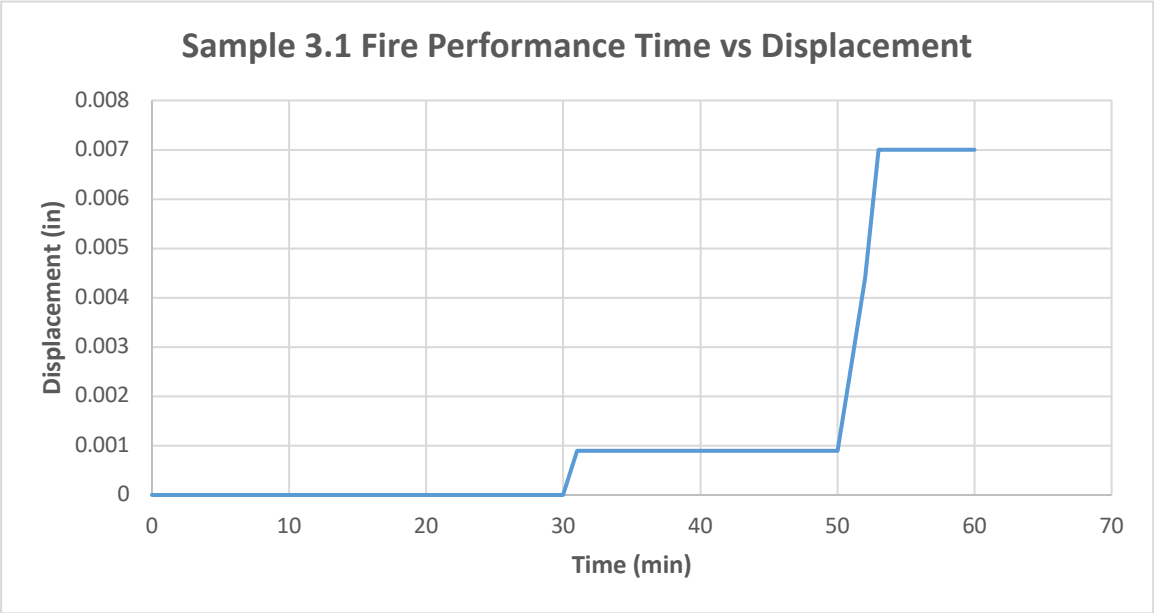

(Note: In both of these experiments samples were under only their own weight plus loading deck)

Assemblies 4 to 7 built out of Aluminum doweled connections. This Appendix also provides some information about these assemblies.

Experimental Research Summery

#	Assembly description	Temperature	Load	Number of tests
A4	GL Beam-to-Beam assembly with 0.5 in. gap between members connected with Aluminum doweled connection. (The connections are **totally exposed** to fire in this assembly)	Ambient temperature	Loaded until failure	3
		30 min fire exposure 60 min fire exposure	Loaded after fire exposure until failure	2
		fire exposure	Constantly Loaded during fire exposure until failure	2
A5	GL Beam-to-Beam assembly with no gap between members connected with Aluminum doweled connection. (The connections are **totally concealed** from fire in this assembly)	Ambient temperature	Loaded until failure	3
		30 min fire exposure 60 min fire exposure	Loaded after fire exposure until failure	2
		fire exposure	Constantly Loaded during fire exposure until failure	2
A6	GL-Beam to CLT-Wall assembly with 0.5 in. gap between members connected with Aluminum doweled connection. (The connections are **totally exposed** to fire in this assembly)	Ambient temperature	Loaded until failure	3
		30 min fire exposure 60 min fire exposure	Loaded after fire exposure until failure	2
		fire exposure	Constantly Loaded during fire exposure until failure	2
A7	GL-Beam to CLT-Wall assembly with no gap between members connected with Aluminum doweled connection. (The connections are **totally concealed** from fire in this assembly)	Ambient temperature	Loaded until failure	3
		30 min fire exposure 60 min fire exposure	Loaded after fire exposure until failure	2
		fire exposure	Constantly Loaded during fire exposure until failure	2

Details of glulam beam to beam assembly with exposed aluminum connections (A4).

Parts	Quantity	Material	Dimensions
Headers	2	Glulam Beam	7.625 in. x 3.125 in. x 18 in.
Joist	1	Glulam Beam	7.625 in. x 3.125 in. x 18 in.
Connection	2	Aluminum doweled connection	Plate A: 3.125 in. x 6.3 in. x 3/16 in. Plate B: 4.125 in. x 6.3 in. x 3/16 in.
Dowel	8	Stainless Steel	1/2 in. diameter, 3.125 in. length
Screw	18	Stainless Steel	1/4 in. diameter, 3 in. length

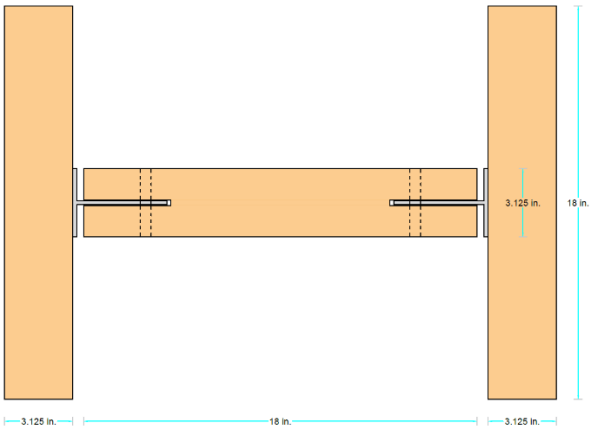

Top and Bottom View

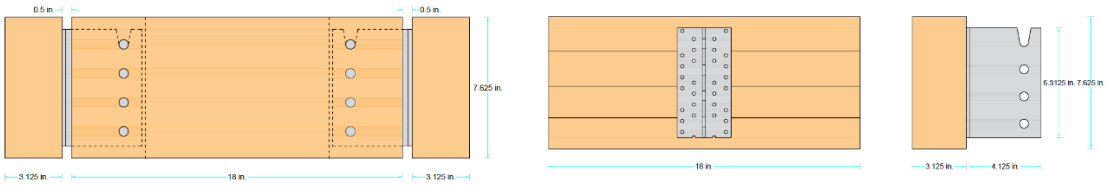

Front View *Side View*

Geometry of glulam beam to beam assembly with exposed aluminum connections (A4).

Details of glulam beam to beam assembly with concealed aluminum connections (A5).

Parts	Quantity	Material	Dimensions
Headers	2	Glulam Beam	7.625 in. x 4.5 in. x 18 in.
Joist	1	Glulam Beam	7.625 in. x 4.5 in. x 18 in.
Connection	2	Aluminum Doweled Connection	Plate A: 3.125 in. x 6.3 in. x 3/16 in. Plate B: 4.125 in. x 6.3 in. x 3/16 in.
Dowel Caps	8	Wooden	0.5 in. diameter and 0.5 in. length
Dowel	8	Stainless Steel	1/2 in. diameter, 3.125 in. length
Screw	18	Stainless Steel	1/4 in. diameter, 3 in. length

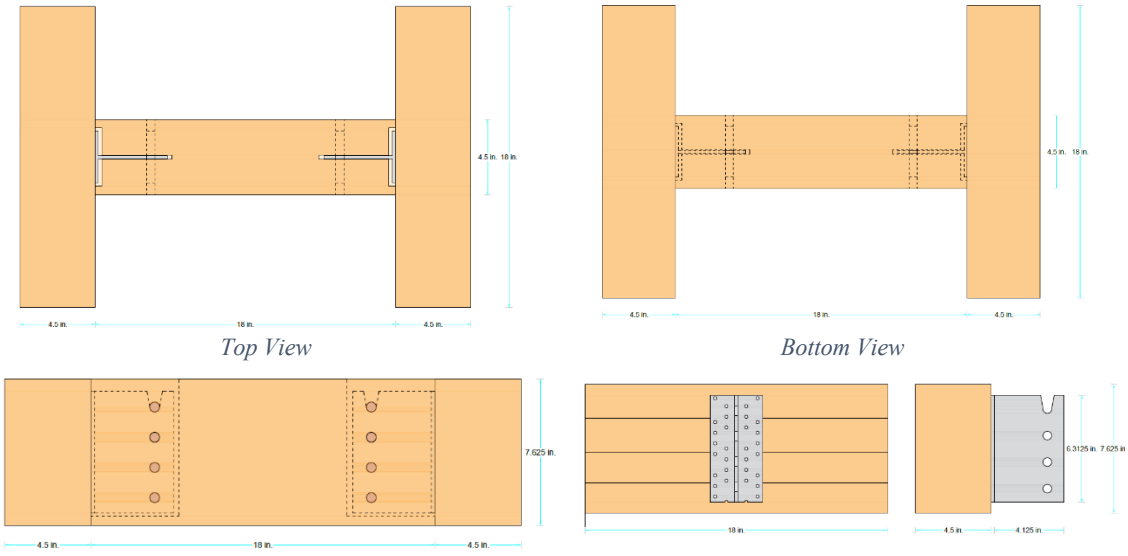

Top View *Bottom View*

Front View *Side View*

Geometry of Glulam Beam to Beam Assembly with Concealed Aluminum Connections (A5).

Details of GL beam to CLT wall assembly with exposed aluminum connections (A6).

Parts	Quantity	Material	Dimensions
Headers	2	CLT Wall	7.625 in. x 3.875 in. x 18 in.
Joist	1	Glulam Beam	7.625 in. x 3.125 in. x 18 in.
Connection	2	Aluminum Doweled Connection	Plate A: 3.125 in. x 6.3 in. x 3/16 in. Plate B: 4.125 in. x 6.3 in. x 3/16 in.
Dowel	8	Stainless Steel	1/2 in. diameter, 3.125 in. length
Screw	18	Stainless Steel	1/4 in. diameter, 3 in. length

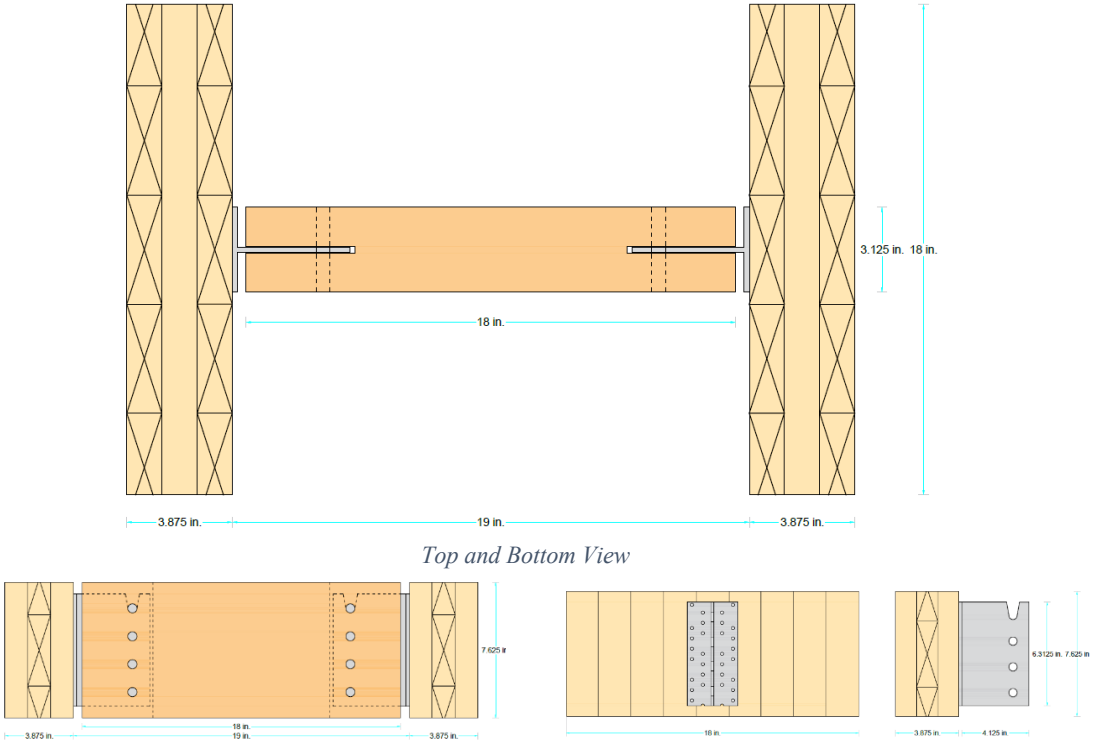

Top and Bottom View

Front View *Side View*

Geometry of GL beam to CLT wall assembly with exposed aluminum connections (A6).

Details of GL beam to CLT wall assembly with concealed aluminum connections (A7).

Parts	Quantity	Material	Dimensions
Headers	2	CLT Wall	7.625 in. x 3.875 in. x 18 in.
Joist	1	Glulam Beam	7.625 in. x 4.5 in. x 18 in.
Connection	2	Aluminum Doweled Connection	Plate A: 3.125 in. x 6.3 in. x 3/16 in. Plate B: 4.125 in. x 6.3 in. x 3/16 in.
Dowel	8	Stainless Steel	1/2 in. diameter, 3.125 in. length
Screw	18	Stainless Steel	1/4 in. diameter, 3 in. length

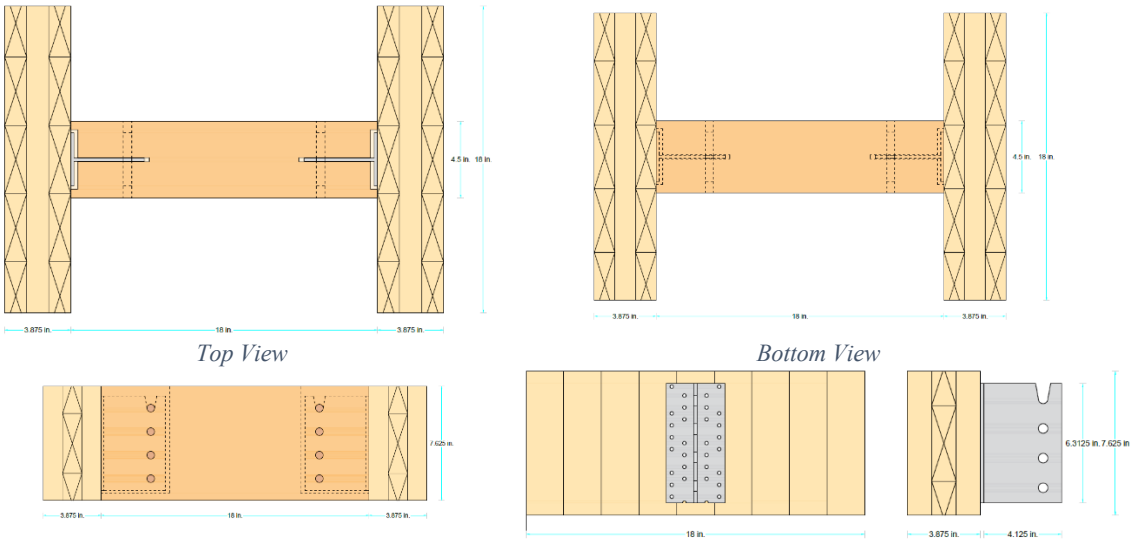

Geometry of GL beam to CLT wall assembly with concealed aluminum connections (A7).

Ambient temperature results summery

Assembly	Test #	Load Carrying Capacity of the System (lbf)	Relative Deflection (in.)	Failure Mode
A4	1	16372	0.61	Splitting
	2	15300	0.78	Splitting
	3	11861.98	0.85	Splitting
A5	1	19476.92	1.067	Splitting
	2	20607.937	1.15	Splitting
	3	20357	1.18	Splitting
A6	1	18155.35	0.7	Splitting
	2	15509.75	1.217	Splitting
	3	18146.38	0.81	Splitting
A7	1	21650	1.52	Splitting
	2	21956	1.537	Splitting
	3	21436.32	0.8335	Splitting

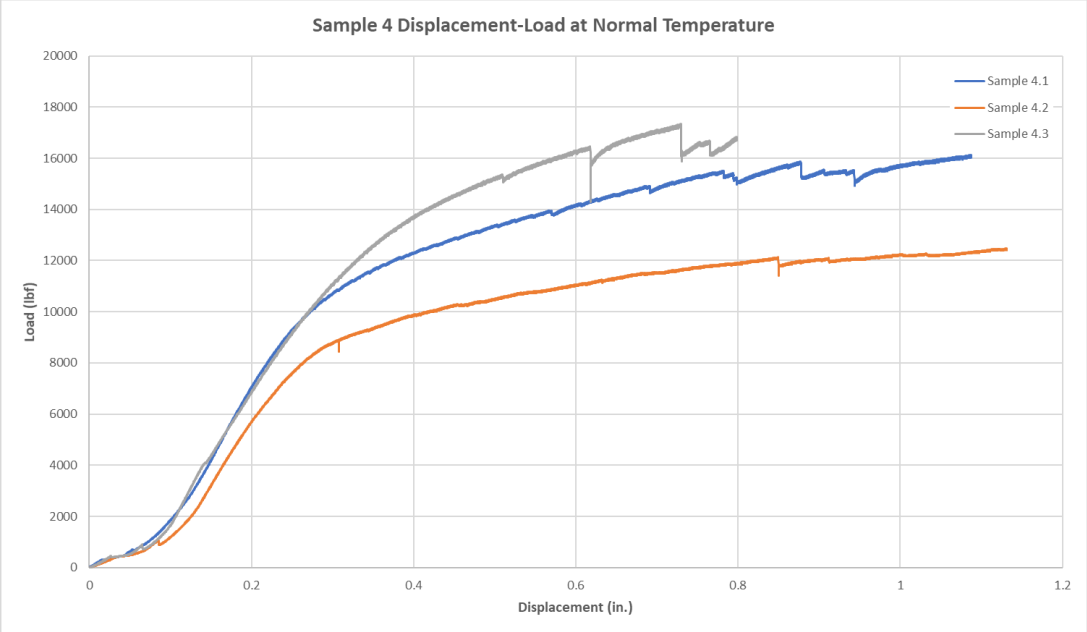

Load-displacement curves of tests A.4.1, A.4.2 and A.4.3 at ambient temperature.

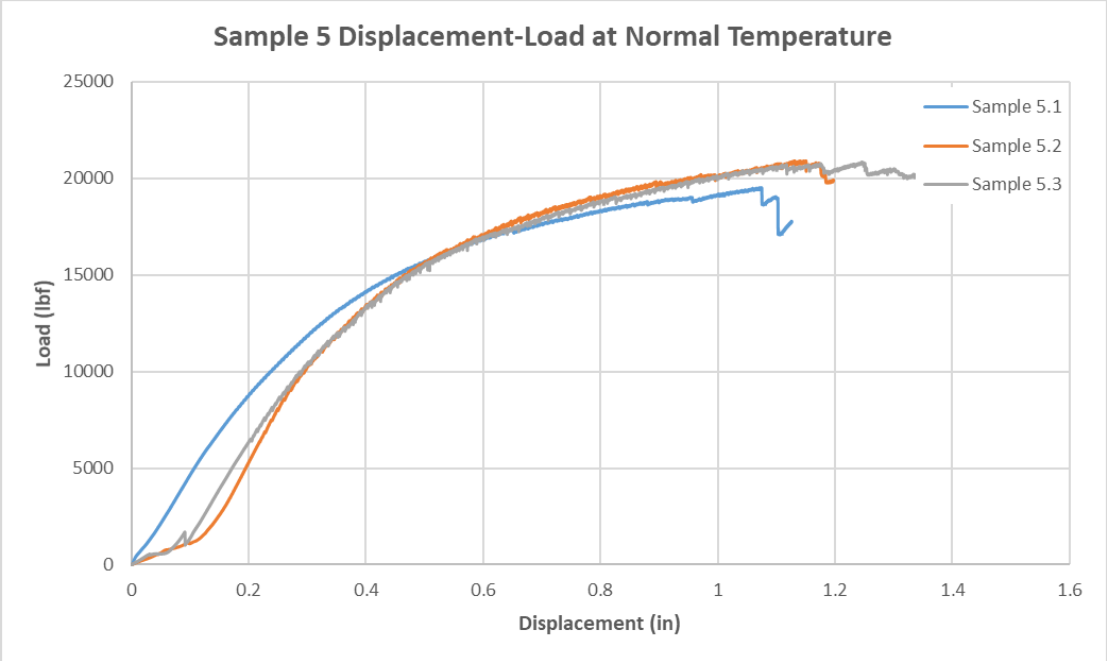

Load-displacement curves of tests A.5.1, A.5.2 and A.5.3 at ambient temperature.

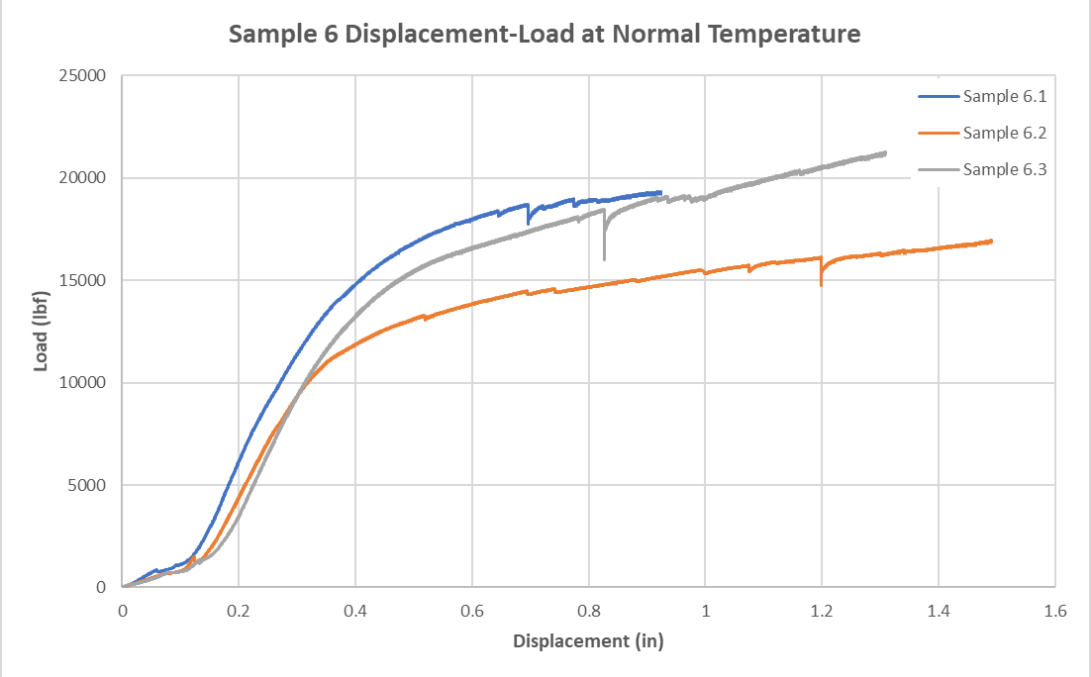

Load-displacement curves of tests A.6.1, A.6.2 and A.6.3 at ambient temperature.

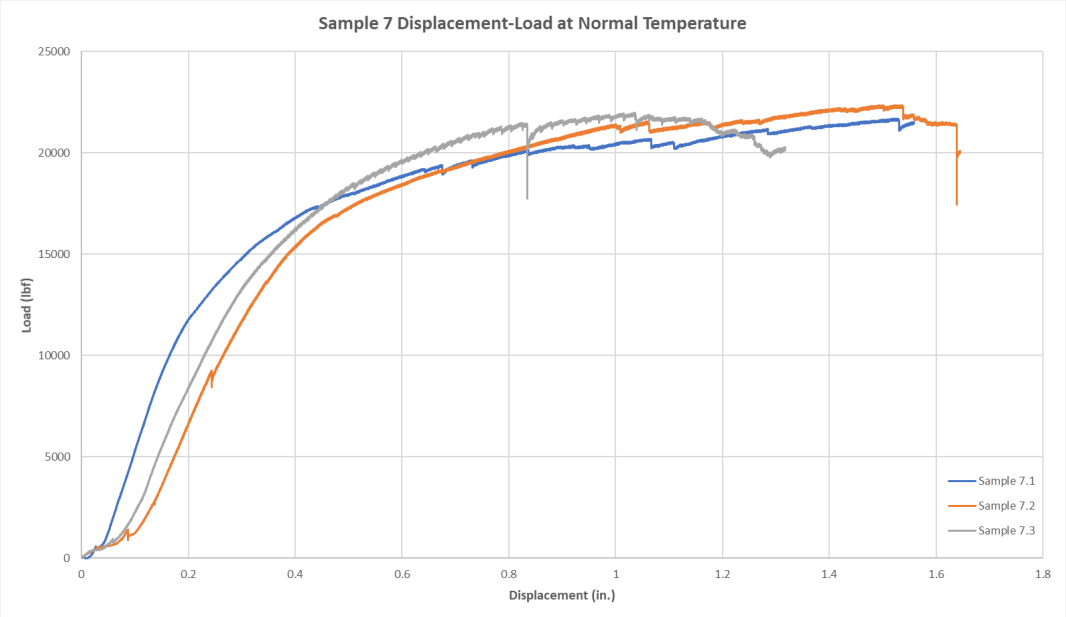

Load-displacement curves of tests A.7.1, A.7.2 and A.7.3 at ambient temperature.

Prepared samples protected by insolation boards

Loading burned sample under imposed downward load

Post-fire performance research summery

Assembly	Test #	Fire Exposure time (min)	Load Carrying Capacity of the System (lbf.)	Relative Deflection (in.)
A4	1	30	13367.428	0.93375
	2	60	9971.37	0.450
A5	1	30	15597	0.602
	2	60	14696.26	0.533
A6	1	60	4526.01	0.312
	2	30	8364.8	0.26801
A7	1	60	12965.43	0.367
	2	30	13731.51	0.6787

Fire performance test setup and loading system.

Strain pod measuring deflection

Assembly	Test #	Load (lbs.)	Maximum Deflection (in.)	Fire Exposure time (min)
A4	1	3500	0.144	37
	2	7000	0.3395	30.1
A5	1	7000	0.0275	33
	2	7000	0.017	56
A6	1	12000	0.227	33.33
	2	6000	0.0116	42
A7	1	13000	0.1	80.06
	2	14000	0.11	60.85

Assembly 1: CLT beam-to-beam at ambient temp.

A1.1 AT

A1.2 AT (Failed)

A1.3 AT

A1.4 AT

A1 PFP 30

A1 FP

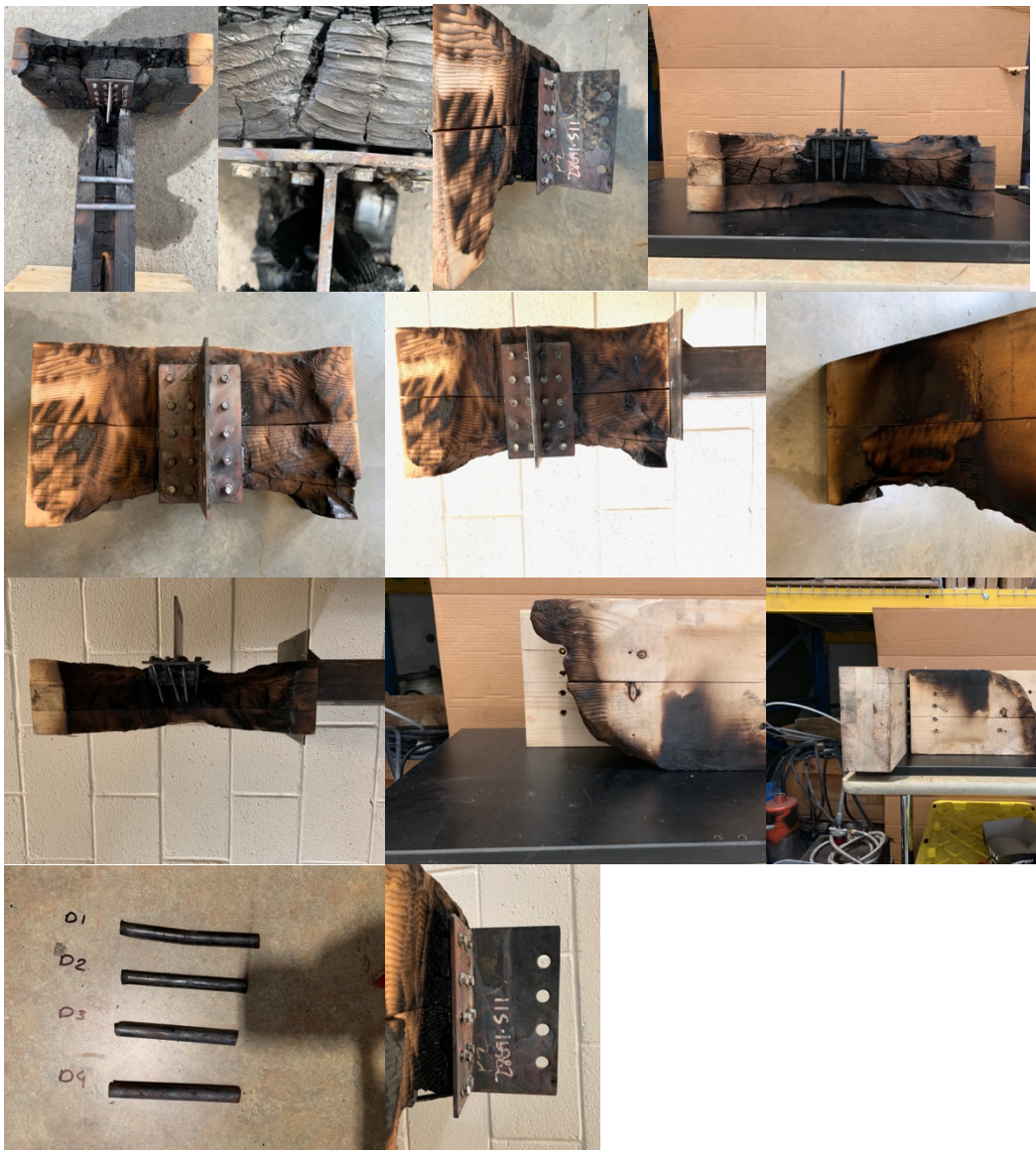
D1
D2
D3
D4

A2: Glulam Beamt to CLT Walls

A2.1 Ambient Temp.

A2.2. AT

A2.3. AT

A2 PFP30

A2 PFP60

A2 FP1 (Jack did not work in this test)

A2 FP2

A3: Glulam beam-to-beam assembley
A3.1 AT




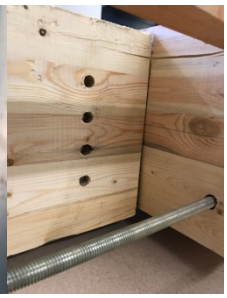
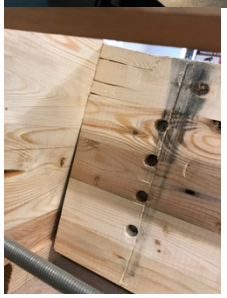

A3.2. AT

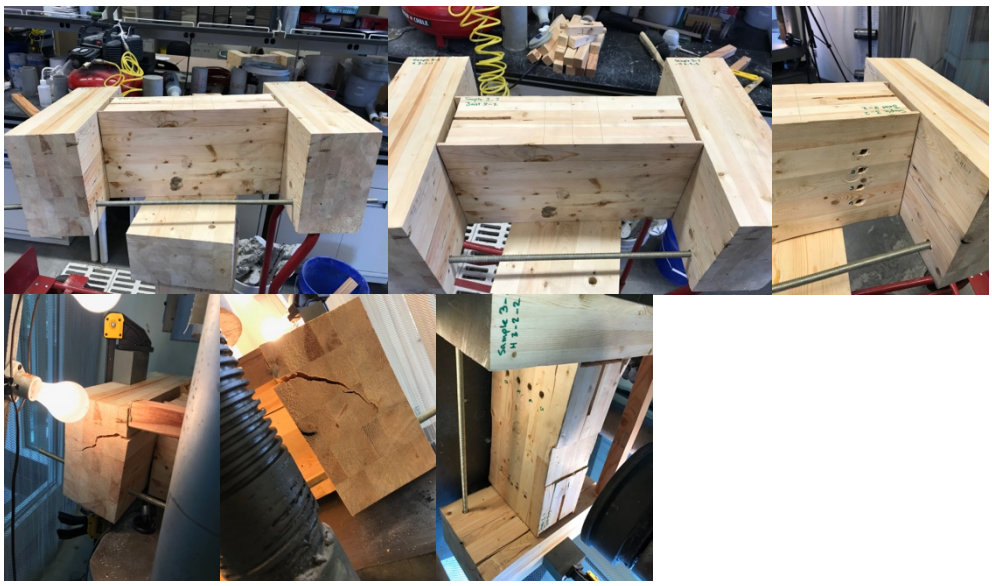

A3.3. AT

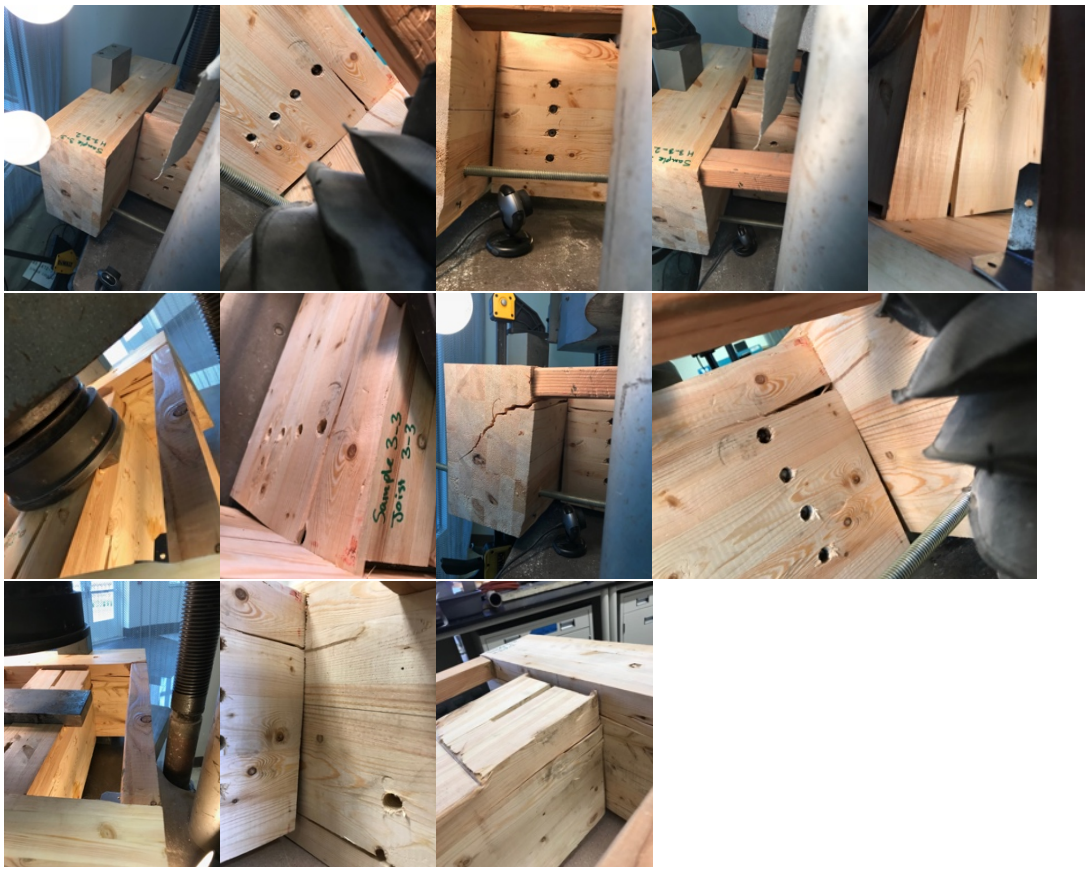

A3 PFP 30

A3 PFP60

A3 FP1 (loading system failed)

A3 FP2

A4 (Glulam beam-to-beam exposed) AT

A4 PFP

A4 FP (42 min and 32 min Fire exposure)

Assembly 5 (Gl beam-to-beam concealed) AT

A5 PFP

A5 FP (63 min and 110 min)

A6 (Glulam beam to CLT walls exposed) AT

A6 PFP

A6 FP (85 min and 45 min fire exposure)

A7 (Glulam beam to CLT walls Concealed) AT

A7 PFP

A7 FP (115 min and 60 min fire exposure)